Overview of MXene/conducting polymer composites for supercapacitors

Wenlong Luo[1], Yong Ma[1,*], Tingxi Li[1,*], Hamdy Khamees Thabet[2]*, Chunping Hou[3], Mohamed M. Ibrahim[4], Salah M. El-Bahy[5], Ben Bin Xu[6], Zhanhu Guo[7,*]

[1] School of Material Science and Engineering, Shandong University of Science and Technology, Qingdao 266590, P. R. China

[2] Chemistry Department, Faculty of Arts and Science, Northern Border University, Rafha, 91911, Saudi Arabia

[3] College of Materials Science and Engineering, North Minzu University, Yinchuan, 750021, P. R. China

[4] Department of Chemistry, College of Science, Taif University, Taif 21944, Saudi Arabia

[5] Department of Chemistry, Turabah University College, Taif University, Taif 21944, Saudi Arabia

[6] Department of Mechanical and Construction Engineering, Faculty of Engineering and Environment, Northumbria University, Newcastle upon Tyne, NE1 8ST, UK

[7] Integrated Composites Laboratory (ICL), Department of Chemical and Biomolecular Engineering, University of Tennessee, Knoxville, TN, 37996, USA

*Correspondence author: mayong@sdust.edu.cn (Y. Ma); litx@sdust.edu.cn (T. Li); hamdy.salem@nbu.edu.sa (H. Khames); zguo10@utk.edu (Z. Guo).

Abstract

Both MXene and conducting polymers are hot research topics on electrode materials for supercapacitors (SCs). The combination of these two different types of materials can solve the defects that exist when they are used as electrode materials alone. Based on theoretical capacity, specific surface area, mass load, flexibility and excellent mechanical properties, MXene/conducting polymers composites demonstrate their potential to become advanced electrode materials. In order to further illustrate the changes brought about by these composites, a large number of examples of MXene/conducting polymers as electrodes are described in details. In general, this review covers the latest developments in the study of SCs based on MXene/conducting polymers composites, including materials preparation, electrode materials, symmetrical supercapacitors (SSCs) and asymmetrical supercapacitors (ASCs). This article aims to understand the application of MXene/conducting polymers composites in the research of SCs, and provides a guideline for further research of these promising materials.

Keywords: MXene; Conducting polymers; Composites; Supercapacitors.

1. Introduction

With the rapid development of science and technology, humanity's demand for energy is increasing. For a long time, the continuous consumption of petroleum, coal and other fossil fuels, the supply of non-renewable energy has been slightly short of, and the contradiction between social development and energy supply has become more and more serious[1-5]. In order to effectively solve the problem of energy supply, it is important to reduce the adverse impact of fossil fuel combustion, and realize the green and sustainable blossom of the ecological environment[6-9]. Developing efficient energy storage devices is considered to be a strategic technology for the development of renewable energy, such as metal ion batteries[10-12], fuel cells[13, 14], phase change energy, solar cells, metal air batteries[15-17] and SCs[18-20]. Among these promising devices, SCs have attracted much attention because of the advantages including wide operating temperature range, high-power density, long cycle life and good recoverability[21-25]. The electrochemical performances of SCs are mainly related to the properties and structures of electrode materials[26-29].

Based on the energy storage mechanism, electrode materials are mainly divided into two categories[30]. One is carbon materials providing good power density because of their fast-physical processes, on the basis of electrochemical double layer capacitor[31-33]. Nevertheless, owing to the lack of rapid reversible reactions, they have lower energy densities[34, 35]. The other is pseudocapacitive materials by taking on Faraday charge transfer reactions at the electrochemically active sites, including transition metal oxides[36, 37], such as MnO_2 and RuO_2,

which can be used as effective electrodes owing to their high theoretical capacitance of 1380 and 1200-2200 F g^{-1}, respectively[38, 39]. However, the cyclic stability of pseudocapacitive materials is poor, which greatly limits its application[40, 41]. Therefore, on the premise of not losing the advantages of excellent rate capacity and large specific capacity, to find a suitable electrode material with good cycling stability becomes more importantly[42, 43].

Because of the remarkably physical and chemical performances, two-dimensional (2D) materials can provide not only electrical double-layer capacitance by ion adsorption/desorption, but also pseudo-capacitance by Faraday redox reaction on the surface[44-46]. Some 2D materials even provide electrical double-layer capacitance and pseudo-capacitance at the same time[47-49]. Because of their unique features, good elasticity, excellent mechanical properties, the quality of load big advantages[50, 51], 2D materials have become important electrochemical active materials in SCs, such as grapheme[52], metal organic framework (MOFs)[53, 54], the layered double hydroxides (LDHs)[55] and MXene[56, 57].

MXene is a large class of 2D transition metal nitrides or carbides, for example Mo_2C[58], Nb_2C[59], Ti_2C[60], V_2C[61], Ti_3C_2[46, 62], etc. Fig. 1 (a) shows the distribution of the main selected elements of MXene in the periodic table. Its general molecular formula is $M_{n+1}AX_n$ (n=1, 2, 3), in which M, A and X separately denote the transition metal, III_A and IV_A group elements and nitrogen or carbon [63, 64]. In the tightly arranged M layer, X atoms are located in the center of the octahedron, and M and A layers are alternately arranged to form the MAX phase, as shown in Fig. 1 (b)[65]. MXene can be obtained through selectively etching element A. And the etching

process is carried out in solution, resulting in the periphery of the material with -O, -OH or -F functional groups[66]. Therefore, its general molecular formula can be expressed as $M_{n+1}X_nT_x$ (n=1, 2, 3)[67], in which M, X and T denote the early transition metal, carbon or nitrogen, and surface terminating groups of -O, -OH or -F[68].

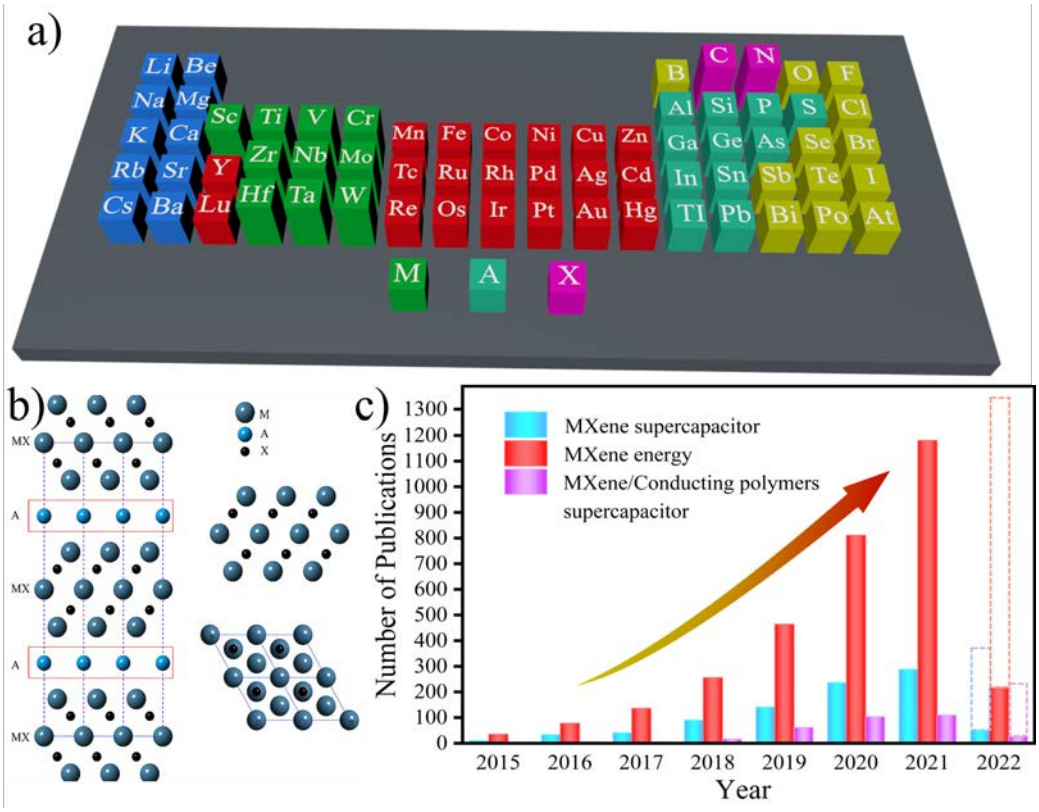

Fig. 1. (a) Fragment of the periodic table showing the main elements of the MAX phase. (b) The illustration of the crystal structure of the MAX phase[65]. Copyright 2013 American Physical Society. (c) Annual publication volume of MXene related articles. [Source: Web of Science. Search index: MXene energy, MXene supercapacitor or MXene/Conducting polymers supercapacitor.]

Since the discovery of MXene by Gogotsi *et al.*[69] in 2011, MXene materials have attracted great attention because of their large specific surface area and excellent electrical conductivity.

Fig. 1 (c) exhibits the number of papers reporting MXene in the field of energy and supercapacitors (SCs) in recent years. The number of articles published each year is rising in a stepwise manner, which also shows that the research of MXene is becoming more and more popular. Lukatskaya *et al*.[70] stripped Ti_3C_2 with dimethyl sulfoxide and then adopted ultrasound to obtain Ti_3C_2 sheets with fewer layers. After centrifugation, filtration and drying, self-supported "Ti_3C_2 paper" electrodes had only 2~20 μm thickness. In the KOH electrolyte, this "paper" electrode provides a volumetric capacitance of 450 F cm^{-3} at 2 mV s^{-1}, and still gives 280 F cm^{-3} even at 100 mV s^{-1}. Ghidiu *et al*.[71] etched Ti_3AlC_2 with hydrochloric acid and lithium fluoride and obtained clayey Ti_3C_2, then rolled the clayey Ti_3C_2 into thin sheets with a roller and directly made an electrode. In 1 M H_2SO_4 electrolyte, its volumetric capacitance is as high as 900 F cm^{-3} at 2 mV s^{-1} and 730 F cm^{-3} at 100 mV s^{-1}. Hydrophilicity, metal conductivity as well as surface redox reaction of MXene are the key to the preparation of electrode materials with good performances. However, under the effect of van der Waals force, the adjacent MXene flakes have a strong tendency to gather or self-accumulate, reducing the specific surface area and further affecting the ion diffusion among the layers. So, it seriously deteriorates the properties in practical applications of MXene based electrodes[72, 73]. Fortunately, the combination of conducting polymers with MXene can improve their electrochemical properties and give them superior mechanical properties[74-77].

The conducting polymers that are most commonly studied for use in SCs devices are polyaniline (PANI), polypyrrole (PPy), polythiophene (PTh) and poly(3,4-ethylenedioxythiophene) (PEDOT)[78-82]. They have good intrinsic conductivity. Table 1[83]

shows the typical conductivity of different conducting polymers in the doping state. Compared to conventional polymers (10 eV), conducting polymers have a lower band gap (1-3 eV). And these polymers possess specific doping/undoping behaviors, various morphologies and rather fast charge and discharge ability[84, 85].

Table 1. Conductivity of typical conducting polymers[83].

Polymer	PANI	PPy	PTh	PEDOT
Conductivity (S cm^{-1})	0.1-5	10-50	300-400	300-500

Since 2015, the development of MXene in the field of energy storage has been rapid, and there are numerous articles for SCs research[86-92]. For example, Xu *et al*.[88] discussed MXene for energy storage in sodium ion batteries, comparing theoretical and experimental differences in electrochemical performance. Nan *et al*.[86] summarized MXene in different energy storage devices and presented some challenges of MXene for future energy storage. Wu *et al*.[87] introduced MXene in potassium ion battery by some examples and explained the potassium storage mechanism of MXene. Nasrin *et al*.[93] elaborated the improvement of 2D/2D MXene heterostructures on the performance of SCs. The reviews of MXene applications in energy storage such as SCs and batteries are relatively numerous, however, there are relatively few reviews of MXene/conducting polymer composites for SCs.

In order to get a quicker and more convenient understanding of the recent research on MXene/conducting polymers in SCs, the recent papers on MXene/conducting polymers for SCs are summarized. This article focuses on the application of 2D materials MXene and

MXene/conducting polymers composites in SCs, including the synthesis and preparation of MXene and composite materials, and the research of advanced electrode materials. Subsequently, the application of these materials in symmetrical supercapacitors (SSCs) and asymmetrical supercapacitors (ASCs) is discussed with detailed examples. Some problems existing in the development of current Mxene/conducting polymers composite materials are pointed out. At last, we look into the application prospects of MXene.

2. Synthetic Methods

2.1. Preparation of MXene

2.1.1. HF etching

There are dozens of known types of MXene. Ti_3AlC_2 is taken as an example to explain the main preparation methods of MXene lamellas[64, 94]. As shown in Fig. 2 (a)[95], the first reported method for preparing MXene is to etch bulk Ti_3AlC_2 with hydrofluoric acid (HF). This preparation method requires the cation intercalation to get layered Ti_3AlC_2 into a single layer or a few layers. However, there is often more than a single reaction in the etching process. The etching reaction of Ti_3AlC_2 in HF is expressed as follows[96]:

$$Ti_3AlC_2(s) + 3HF(aq) = AlF_3(a) + Ti_3C_2(s) + \frac{3}{2}H_2(g) \quad (1)$$

$$Ti_3C_2(s) + 2H_2O(aq) = Ti_3C_2(OH)_2(s) + H_2(g) \quad (2)$$

$$Ti_3C_2(s) + 2HF(aq) = Ti_3C_2F_2(s) + H_2(g) \quad (3)$$

Equation (1) is an essential step for the formation of layered Ti_3C_2. Equation (2) and (3) are

reactions that generate the corresponding surface terminals (-OH, -F) on the Ti_3C_2 lamellae, and the actual terminal is most likely a combination of the -OH and -F. In the whole reaction, the solid dense Ti_3AlC_2 is treated by HF, and then the Al atoms are selectively stripped to form a loosely stacked accordion-like $Ti_3C_2T_x$ (Fig. 2 (b)[97] and Fig. 2 (c)[97]). The $Ti_3C_2T_x$ was then dispersed by ultrasound to form single-layer or few-layer MXene. In Fig. 2 (d)[98], after the Al atoms are stripped, the exfoliated Ti_3C_2 layers have two naked Ti atoms per unit formula, and they would be satisfied through suitable ligands. As the experiment was carried out in the aqueous solution, the system is rich in ligands of fluorine ions, -OH and -F[98]. HF etching is a dynamic process. During the etching process, the etching conditions including HF dosage, reaction time, reaction temperature, etc. play roles in affecting the resulting morphology, yield and the proportion of surface terminating groups of $Ti_3C_2T_x$[99-101].

2.1.2. Fluoride-based salt etching

The preparation of Ti_3C_2 by HF etching has been widely used. However, this preparation involves HF, which is itself a colorless, smoky, highly irritating, and highly corrosive liquid. Therefore, researchers have been working to find a gentler and safer etching method to replace HF etching. In 2014, Ghidiu *et al.*[102] for the first time, etched Ti_3AlC_2 with a mixture consisting of LiF and HCl to obtain $Ti_3C_2T_x$ MXene. The resulting MXene has clay-like plasticity after absorbing water, and can be rolled into thin film with a thickness of tens of micron meters. The dried solid powder particles have high electrical conductivity. In addition, Fig. 2 (e&f)[103] shows the morphology of $Ti_3C_2T_x$ obtained after LiF-HCl etching the MAX phase. In the etching process,

the use of a much gentler and environmentally friendly LiF-HCl etching agent to treat MAX facilitates the pre-intercalation of Li^+, which increases the MXene layer spacing and weakens the interlayer interaction[104, 105]. This makes it easier to delaminate MXene during ultrasonic processing to obtain small or single layer MXene flakes. It is important to note that LiF-HCl is one of the most extensive in-situ HF etching agents currently used to synthesize high-quality MXene[106]. Inspired by LiF-HCl etching, more groups of acids and fluoride salts including NaF, KF, NH_4F, etc. are applied. When H_2SO_4 is used instead of HF, the etched $Ti_3C_2T_x$ can still be obtained[102]. The reason is that fluoride salt and acids react to obtain HF. Interestingly, in the aqueous solution of fluoride salt, a large number of cations and H_2O molecules spontaneously intercalate among Ti_3C_2 sheets. Then, MXene having surface modification and larger interlayer spacing is prepared[107, 108].

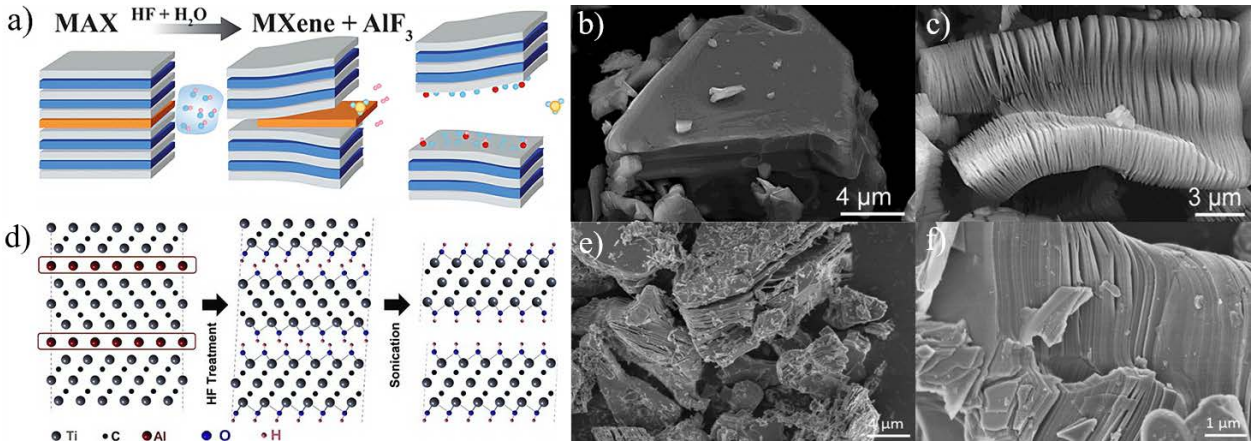

Fig. 2. (a) Illustration of layered Ti_3C_2 MXene synthesized by HF etching[95]. Copyright 2016 American Chemical Society. SEM images of (b) MAX phase before treatment and (c) Ti_3AlC_2 after HF treatment[97]. Copyright 2012 American Chemical Society. (d) illustration of Ti_3AlC_2 exfoliation process [98]. Copyright 2011

WILEY-VCH Verlag GmbH & Co. KGaA, Weinheim. (e) (f) SEM images of Ti_3AlC_2 after LiF-HCl treatment[103]. Copyright 2016 Elsevier B.V. All rights reserved.

2.2. Preparation of conducting polymers

2.2.1. Hard template

In the case of fabricating regular nanostructures, hard template method is a general and resultful method[109]. The course is as follows: (1) penetration or adsorption of monomers to the surface of the template or into the void of the template, (2) in-situ reaction or curing of the dispersed monomers, and (3) removal of the template[110, 111]. Common templates include silica nanomaterials, anodic aluminum oxide (AAO), orbital etching films, and other non-conducting polymers nanomaterials[112-115]. These templates usually appear as a porous cylinder or hollow structure. Therefore, the size of the prepared structure is directly depended on the pore size of the template, and their structure and length are regulated through varying the reaction conditions and monomer concentration[116, 117]. This leads to the possibility of two extreme modes of nanostructured conducting polymers polymerized by the hard template method. One is that at a slow reaction rate and with sufficient monomer supply, the monomers can be slowly diffused into the template for filling, forming nanowires structures[111, 118]. In the other case, due to the interaction between the polymer and the pore wall surface, the monomers rapidly diffuse from the bulk solution to the pore wall and polymerize to form the nanotubes structure under the condition of fast reaction rate and insufficient monomer supply[119, 120]. Fig. 3 (a)[121] presents the preparation of conducting polymer nanostructures using porous membranes, nanofibers and

colloidal particles as hard templates.

Xue *et al*.[122] discovered that PPy nanotubes arrays could be grown inside the AAO template via lowering the template temperature, and prepared the sample using micro-cold wall vapor deposition technology. However, the traditional sacrificial template has some unavoidable disadvantages. For example, in sacrificial templates (such as AAO templates), the structure of the conducting polymers is affected by the morphology and shape of the electrode. Fortunately, in Fig. 3 (b), Park *et al*.[123] prepared PANI nanosheets by employing ice as a movable template[123]. Due to the low energy and orderly suspended -OH groups on the ice surface, the use of ice can effectively limit the growth of polymer films. In addition, the ice template removal process is simple, while ensuring the continuity and integrity of the film[124]. However, it is very difficult to prepare complex nanostructured conducting polymers by hard template method due to the limited types of template structures available. Therefore, it is necessary to choose other preparation methods, such as soft template method.

2.2.2. Soft template

In comparison with the hard template method, soft template method is relatively simple and fits the synthesis of nanostructured conducting polymers in a large scale. The soft template method usually uses colloidal materials, surfactants, and directed structural molecules to fabricate micelles, which direct the growth of conducting polymers in the nanoscale to form nanomaterials in turn[109, 125, 126]. Fig. 3 (c)[121] shows the illustration of the preparation of nanotubes, nanospheres and nanoarrays using micelles, nanowires and monomer droplets as soft templates. The size and

morphology of nanostructures of conducting polymers prepared by soft template method are highly related to the reaction conditions, for example, the nature and concentration of dopant, the concentration of oxidant and monomer, reaction temperature and so on[127-129]. These parameters can be used as a simple means to regulate the molecular structure and size[109, 110]. The most used surfactants have hydrophilic heads and hydrophobic tails (mainly alkyl chains). In a synergistic action between molecules, these surfactants form nanotube structures that act as templates to control the growth of conducting polymers.

Soft templates with tunable structures offer a good opportunity to fabricate complex three-dimensional (3D) nanostructures that are not possible with hard template methods[110]. Ma *et al*.[130] prepared different PANI nanostructures (Fig. 3 (d)[130]). In other words, under room temperature and low acid environment, by changing the type of surfactant, PANI with different structures such as spherical (Fig. 3 (e)[130]), diamond plate-shaped (Fig. 3 (f)[58]), flower-shaped (Fig. 3 (g)[130]), cylindrical (Fig. 3 (h)[130]), block-shaped (Fig. 3 (i)[130]), branch-shaped (Fig. 3 (j)[130]), cloud-shaped, and rose-shaped etc., can be prepared. The complex nanostructures are difficult to be fabricated using hard templates.

Besides, the structures and performances of the conducting polymers are adjusted through changing the soft template materials and reaction conditions. However, the poor stability and the uncontrollable final form of soft templates are challenging. Besides, some soft templates, for instance, tobacco Mosaic virus, DNA and sodium alginate, are dear to produce conducting polymers[110, 131, 132].

2.2.3. Electrochemical polymerization

Electrochemical polymerization is a reliable method to prepare electrode-type conducting polymers, whose thickness and morphology are regulated via deposition rate and charge[133-136]. In the method, the doped conducting polymers are directly grafted onto the electrode surface without the need of additional catalysts[119, 137]. However, conducting polymers synthesized by electrochemical polymerization alone are usually irregular in structure[138]. For obtaining the target morphology, a template needs to be found in the combination with the structure and size of conducting polymers.

Many attempts have been made to get rid of templates. For example, conducting polymers nanowires are electrochemically prepared on bias electrodes in the presence of an aqueous monomer solution[139, 140]. The nature of this method is the combination of electrode-conductor-electrode or electrode-conductor-target[139]. As shown in Fig. 3 (k&l)[138], Chouvy *et al*.[138] used this method to prepare oriented PPy nanowires and found that as the solution contains a low concentration of non-acidic anions and a high concentration of weakly acidic anions, the size of the sample increases. Since electrochemical reaction is a controllable method to prepare conducting polymers and their nanostructures, electrodeposition in the inter-electrode channel has attracted attention in the preparation of molecular devices[138, 139, 141].

2.2.4. Interfacial polymerization

Different from the traditional polymerization in aqueous solution, the interfacial polymerization is carried out in an organic and aqueous immiscible two-phase system, which

initiates the polymerization reaction with fewer nucleation sites[142]. As shown in Fig. 3(m), interfacial polymerization is a templateless method, in which dopant anions and monomer are used at the liquid/liquid interface to facilitate the aggregation of monomer-anions. It can synthesize conducting polymers films with high specific surface area or electrochemical properties[142, 143]. At the interface, conducting polymers form and rapidly diffuse into the aqueous phase, allowing the interface to react further. The polymerization rate is affected through the concentration of monomer and oxidant, and the types of nanostructures obtained depend on organic solvent, acid dopant, reaction time and other factors[144]. For instance, the length of PANI nanofibers increases as the acid strength increases[110, 142]. The interfacial polymerization method displays many advantages: (1) synthesis and purification processes are carried out without any templates, (2) this method has high yield and is easy to be expanded and repeated, and (3) the obtained product is easily dispersed in aqueous phase, facilitating biological applications and environmentally friendly processes in environment[110, 142, 145].

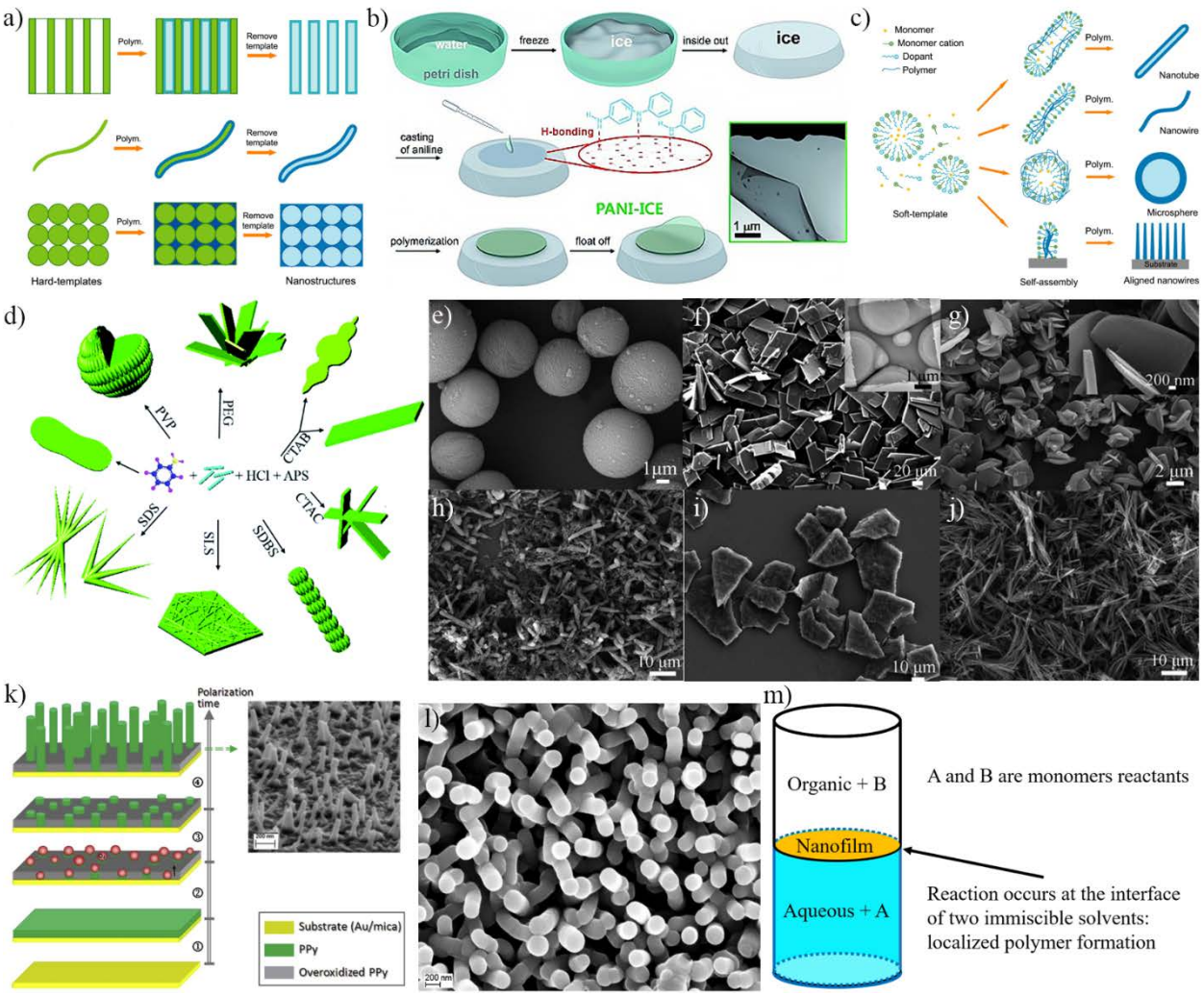

Fig. 3 (a) Illustration of the preparation of conducting polymer nanostructures using porous membranes, nanofibers and colloidal particles as hard templates[121]. (b) The preparation processes of 2D PANI nanosheets on ice surfaces (Inset: the transmission map of the complete 2D nanosheet)[123]. Copyright 2015 WILEY-VCH Verlag GmbH & Co. KGaA, Weinheim. (c) Illustration of the preparation of nanotubes, nanospheres and nanoarrays using micelles, nanowires and monomer droplets as soft templates[121]. (d) Schematic diagram of PANI preparation with different structures[130]. SEM images of PANI with different structures, such as (e) spherical[130], (f) diamond plate-shaped[130], (g) flower-shaped[130], (h) cylindrical[130], (i) block-shaped[130] and (j) dendritic-shaped[130]. Copyright Royal Society of Chemistry. (k) Schematic diagram of the

preparation of PPy nanowires by electrochemical polymerization (Inset: SEM image of PPy nanowires)[138]. (l) SEM image of PPy nanowire from the top view[138]. Copyright 2018 Elsevier Ltd. (m) Schematic of an interfacial polymerization reaction.

2.3. Preparation of MXene/conducting polymers composites

As a high-performance electrode material, MXene has shown great application prospects in the field of SCs[46, 146]. However, similar to other 2D materials, thin films made of MXene are prone to re-stacking, thereby reducing ion transport inside the electrode, which seriously affects the specific capacitance and rate capability of the independent electrode[147, 148]. To overcome this problem, many researches have been focused on designing the MXene electrode structure and improving its ion transport properties. These include the preparation of microporous and hydrogel $Ti_3C_2T_x$ thin films, and the design of mixed electrodes of $Ti_3C_2T_x$ and carbon nanomaterials[149-151]. Although some of these strategies can effectively improve the ion transport and high-speed electrochemical performance of the electrode, they will reduce the electrode density, resulting in a decrease in the electrode volume capacitance, rate capability, and energy density[152-154]. In recent years, studies have shown that depositing conducting polymers (such as PANI, PPy and PEDOT) on the surface of MXene sheets can promote the electrochemical properties of independent MXene electrodes[155-158].

2.3.1. Preparation of MXene/PANI composites

Xu *et al*.[159] came up with a new strategy for producing MXene/PANI composites by chemically oxidizing polymerizing aniline monomers on $Ti_3C_2T_x$ MXene nanosheets under acidic

conditions. The surface of MXene nanosheets is rich in -O, -F, -OH functional groups, which can provide nucleation sites for the deposition of aniline on the surface of MXene[160]. With the continuous dripping of ammonium persulfate (APS), the aniline monomer began to continuously polymerize on the functional groups on the surface of MXene. Finally, irregular porous PANI was formed on the MXene nanosheets to provide channels for the transport of electrolyte ions. With more ion transport channels, the electron transfer efficiency and electrochemical activity of the MXene/PANI composite have also been improved. In addition, Zhao *et al.*[161] used the method of in situ polymerization at low temperature to reasonably modify PANI nanoparticles on the surface or between MXene nanosheets, as shown in Fig. 4 (a)[161]. One can see from Fig. 4 (b)[161] that PANI nanoparticles in the MXene/PANI composite are relatively regular and distributed relatively uniformly. This method effectively reduced the damage to MXene nanosheets and ensured the polymerization quality of PANI as much as possible[162, 163].

Beidaghi *et al*.[155] reported a method for preparing MXene/PANI composites by oxidant-free polymerization, which uses aniline monomers to synthesize MXene/PANI composites on the periphery of MXene nanosheets through in-situ polymerization without adding additional oxidants，as shown in Fig. 4 (c)[155]. The amount of polymer deposition on the periphery of MXene nanosheets is a key parameter affecting the electrochemical performance of the electrodes. The cross-sectional SEM image (Fig. 4 (d)[155]) shows that MXene and PANI nanoparticles are closely combined to form a dense interlayer structure with pores. Under the premise of not reducing the electrochemical performance, the MXene/PANI composite electrode prepared when

the quality of the PANI deposited on the surface of the MXene layer is minimized shows 503 F g^{-1} mass capacitance and 1682.3 F cm^{-3} volume capacitance (1682.3 F cm^{-3}). The composite method can effectively control the amount of PANI so that the electrode has a higher ion transport capacity, improves the electrochemical performance of the electrode, and has excellent cycle performance (the capacitance retention rate after 10000 cycles is 98.3%). Compared with the original $Ti_3C_2T_x$ electrode previously reported, this method can prepare high-quality load or high-thickness MXene/PANI electrode without affecting the electrochemical performance.

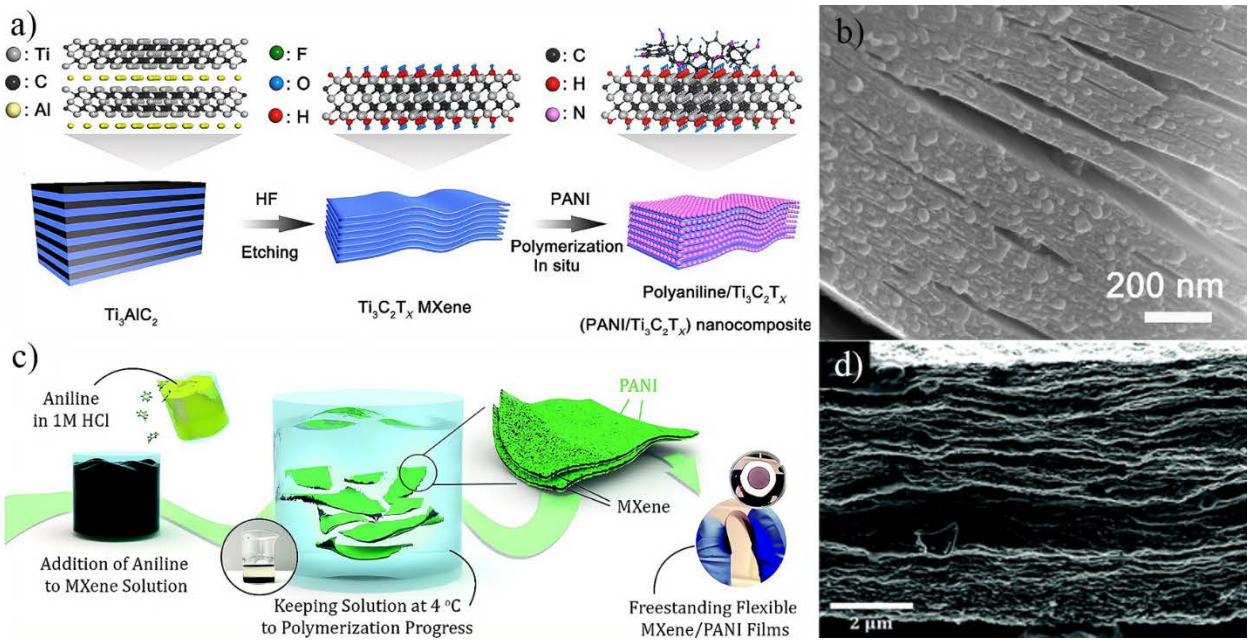

Fig. 4 (a) Diagram of preparation of PANI/$Ti_3C_2T_x$ by in situ polymerization at low temperature[161]. (b) SEM image of MXene/PANI composites[161]. Copyright 2019 The Authors. (c) Diagram of preparation of PANI/MXene by oxidant-free polymerization[155]. (d) Cross-sectional SEM image of MXene/PANI films[155]. Copyright Royal Society of Chemistry.

2.3.2. Preparation of MXene/PPy composites

As shown in the mechanism diagram of Fig. 5 (a)[164], Jian *et al.*[164] used a one-step co-electrodeposition route for preparing MXene/PPy composite films on ITO glass. With MXene nanosheets as the core of polymerization, pyrrole monomers gradually polymerize on the surface or between the MXene nanosheets to obtain a 3D carambola-like MXene/PPy composite film, as shown in Fig. 5 (b)[164]. The introduction of PPy with pseudo-capacitance characteristics can produce a higher capacitance than pure MXene. At the same time, due to the introduction of $Ti_3C_2T_x$, the expansion problem of PPy during charging and discharging is alleviated[165, 166]. It is worth noting that PPy intercalates the $Ti_3C_2T_x$ nanosheets, increasing the interlayer spacing of $Ti_3C_2T_x$ and further improving electrochemical performance of the material. Besides, Zhang *et al*.[167] fabricated Ti_3C_2/PPy film via HCl-LiF in-situ etching, electrophoretic deposition and electrochemical polymerization (Fig. 5 (c)[167]). From the comparison of Fig. 5 (d&e)[167], it can be clearly seen that the cross-sections of the PPy film and the Ti_3C_2/PPy film are significantly different. Under the condition of 1 mA cm^{-2}, affected by the synergistic effect of Ti_3C_2 and PPy, the planar SCs prepared by Ti_3C_2/PPy composite films showed 109.4 mF cm^{-2} and 86.7 mF cm^{-2} area capacitance in 2 M H_2SO_4 solution and PVA/H_2SO_4 solid electrolyte, respectively.

Wu *et al*.[168] prepared PPy/Ti_3C_2 MXene heterostructure nanocomposites by one-step in situ polymerization, as shown in Fig. 5 (f)[168]. In the introduction of uniformly dispersed Ti_3C_2 nanosheet suspension, the pyrrole monomer was in situ polymerized to generate PPy nanospheres on the periphery of the MXene sheet layers to generate a PPy/Ti_3C_2 MXene heterostructure nanocomposite material. As can be seen in Fig. 5 (g)[168], PPy and Ti_3C_2 form a heterogeneous

composite material with a regular particle size and a uniform distribution. The heterogeneous structure of PPy/Ti_3C_2 MXene composites provides many active sites for charge or ion transfer, accelerates the rapid accessibility and penetration of ions in the electrolyte, and reduces the inherent resistance and charge transfer resistance[169, 170], improving the electrochemical properties significantly.

In addition, MXene nanosheets exhibit good hydrophilicity because of the -F, -O, -OH groups of the surface. These functional groups provide more nucleophilic reaction sites for polymerizing pyrrole monomers[171]. MXene nanosheets and PPy framework are tightly combined through beneficial π-π conjugation and electrostatic force. The effective combination of the Ti_3C_2 ultra-flake layers and the PPy nanospheres can prevent the spontaneous agglomeration and accumulation of the Ti_3C_2 layers[168].

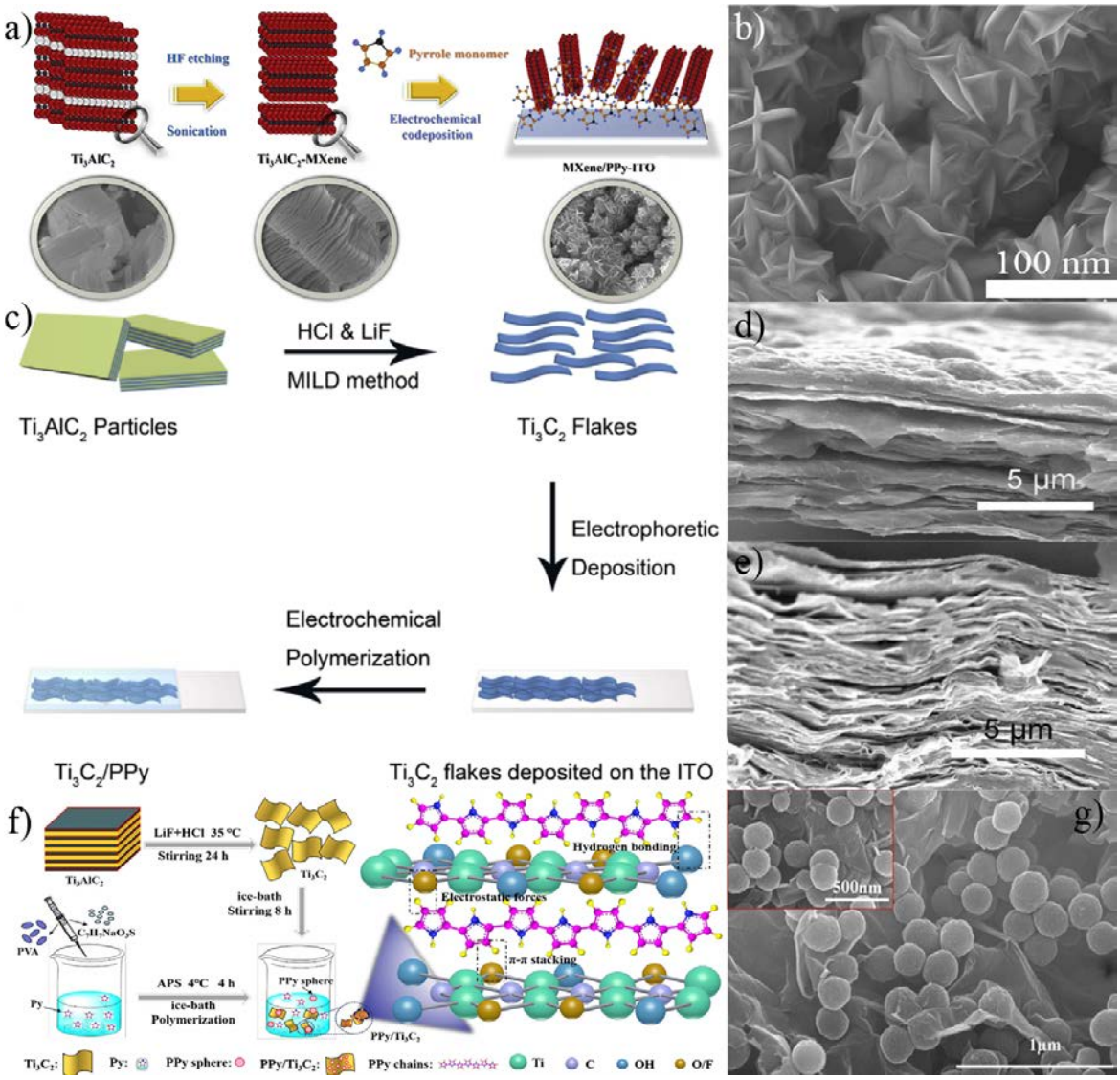

Fig. 5 (a) The mechanism diagram of MXene/PPy composite preparation. Inset: SEM images of Ti_3AlC_2, Ti_3AlC_2-MXene and MXene/PPy[164]. (b) SEM image of 3D starfruit-like MXene/PPy composite[164]. Copyright 2019 Elsevier Ltd. (c) Flow chart of preparation of $Ti_3C_2T_x$/PPy composite membrane by electrochemical polymerization[167]. SEM image of the hybrid $Ti_3C_2T_x$/PPy membrane (d)[167] and the pure $Ti_3C_2T_x$ film (e)[167]. Copyright 2019 Elsevier Ltd. (f) Synthetic schematic diagram of PPy/Ti_3C_2 nanocomposite[168]. (g) SEM image of PPy/Ti_3C_2 composite[168]. Copyright 2020 Elsevier B.V.

2.3.3. Preparation of MXene/PEDOT composites

Zhu *et al*.[172] prepared a flexible MXene/PEDOT: poly(styrenesulfonate) (PEDOT: PSS) film using the vacuum assisted filtration method, as shown in Fig. 6 (a)[172]. In this method, the prepared MXene solution is mixed with the PEDOT: PSS dispersion in proportion, and the MXene/PEDOT: PSS composite film (Fig. 6 (b) [172]) is obtained by vacuum filtration. For improving the conductivity of the composite film, MXene/PEDOT: PSS composite film is treated with H_2SO_4 to get rid of the non-conducting PSS, and a flexible and independent high-performance MXene/PEDOT composite film (Fig. 6 (c)[172]) is obtained. From the comparison of the two cross-sectional SEM images, it can be seen that the regularity of the composite membrane after treatment with concentrated H_2SO_4 is better, which also leads to an improvement in its performance. As shown in Fig. 6 (d)[172], it can be seen from the stress-strain curve that after adding a handful of PEDOT: PSS and H_2SO_4, the tensile strength of the film is significantly improved. In addition, compared with pure MXene film and other MXene/polymer composite films, the MXene/PEDOT: PSS composite film greatly enhances the mechanical performance and maintains good electrical conductivity[173-175]. This method provides ideas to prepare lightweight, flexible, and high-performance MXene/PEDOT composites with high mechanical strength.

Chen *et al*.[176] prepared 1,5-naphthalenedisulfonic acid doped MXene/PEDOT (MPT) composites by in-situ chemical oxidation. NP-MPT and NA-MPT composites were prepared by co-doping with phosphomolybdic acid and anthraquinone-2-sulfonate. Among them, NA-MPT shows a good layered composite structure, with a large voltage window as high as 1.8 V and a

specific capacitance of 323 F g^{-1}. The latter value is more than twice that of pure PEDOT and pure MXene, as shown in Fig. 6 (e)[176]. This co-doping method can be used for reference in other MXene/polymer composite applications[21, 177].

In addition, Gogotsi *et al*.[178] imitated the preparation of MXene/PPy composites by in-situ polymerization without oxidants to prepare MXene/PEDOT composites, as shown in Fig. 6 (f)[178]. Compared with conventional PEDOT polymerization, although the degree of oxidation of EDOT is not high enough, it is sufficient to achieve the conditions for PEDOT to complete doping polymerization in MXene[179, 180]. This method does not need any oxidizing agent. It only needs to simply mix the etched $Ti_3C_2T_x$ MXene solution and the EDOT aqueous solution to realize the polymerization of EDOT on the periphery of the MXene sheets[181, 182]. In comparation with MXene and pure PEDOT, composite material has good cycle stability and rate performance. The effective combination of $Ti_3C_2T_x$ and PEDOT improves the ion and charge storage capacity[183-186].

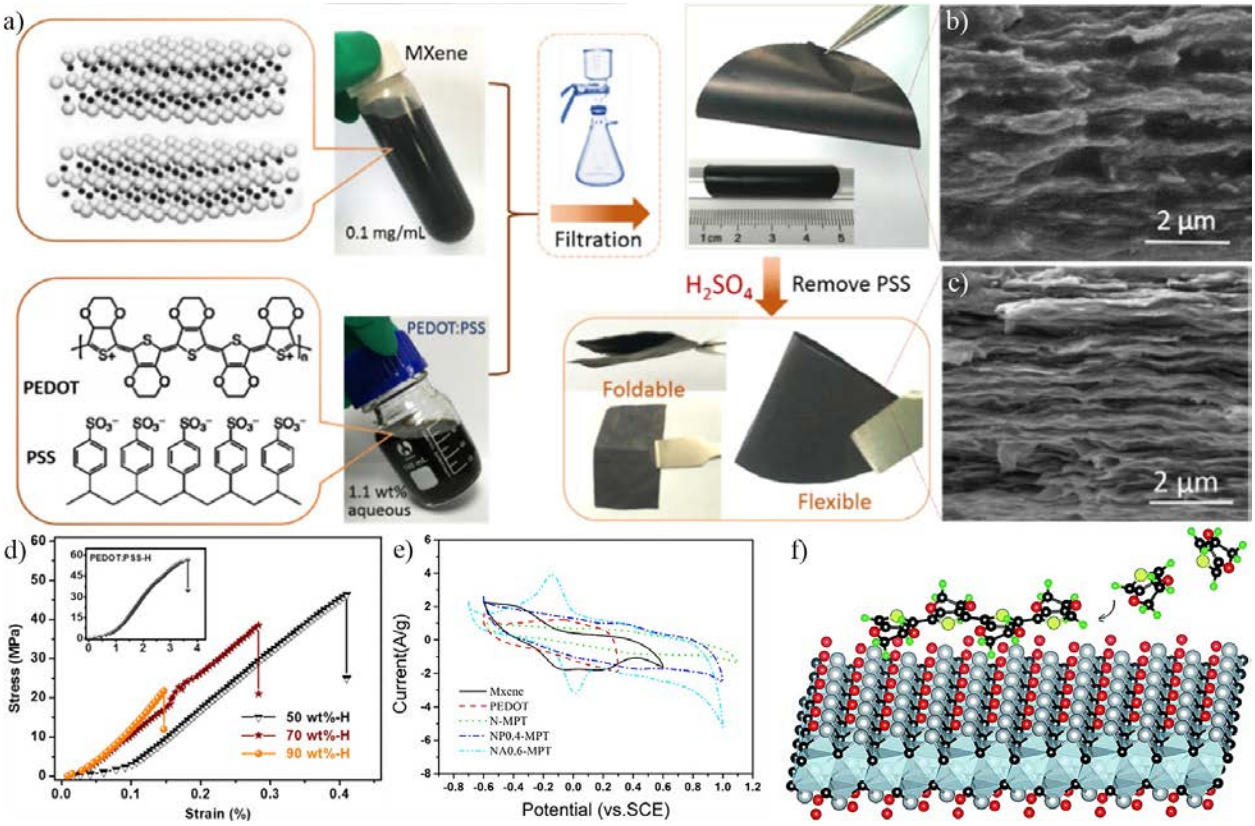

Fig. 6 (a) Flow chart of preparing MXene /PEDOT: PSS composite membrane by vacuum assisted filtration method[172]. SEM image of MXene/PEDOT: PSS composite membrane (b)[172] and MXene/PEDOT composite membrane treated with concentrated H_2SO_4 (c)[172]. (d) Stress-strain curves of MXene /PEDOT: PSS composite films with different mass ratios[172]. Copyright 2020 Elsevier Ltd. (e) CV curves of obtained samples at 10 mV s^{-1} [176]. Copyright 2018 Elsevier B.V. (f) Illustration of polymerizing EDOT on the surface of MXene[178]. Copyright Royal Society of Chemistry.

3. Electrode based on MXene/conducting polymers

The performance of SCs is affected by many factors, such as electrode material[187, 188], the choice of electrolyte[189], and the size of potential window[190, 191], among which the electrode material is a key factor affecting the performance of the capacitor[192, 193]. Therefore,

a lot of efforts have been invested in the research and development of reasonable structure design for electrode materials to promote the effective electron transmission and ion diffusion of SCs[191, 194]. Advanced electrode materials must have the characteristics of temperature stability, high conductivity, high specific surface area, good chemical stability, corrosion resistance, etc., and must be green and environmentally friendly and low in cost[92, 195, 196]. At present, the most researched electrode materials mainly include carbon-based materials[197], conducting polymers[198-200], and transition metal oxides[201, 202]. This article will focus on the MXene/conducting polymers composites electrode and its application in SCs.

3.1. MXene-based electrodes

Since its introduction in 2011, MXene has been widely used in a variety of studies, and new types of MXene have been continuously confirmed. So far, more than half of MXene research focuses on $Ti_3C_2T_x$ MXene, owing to the superior 6000-10000 S cm^{-1} electrical conductivity and mechanical stability[203-205]. Yan *et al*.[152] prepared a stand-alone and binderless MXene film electrode with excellent volume performance by vacuum assisted filtration and assembly of stand-alone membrane technology. This MXene film electrode is based on its ultra-high density and excellent pseudo-capacitance energy storage mechanism, showing 1222 F cm^{-3} volume capacitance[152]. However, this case has significant limitations and can only be achieved at low scan rates. The volumetric capacitance of MXene film will be degraded seriously under high scanning rate or rapid charge and discharge conditions[66, 206, 207]. Li *et al*.[208] prepared a flexible suspended $Ti_3C_2T_x$ MXene film with a wave structure (Fig. 7 (a)[208]) using a mechanical

compression method. The wavy structure reduces the problem of self-stacking to a certain extent. At the same time, the wavy structure provides a stable channel for the rapid and effective transfer of ions/charges. The compact structure of $Ti_3C_2T_x$ MXene film electrode provides an ultra-high-volume capacitance of 1277 F cm^{-3} at 10 mV s^{-1} in 3 M H_2SO_4; even at 5000 mV s^{-1}, it still has a capacity of 790 F cm^{-3}, as shown in Fig. 7 (b)[208].

Fan *et al*.[209] were inspired by porous graphene film electrodes and processed 3D MXene aerogels into dense porous MXene films by mechanical pressing, as shown in Fig. 7 (c)[209]. From the across-sectional scan of Fig. 7 (d)-(f)[209], it can be seen that when the mechanical pressure increases, the structure of the MXene film becomes denser and the sample layer arrangement becomes more regular, which is more conducive to improving the volumetric capacitance. According to the reports, at 500 mV s^{-1}, the MXene film obtained at a mechanical pressure of 40 MPa still has a volume capacitance of 462 F cm^{-3}, while the value of the traditional MXene film is reduced to 395 F cm^{-3} [209]. The folded structure of MXene nanosheets are combined to form a tightly connected pore structure, which greatly increases the accessibility of electrolyte ions to active sites, thereby improving transport efficiency and the subsequent electrochemical storage capacity, as shown in Fig. 7 (g)[209].

In addition, this dense MXene film having a folded morphology is independent and adhesive-free, which is applied directly as the working electrode. Compared with the traditional MXene film prepared by vacuum-assisted filtration, its rate performance and volume capacitance are greatly improved, and it is more suitable for mass production[209]. However, it should be pointed out that

due to the abundant pore structure, the density and conductivity of the prepared film are not as good as the traditional MXene film, which also leads to a volume capacitance of only 932 F cm^{-3} at low scan rates[155]. MXene has natural advantages for SCs, but the application of independent membranes is very limited due to the performance problems[210].

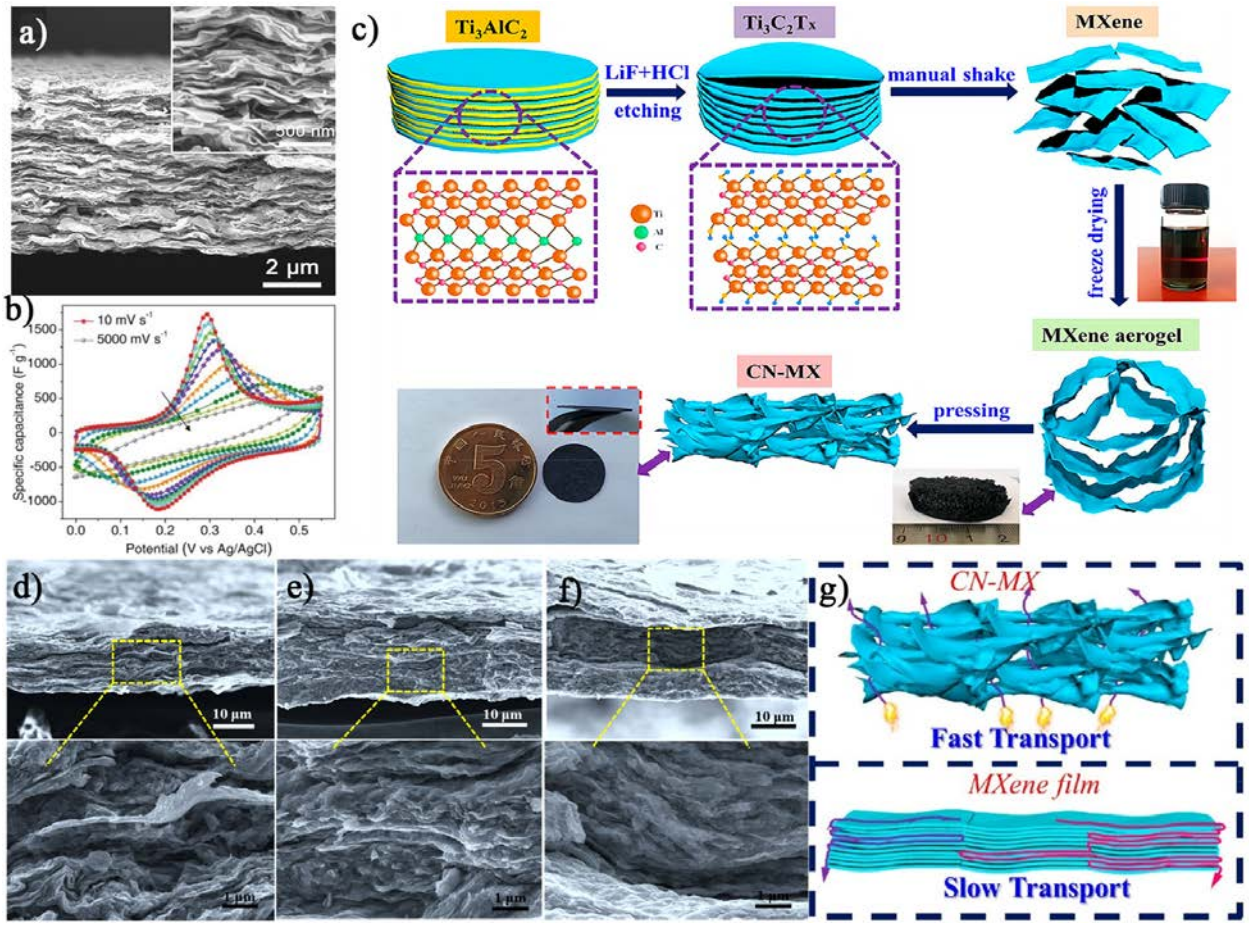

Fig. 7 (a) SEM image of wavy MXene[208]. (b) CV curve of $Ti_3C_2T_x$ MXene film electrode tested in the range of 10 to 5000 mV s^{-1}[208]. Copyright 2020 Elsevier Ltd. (c) Schematic diagram of the preparation process of MXene film[209]. SEM images of cross sections of films prepared under different mechanical pressures: (d) CN-MX_{20}[209], (e) CN-MX_{40}[209], and (f) CN-MX_{50}[209]. (g) Schematic diagram of ion diffusion of CN-MX and MXene films[209]. Copyright 2020 American Chemical Society.

3.2. MXene-conducting polymers binary composite electrodes

3.2.1. MXene/PANI composite electrodes

Wu *et al*.[211] successfully prepared organ-like amino-Ti_3C_2 (N-Ti_3C_2)/PANI composites by applying a two-step electrochemical route. In Fig. 8 (a)[211], N-Ti_3C_2 is first deposited or coated on the FTO-glass substrate through an electrochemical reaction. Then the ordered structure of Ti_3C_2 MXene was used as the carrier, under the action of constant voltage, the PANI chain was connected to the FTO-glass substrate through electrochemical polymerization. From the SEM image of Fig. 8 (b)[211] and EDS spectrum of Fig. 8 (c)-(e)[211], it can be seen that N-Ti_3C_2 and PANI are effectively combined. Fig. 8 (f)[211] shows the special binding method between N-Ti_3C_2 and PANI, which is different from the general TI_3C_2 binding directly to PANI. The amine nitrogen on the PANI chain and the amino group carried by N-Ti_3C_2 are tightly combined through chemical bonds, which increase the spacing and accessible surface area of Ti_3C_2 MXenes, effectively preventing the self-stacking of MXene sheets.

In addition, the organ-like N-Ti_3C_2/PANI composites formed by covalent grafting can also provide a precise and fast channel to transfer charges and ions, and make the charge transfer rate of the composites more rapidly. The special structure and special bonding method make N-Ti_3C_2/PANI have good electrochemical performance. Among them, in the 0.5 M H_2SO_4 electrolyte solution, at 5 mV s^{-1}, the N-Ti_3C_2/PANI shows the best performance with a maximum surface capacitance of 228 mF g^{-1}, which is 32 times higher than that of the original Ti_3C_2 film, as shown in Fig. 8 (g)[211]. In addition, the N-Ti_3C_2/PANI composite electrode shows 85% capacitance

retention rate after 1000 cycles.

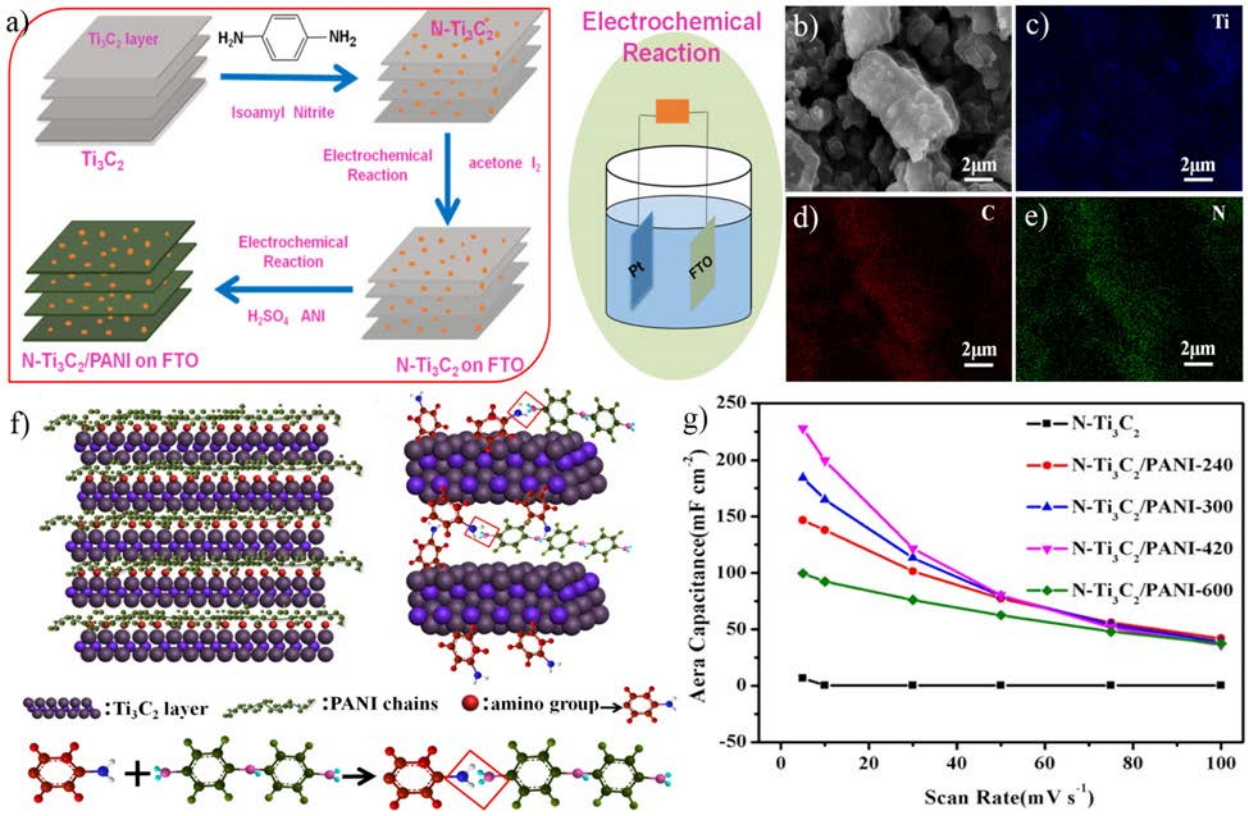

Fig. 8 (a) Schematic diagram for the preparation of N-Ti_3C_2/PANI[211]. (b) SEM image of N-Ti_3C_2/PANI[211]. EDS spectrum[211]: (c) Ti, (d) C, and (e) N. (f) Atomic schematic diagram of PANI intercalation N-Ti_3C_2[211]. (g) The specific capacitance of pure N-Ti_3C_2 and N-Ti_3C_2/PANI electrodes from 5-100 mV s^{-1}[211]. Copyright 2019 Elsevier B.V.

Li *et al.*[212] fabricated MXene/PANI material covered with PANI chains via the hydrothermal method. MXene serves as the supporting framework, while PANI serves to link adjacent MXene layers. In the prepared composites, MXene can improve flexibility and form a 3D network structure. The introduction of PANI expands the MXene interlayer spacing and accelerates the transfer of ions and charges[213]. In the 6 M KOH solution, the MXene/PANI

composite electrode displays a mass specific capacitance of 563 F g^{-1} at 0.5 A g^{-1}, which is almost 2.3 times than that of pure MXene (Fig. 9 (a&b)[212]). In addition, at 5 A g^{-1}, the capacitance retention rate after 10000 cycles is as high as 95.15%.

Chen *et al*.[214] used simple chemical oxidation polymerization method to study a new type of MXene/PANI composite as a synthesis method for high-performance SCs electrode, as shown in Fig. 9 (c)[214]. In this method, the dopant DL-tartaric acid (DLTA) is added to the $Ti_3C_2T_x$ MXene solution and mixed uniformly, and the supramolecular self-assembly technology is used to assemble DLTA on the periphery of MXene. Then, in the supramolecular self-assembly process, rich electronegative oxygen-containing functional groups result in the aniline monomers to conduct the ordered mechanism polymerization, thus obtaining the $Ti_3C_2T_x$ MXene-DLTA/PANI (TDP) self-assembly composites with satisfactory microstructure (Fig. 9 (d))[214].

The realization of supramolecular self-assembly mainly relies on the chiral interaction of MXene, and the flexible spatial distribution of DLTA with abundant negatively charged oxygen-containing functional groups (-OH, -COOH). As can be seen from Fig. 9 (e)[214], in 1 M H_2SO_4 electrolyte solution, the TDP electrode material prepared with a mass ratio of MXene and aniline of 2:8 exhibits a specific capacitance of 452 F g^{-1} at 1 A g^{-1}, much higher than that of MXene (61 F g^{-1}) and PANI (263 F g^{-1}). In addition, the TDP electrode also has a voltage window of up to 1.9 V. At 4 A g^{-1}, and it still has a capacitance retention rate of 61% after 2000 cycles, as shown in Fig. 9 (f)[214]).

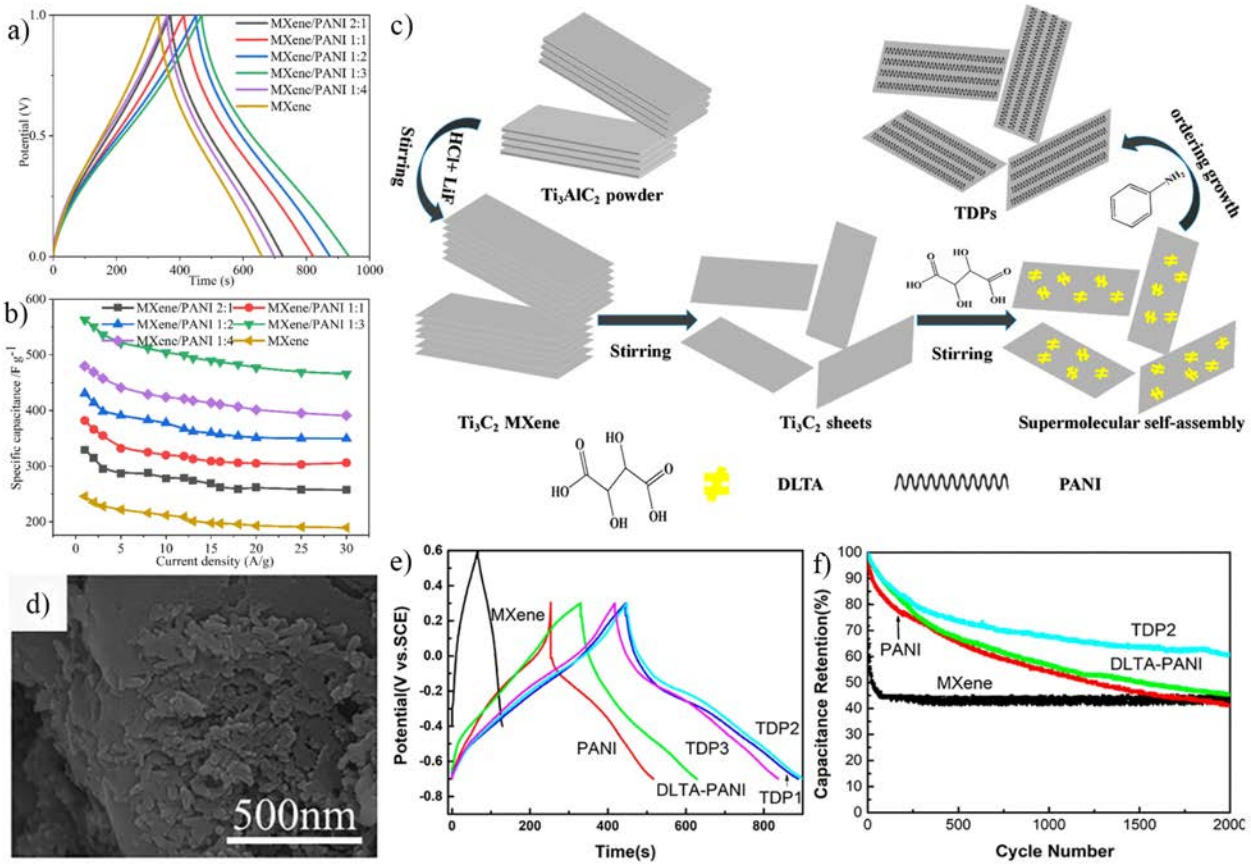

Fig. 9 (a) GCD curves and (b) specific capacitance of pure MXene and MXene/PANI electrodes with different mass ratios at 0.5 A g^{-1}[212]. Copyright 2020 Elsevier B.V. (c) Schematic diagram of the preparation procedure of TDPs[214]. (d) SEM image of TDP2. (e) GCD curves at 1 A g^{-1} and (f) cyclic curves at 4 A g^{-1} of MXene, PANI, DLTA-PANI and TDPs [214]. Copyright 2020 American Chemical Society.

3.2.2. MXene/PPy composite electrodes

Wu *et al.*[215] prepared organ-like $Ti_3C_2T_x$/PPy nanocomposites by low-temperature chemical oxidation, that is, pyrrole monomer was polymerized in situ on $Ti_3C_2T_x$ nanosheets at low-temperature to form clear and uniformly dispersed PPy nanoparticles, as shown in Fig. 10 (a)[215] and Fig. 10 (b)[215]. As a polymeric skeleton, $Ti_3C_2T_x$ nanosheets limited the growth of PPy, effectively prevented the self-stacking of PPy, and promoted the structural stability of

$Ti_3C_2T_x$/PPy composites. The composite material prepared by this method mainly relies on the hydrogen bond and electrostatic force combination between $Ti_3C_2T_x$ nanosheets and PPy chains. In addition, the intercalation effect of homogeneous PPy nanoparticles expanded the interlayer spacing of $Ti_3C_2T_x$ nanosheets. At the same time, the highly oriented polymer molecular chains provide more channels for charge transfer and electrolyte ion diffusion, thus increasing the specific capacitance and reducing the charge transfer resistance. It is worth noting that in Fig. 10 (c)[215], $Ti_3C_2T_x$/PPy composite electrode with the best ratio shows a specific capacitance of 184.36 F g^{-1} at 2 mV s^{-1}, 37% higher than that of the pure $Ti_3C_2T_x$ MXene electrode (133.91 F g^{-1}). At 1 A g^{-1}, the capacitance of the $Ti_3C_2T_x$/PPy composite electrode remains 83.33% after 4000 charge-discharge cycles (Fig. 10 (d)[215]). The improvement of material electrochemical performance and cycle stability is attributed to the synergy between $Ti_3C_2T_x$ nanosheets and PPy nanoparticles and different energy storage mechanisms. Most importantly, it exhibits a low-cost and convenient route to prepare $Ti_3C_2T_x$/PPy composites in large-scale.

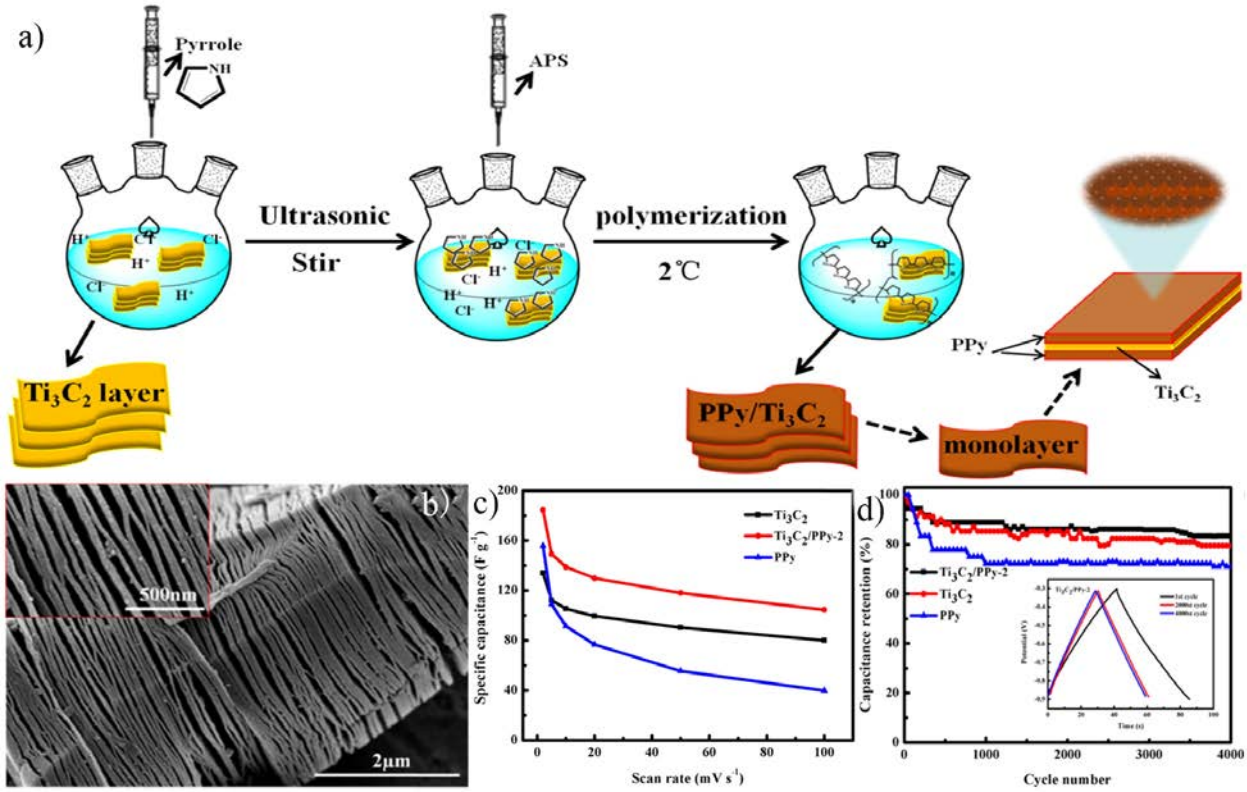

Fig. 10 (a) Schematic illustration of preparing $Ti_3C_2T_x$/PPy composites through low-temperature in-situ polymerization of PPy on Ti_3C_2 nanosheets[215]. (b) SEM image of $Ti_3C_2T_x$/PPy. (Inset of a partially enlarged view)[215]. (c) The specific capacitance of PPy, Ti_3C_2, and Ti_3C_2/PPy at different scanning rates[215]. (d) Cycle curves of PPy, Ti_3C_2, and Ti_3C_2/PPy at 1 A g^{-1}[215]. Copyright 2019 Elsevier Ltd and Techna Group S.r.l.

Tong *et al*.[216] successfully prepared an independent $Ti_3C_2T_x$/PPy composite film electrode by electrochemically depositing PPy on the $Ti_3C_2T_x$ film prepared through the vacuum assisted filtration method (Fig. 11 (a)[216]). The $Ti_3C_2T_x$/PPy composite film has a special structure, in which PPy is formed on the periphery of the $Ti_3C_2T_x$ film and inserted into the gap between the $Ti_3C_2T_x$ nanosheet layers, as shown in Fig. 11 (b)-(e)[216]. This special structure results in an effective strong binding between $Ti_3C_2T_x$ and PPy. The good combination between $Ti_3C_2T_x$ and

PPy increases the tensile strength of $Ti_3C_2T_x$/PPy film (48.2 MPa), which is much higher than that of the original $Ti_3C_2T_x$ electrode (9.9 MPa). More importantly, due to this special structure and the cooperation effect of different parts, the optimal $Ti_3C_2T_x$/PPy film electrode shows a specific capacitance of 420.2 F g^{-1} at 1 A g^{-1}, much higher than that of Ti_3C_2 and PPy (Fig. 11 (f&g)[216]). In addition, even at 20 A g^{-1}, after 10000 cycles, the capacitance retention rate of the $Ti_3C_2T_x$/PPy film electrode still reached 86%, showing good electrochemical stability, indicating that $Ti_3C_2T_x$/PPy film can be as SCs electrode.

Lee et al.[217] used in-situ synthesis to prepare 3D $Ti_3C_2T_x$@PPy nanocomposites. The multilayer MXene nanosheet structure is wound in a 3D PPy nanowire matrix to form a MXene/PPy composite with an ideal 3D interconnected porous structure and high conductivity, as shown in Fig. 11 (h)-(j)[217]. The special structure formed by the entanglement of MXene and PPy ensures the rapid diffusion of electrolyte ions and a short and continuous charge transfer path, which maximizes the utilization of active materials. In addition, the porous interconnected 3D network connects the MXene sheets while preventing them from self-stacking. As can be seen from Fig. 11 (k&l)[217], at 0.5 A g^{-1}, 3D $Ti_3C_2T_x$@PPy displays a specific capacitance of 610 F g^{-1}, while the previously reported $Ti_3C_2T_x$@PPy and pure $Ti_3C_2T_x$ MXene separately exhibit 298 F g^{-1} and 138 F g^{-1}. 3D $Ti_3C_2T_x$@PPy has more than doubled the specific capacitance than the previously reported $Ti_3C_2T_x$@PPy. Significantly, at 4 A g^{-1}, after 14000 cycles, 3D $Ti_3C_2T_x$@PPy electrode maintains almost 100% stability, better than those of other advanced MXene-based SCs.

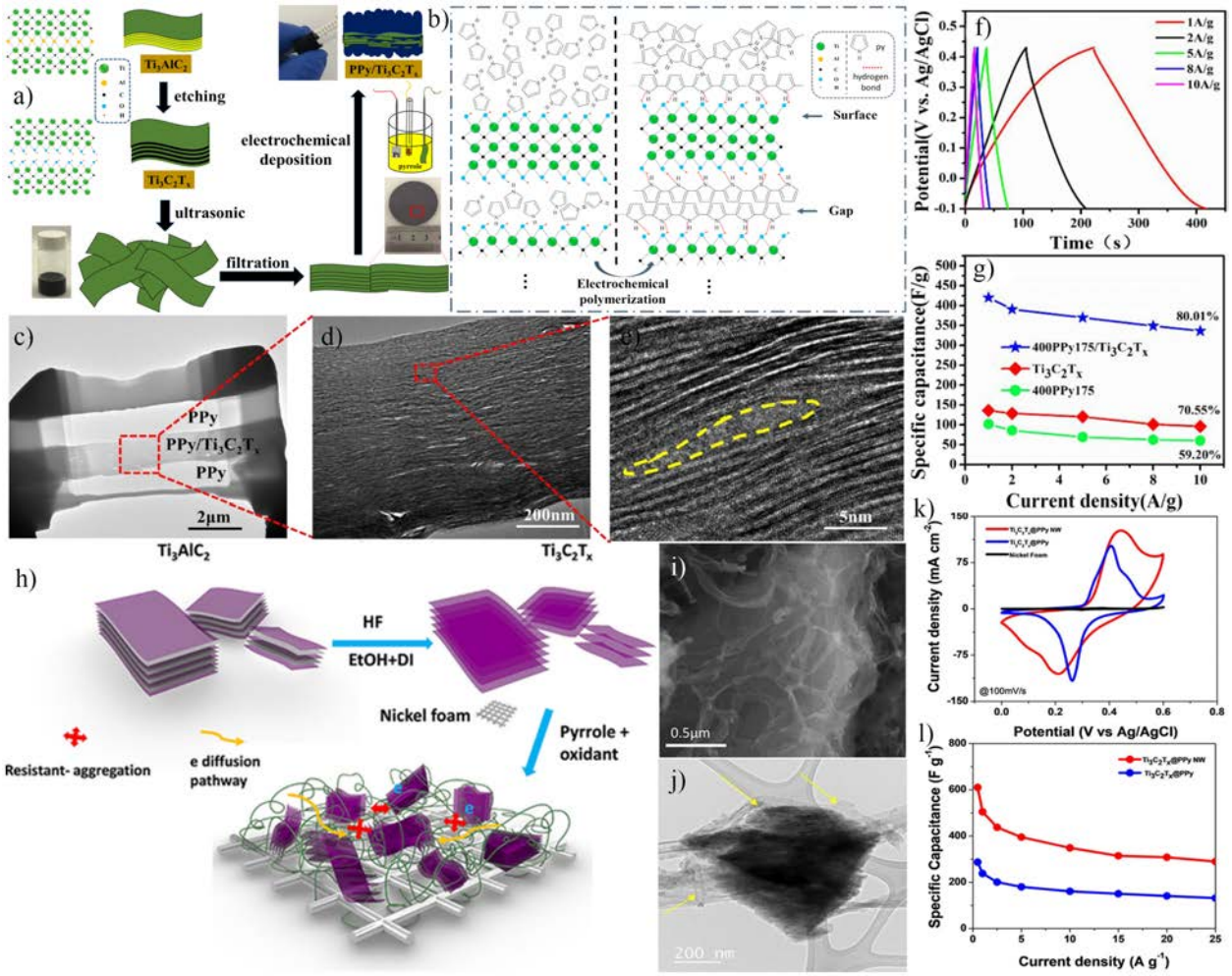

Fig. 11 (a) Flow chart for preparing $PPy/Ti_3C_2T_x$ by electrodeposition of PPy on $Ti_3C_2T_x$ thin film[216]. (b) Schematic illustration of electrochemical polymerization of PPy on the surface and gap of Ti_3AlC_2 film[216]. (c)-(e) TEM images of $PPy/Ti_3C_2T_x$ with different scales[216]. (f) GCD curves of $PPy/Ti_3C_2T_x$ electrode at various current densities[216]. (g) The specific capacitance of $PPy/Ti_3C_2T_x$, pure $Ti_3C_2T_x$, and PPy electrode at different current densities[216]. Copyright 2020 Elsevier B.V. (h) Schematic illustration of 3D $Ti_3C_2T_x$@PPy nanowire preparation[217]. SEM image (i) and TEM image (j) of 3D $Ti_3C_2T_x$@PPy nanowire[217]. (k) CV curves of different electrodes[217]. (l) The specific capacitance of $PPy/Ti_3C_2T_x$ nanowire and $PPy/Ti_3C_2T_x$ electrode at different current densities[217]. Copyright 2019 Wiley-VCH Verlag GmbH & Co. KGaA,

Weinheim.

3.2.3. MXene/PEDOT composite electrodes

Tao *et al*.[218] proposed a preparation way of vacant $Mo_{1.33}C$ MXene. This vacant MXene film has a high-volume capacitance of 1153 F cm^{-3} and a high conductivity of 29674 S m^{-1}. Based on the vacant $Mo_{1.33}C$ MXene, Qin *et al.*[219] prepared $Mo_{1.33}C$ MXene/PEDOT: PSS film by simple hydrothermal method and vacuum assisted filtration method. For further optimizing the electrochemical properties, the $Mo_{1.33}C$ MXene/PEDOT: PSS film was soaked in concentrated H_2SO_4 for 24 h to remove the non-conducting PSS (Fig. 12 (a)[219]). Comparing Fig. 12 (b)[219] and Fig. 12 (c)[219], it is easy to see the difference between the MXene/PEDOT: PSS film before and after immersion in concentrated H_2SO_4. The MXene/PEDOT film after soaking the non-conductive PSS has a more obvious layered structure, which is beneficial to ion transport.

In addition, the resistivity of the composite film is greatly reduced, and the capacitance value is also increased (the maximum volume capacitance reaches 1310 F cm^{-3}) after the concentrated H_2SO_4 treatment. The conductive PEDOT intercalation expands the interlayer spacing of the MXene sheets, and meanwhile, the oriented PEDOT nanofibers fabricate a network structure between the MXene sheets, providing a fast channel for ion transmission and realizing a fast and reversible redox reaction. The GCD curves of Fig. 12 (d)[219] and capacitance curves of Fig. 12 (e)[219] results show that the $Mo_{1.33}C$ MXene/PEDOT: PSS film with a mass ratio of 10:1 has excellent specific capacitance (2 mV^{-1}, 1310 F cm^{-3} or 452 F g^{-1}) after concentrated H_2SO_4 treatment, which is superior to the MXene-based electrode materials reported in previous

literature[102, 220, 221].

Inal *et al*.[173] prepared PEDOT: PSS: MXene films by electrochemical polymerization and co-doping. Compared with a thin film composed of a single dopant and PEDOT, the integration of PSS and MXene as a co-dopant with PEDOT can better combine the characteristics of MXene with PEDOT to obtain a polymer composite with higher specific capacitance and energy density. From CV curves of Fig. 12 (f)-(h)[173] and the cycle curve of Fig. (i)-(k)[173], it can be seen that under the same conditions, PEDOT: PSS: MXene film (607 ± 85.3 F cm^{-3}, the capacity retention rate after 500 cycles is 78%) has a higher capacity than PEDOT: PSS (195.6 ± 1 F cm^{-3}, 37%) and PEDOT: MXene (358.9 ± 16.7 F cm^{-3}, 58%) higher volume capacitance and stability. The co-doping method significantly improves the electrochemical performance and stability of the PEDOT films, and electrochemical polymerization is a simple and easy-to-operate single-step polymerization method[222, 223]. Both methods provide an effective way for the combination of high-performance materials with different characteristics. In general, the combination of MXene and conducting polymers can significantly improve its electrochemical performance, and MXene/conducting polymers has good application prospects. Table 2 summarizes the applications of MXene/conducting polymers composite electrodes in SCs.

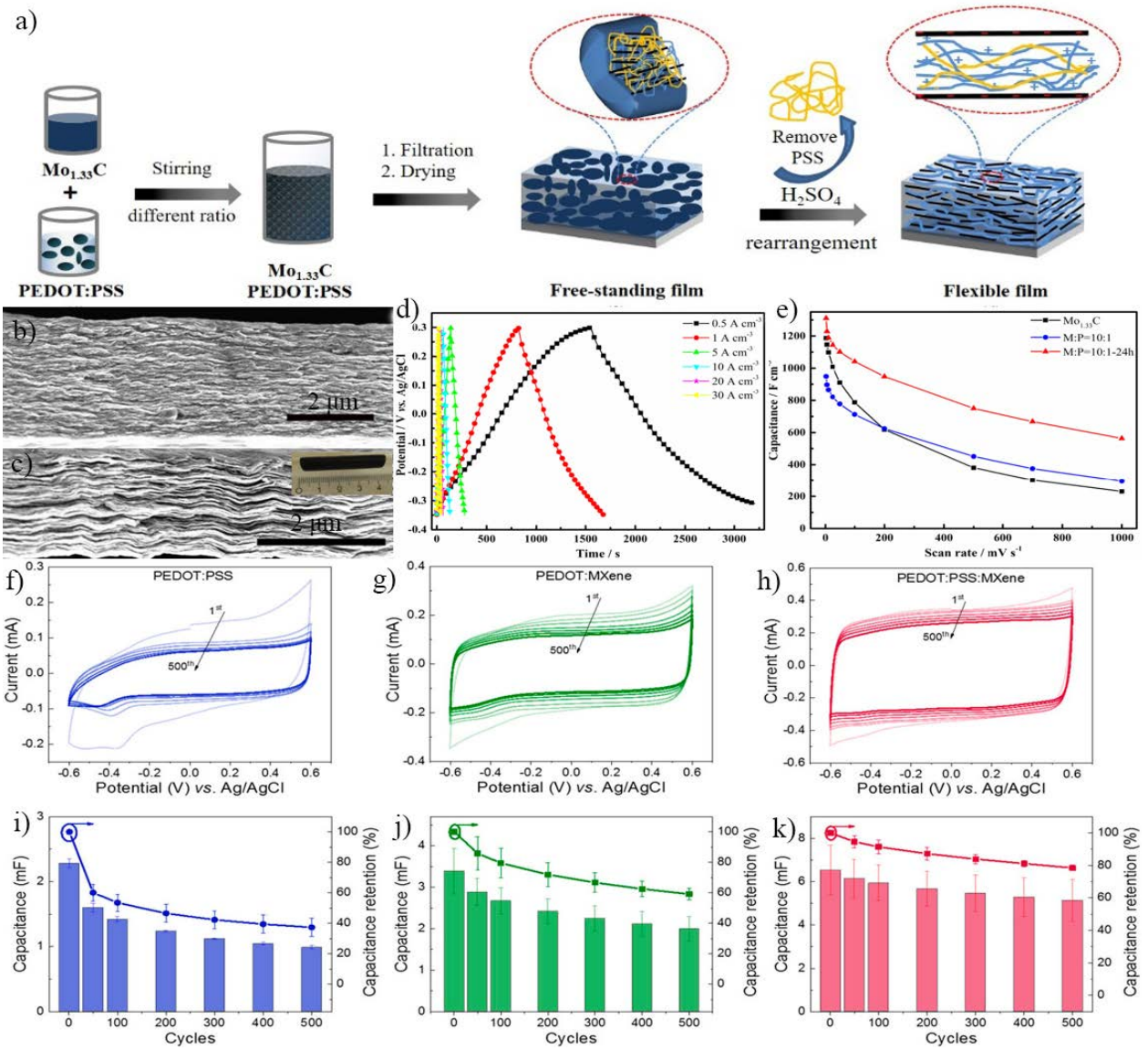

Fig. 12 (a) Schematic diagram of the preparation of MXene/PEDOT film[219]. SEM images of (b) MXene/PEDOT: PSS[219] and (c) MXene/PEDOT[219]. (d) GCD curves of MXene/PEDOT: PSS after immersion in concentrated H_2SO_4 for 24 h at different current densities[219]. (e) The specific capacitance of $Mo_{1.33}C$, MXene/PEODT: PSS, and MXene/PEDOT electrode at different scan rates[219]. Copyright 2017 WILEY-VCH Verlag GmbH & Co. KGaA, Weinheim. CV curves of PEDOT: PSS (f)[173], PEDOT: MXene (g)[224], and PEDOT: PSS: MXene (h)[173] upon 500 CV cycles at 100 mV s^{-1}. Cycling stability of PEDOT:

PSS (i)[173], PEDOT: MXene (j)[173], and PEDOT: PSS: MXene (k)[173]. Copyright 2020 Author(s).

4. Supercapacitors

In order to perform better calculations related to SCs, taking sandwich type face-to-face SCs as an example, the commonly used calculation formulas are listed[46, 225].

Gravimetric capacitance is calculated by using CV curves:

$$C_g = \frac{S}{m \times \nu \times \Delta u} \tag{4}$$

where C_g (F g^{-1}) stands for gravimetric capacitance, S (cm^2) is the area of the CV curve, m (g) denotes to the mass of the active substance loaded by the electrode, ν (mV s^{-1}) represents the scan rate, and Δu (V) refers to the voltage window of the test.

Gravimetric capacitance calculated by using GCD curves:

$$C_g = \frac{I \times \Delta t}{m \times \Delta u} \tag{5}$$

where C_g (F g^{-1}) stands for gravimetric capacitance, I (A) is the current of the GCD test, Δt (s) represents the discharge time of a charge-discharge test, m (g) represents the mass of the active substance loaded by the electrodes, and Δu (V) refers to the voltage window of the test.

$$C_A = \frac{m}{A} \times C_g \tag{6}$$

$$C_V = \frac{m}{V} \times C_g \tag{7}$$

Here, C_A (F cm^{-2}) and C_V (F cm^{-3}) represent area specific capacitance and volume specific capacitance, respectively, m (g) represents the mass of the active substance loaded by the electrode, A (cm^2) represents the electrode area, V (cm^3) stands for the electrode volume, and C_g (F g^{-1}) is the mass specific capacitance.

Energy density and power density of SCs are calculated based on the specific capacitance:

$$E = \frac{1}{2} \times C_g \times (\Delta u)^2 \quad (8)$$

$$P = \frac{E}{\Delta t} \times 3600 \quad (9)$$

where, E (Wh kg^{-1}) stands for energy density, P (W kg^{-1}) represents power density, C_g (F g^{-1}) is the above-mentioned gravimetric capacitance, and Δu (V) and Δt (s) separately denote to the voltage window and the discharge time of the charge-discharge test.

It is worth noting that energy matching needs to be considered for better device performance when assembling asymmetric supercapacitors, with the following equation:

$$C_+ \times \Delta u_+ \times m_+ = C_- \times \Delta u_- \times m_- \quad (10)$$

where C_+ (F g^{-1}) and C_- (F g^{-1}) represent the gravimetric capacitance of the positive and the negative electrodes, respectively, Δu_+ (V) and Δu_- (V) stand for the voltage windows of the positive and the negative electrodes, respectively, m_+ (g) and m_- (g) represent the mass of the active material of the positive and the negative electrodes, respectively. Here, the areas of positive and negative electrodes are the same.

Furthermore, the formula for calculating the pseudocapacitance percentage from the CV curve is as follows:

$$i_{cap} = k_1 \times \nu \quad (11)$$

$$i_{diff} = k_2 \times \nu^{0.5} \quad (12)$$

$$i = i_{cap} + i_{diff} \quad (13)$$

$$\frac{i}{v^{0.5}} = k_1 \times v^{0.5} + k_2 \quad (14)$$

where, i_{cap} (A), i_{diff} (A) and i (A) denote to the current in the capacitive part corresponding to the surface control (pseudocapacitance), the current in the capacitive part corresponding to the diffusion control and the total current obtained from the calculation, k_1 and k_2 are the constant coefficients in the calculation process, respectively, and v (mV s^{-1}) represents the range of the voltage window.

4.1. Symmetric supercapacitors

4.1.1. MXene for symmetric supercapacitors

MXene has attracted much attention since its inception. With high specific surface area and good conductivity of metal-like materials, it has been widely used in research in the fields of batteries and SCs[86, 87, 226-228]. As shown in Fig. 13 (a&b)[229], Xia *et al*.[229] used the very representative $Ti_3C_2T_x$ MXene material to prepare $Ti_3C_2T_x$//$Ti_3C_2T_x$ SSCs with an unconventional electrolyte (simulating seawater electrolyte). At 0.25 A g^{-1}, the SSC device exhibits a volumetric capacitance of 27.4 F cm^{-3}. In the case of 3 A g^{-1}, the device still exhibits a high-volume capacitance of 12.6 F cm^{-3} (Fig. 13 (c&d)[229]). The device separately provides volume energy densities of 1.74×10^{-3} Wh cm^{-3} and 0.68×10^{-3} Wh cm^{-3} at power densities of 0.15 W cm^{-3} and 1.53 W cm^{-3}. Moreover, the cycle stability of $Ti_3C_2T_x$ electrode was tested at 10 A g^{-1}, and the capacitance retention rate of 96.6% was achieved after 5000 charge-discharge cycles, which is better than those of previously reported similar systems.

Yang *et al*.[230] fabricated a flexible, independent, as well as ultra-dense delamination

$Ti_3C_2T_x$ film by mechanically pressing the conventional $Ti_3C_2T_x$ film, directly as a binderless electrode to assemble SCs. The mechanical high pressure increases the density (Fig. 13 (e)[230]), electrical conductivity (Fig. 13 (f)[230]) and wettability of the $Ti_3C_2T_x$ film. At the same time, the interconnected and enriched mesoporous channels promote the insertion/deintercalation of cations during charging-discharging. Experiments show that with the increase of mechanical pressure, the volume performance of SCs assembled from $Ti_3C_2T_x$ films increases. However, this increase is not endless, and the thin-film electrode prepared under the condition of 40 MPa has the best electrochemical performance. From Fig. 13 (g&h)[230], we can see that a typical SSC stemming from the $Ti_3C_2T_x$ film under 40 MPa in 1 M Li_2SO_4 offered a volumetric capacitance of 633 F cm^{-3} at 2 mV s^{-1}, volumetric energy density of 22 Wh L^{-1}, and capacitance retention of 95.3% after 10000 cycles. It is worth noting that when 1 M Li_2SO_4 is replaced by 1 M $EMIMBF_4$/AN, the voltage window provided by the supercapacitor device is up to 2.2 V. Moreover, it exhibits an ultra-high volumetric energy density of 41 Wh L^{-1}. This is the highest value currently available in organic electrolytes for SCs based on MXene materials.

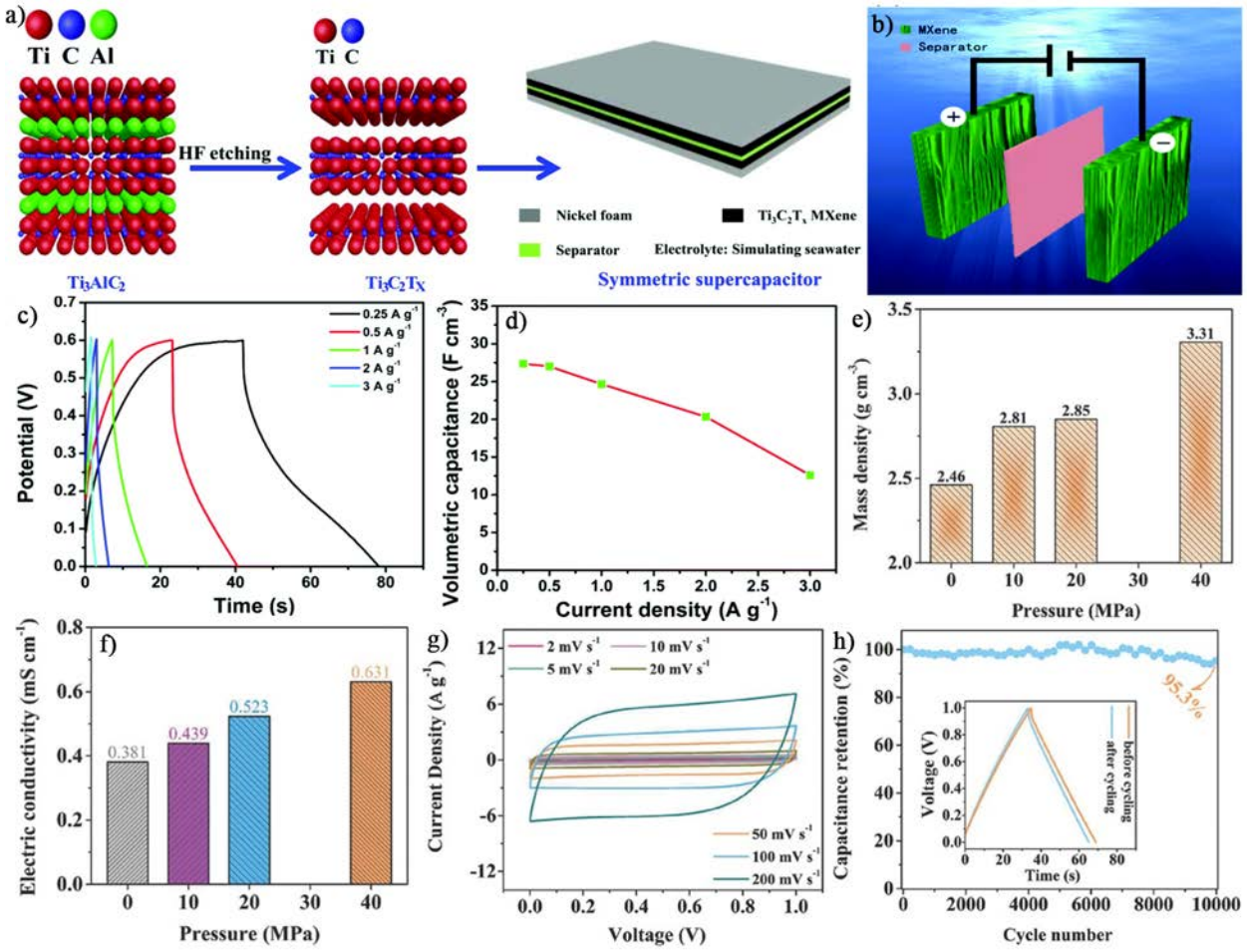

Fig. 13 (a) Schematic diagram of the $Ti_3C_2T_x$//$Ti_3C_2T_x$ SSC presenting process[229]. (b) Schematic diagram of $Ti_3C_2T_x$//$Ti_3C_2T_x$ SSC simulation[229]. GCD curves (c) and specific capacitance (d) at different current density[229]. Copyright Royal Society of Chemistry. Mass density (e) and electrical conductivity (f) of $Ti_3C_2T_x$ films under different pressures[230]. (g) CV curves of $Ti_3C_2T_x$ films prepared under 40 MPa at different scan rates[230]. (h) Cyclic performance of $Ti_3C_2T_x$ films prepared under 40 MPa at 2 A g^{-1}. (Inset of the GCD curves at the beginning and end at 1 A g^{-1})[230]. Copyright 2018 WILEY-VCH Verlag GmbH & Co. KGaA, Weinheim.

Zhang *et al*.[231] proposed an in-situ ice template method to prepare independent and flexible 3D porous $Ti_3C_2T_x$/CNTs SC film (3D-PMCF) electrodes, as shown in Fig. 14 (a)[231]. Unlike $Ti_3C_2T_x$ MXene prepared by traditional vacuum drying method, the in-situ ice template method

does not cause stacking of MXene materials. By freeze-drying the $Ti_3C_2T_x$/CNTs water film, the water molecules between the MXene layers are converted into the form of small particles of ice. Then the small particles of ice serve as a template to sacrifice themselves, preserving the 3D porous structure. In comparison with Fig. 14 (b&c)[231], it can be seen that MXene films are stacked in layers, while 3D-PMCF has many interactive channels. The 3D-PMCF has a large number of active sites, which realizes the rapid transmission of ions, thus exhibiting excellent electrochemical performance. As shown in Fig. 14 (d)[231], in 3 M H_2SO_4, the flexible 3D-PMCF provides a specific capacitance of 375 F g^{-1} at 5 mV s^{-1}. Even in the situation of 10000 mV s^{-1}, 3D-PMCF still displays a specific capacitance of 92.0 F g^{-1} (Fig. 14 (e)[231]). What's more, at 10 A g^{-1}, after 10000 cycles, the 3D-PMCF electrode capacitance retention rate reached 95.9%. After further assembling the 3D-PMCF into an SSC, the device provides an energy density of 9.2 Wh kg^{-1}.

Zhu *et al*.[232] prepared a Ti_2CT_x//Ti_2CT_x SSC with excellent energy and power density. Experiments have proved that when the mass ratio of Ti_2AlC: HF is 1:2, the etched Ti_2CT_x has the best performance. From Fig. 14 (f&g)[232], one can see that in 1 M KOH, the sample 1:2 provides 517 F cm^{-3} and 307 F cm^{-3} volume specific capacitance at 2 mV s^{-1} and 100 mV s^{-1}, respectively. This is similar to the performance of $Ti_3C_2T_x$/PVA electrode (2 mV s^{-1}, 528 F cm^{-3} and 100 mV s^{-1}, 306 F cm^{-3}) in 1 M KOH reported by Ling et al.[233]. It is worth noting that the Ti_2CT_x//Ti_2CT_x SSC has a capacitance retention rate of 100% after 3000 charge-discharge cycles at 20 A g^{-1}, showing the excellent cycle stability of the device.

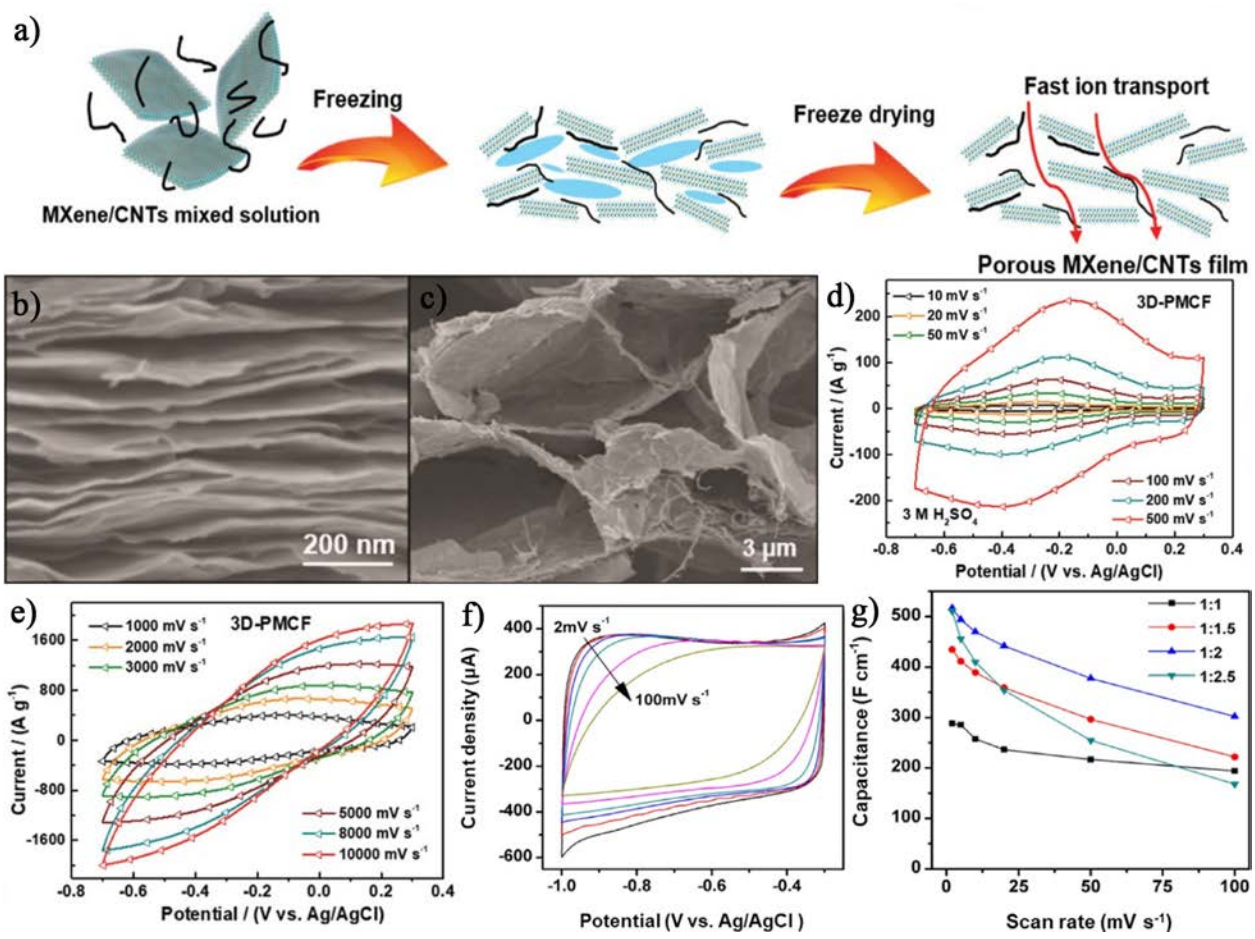

Fig. 14 (a) Schematic illustration presenting the preparation of 3D-PMCF film[231]. SEM images of MXene films (b) and 3D-PMCF (c)[231]. CV curves of 3D-PMCF at various scan rates: (d) 10-500 mV s^{-1}; (e) 1000-10000 mV s^{-1}[231]. Copyright 2020 WILEY-VCH Verlag GmbH & Co. KGaA, Weinheim. CV curves (f) and specific capacitance (g) at different scan rates[232]. Copyright 2018 Science Press and Dalian Institute of Chemical Physics, Chinese Academy of Sciences. Published by Elsevier B.V. and Science Press.

Wu *et al.*[234] reconstructed $Ti_3C_2T_x$ microgels and $Ti_3C_2T_x$ monolayer nanosheets to construct independent flexible reassembled MXene (RAMX) film electrodes with tunable porous structure, as shown in Fig. 15 (a)[234]. It is still the morphology of the film on the macro scale. However, on the micro scale, the stacked $Ti_3C_2T_x$ MXene sheets became a 3D network structure

with dense mesopores (Fig. 15 (b)[234]). From Fig. 15 (c)[234], we can see that the $Ti_3C_2T_x$ microgels and the $Ti_3C_2T_x$ monolayer nanosheets reassembled with different mass ratios maximize the space utilization. When the mass ratio of the microgels reaches 50%, the rate capability of the MXene film is maximized. The MXene film provides a specific capacitance of 978 F cm^{-3} at 10 mV s^{-1} in 3 M H_2SO_4, and even at 2000 mV s^{-1}, it still provides a specific capacitance of 736 F cm^{-3} (Fig. 15 (d)[234] and Fig. 15 (e)[234]). The thin-film electrode assembly $Ti_3C_2T_x$//$Ti_3C_2T_x$ SSC delivered a high energy density of 40 Wh L^{-1} at a power density of 0.83 kW L^{-1}. Even in the case of 41.5 kW L^{-1}, it still shows 21 Wh L^{-1}. Besides, at 1000 mV s^{-1}, the SSC still keeps a capacitance value of 91.14% after 20000 charge-discharge cycles (Fig. 15 (f)[234]), which is the highest value of SSCs in an aqueous electrolyte.

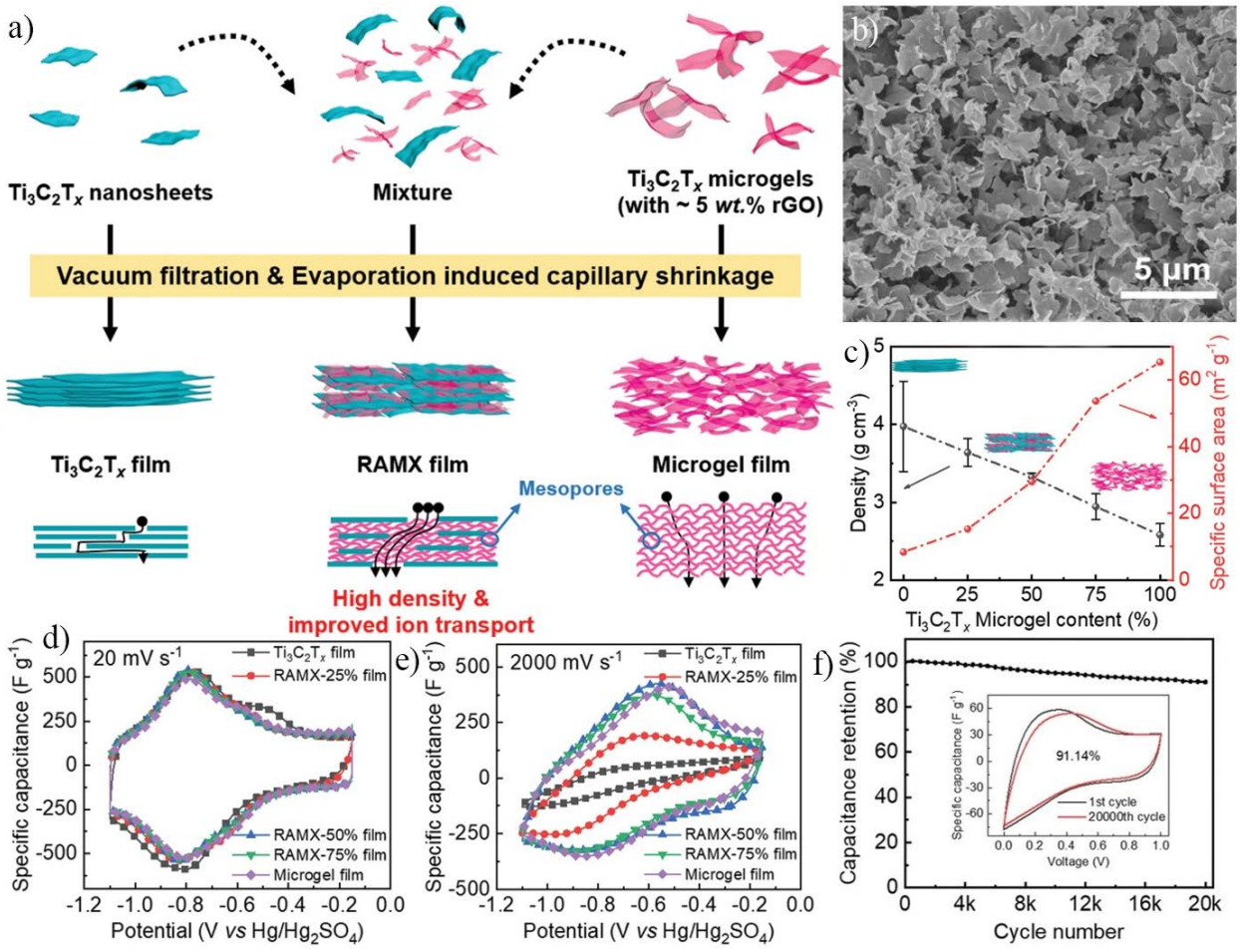

Fig. 15 (a) Schematic diagram for the preparation of RAMX film[234]. (b) SEM image of RAMX film[234]. (c) The RAMX film density and specific surface area versus $Ti_3C_2T_x$ microgel content[234]. CV curves of RAMX electrodes with different contents at different scanning rates: (d) 20 mV s^{-1} and (e) 2000 mV s^{-1} [234]. (f) Cycling performance after 20000 cycles at 1000 mV s^{-1}. (Inset of the CV curves of the 1st and 20000th cycle)[234]. Copyright 2021 Wiley-VCH GmbH.

4.1.2. MXene/conducting polymers for symmetric supercapacitors

MXene has a graphene-like 2D sheet structure and metal-like high conductivity, and has huge application potential in electrochemical energy storage[235-237]. Conducting polymers are shining in the study of SCs because of their ultra-high stability, high conductivity in the doped

state, and fast redox reaction performance[200, 238]. For further improving the performance of electrode materials, researchers continue to explore composite materials with high performance. Combining the excellent properties of MXene and conducting polymers materials with their own characteristics, MXene/conducting polymers composites are extensively applied as electrode materials in SCs[239-242].

Boota *et al.*[160] prepared MXene/PPy composites by in-situ polymerization of pyrrole between $Ti_3C_2T_x$ MXene nanosheets. MXene/PPy composites electrode has a capacitance value of nearly 1000 F cm^{-3} and capacitance remaining 92% after 25000 cycles. Jian *et al.*[164] used a one-step co-electrodeposition way to prepare MXene/PPy composite films. In Fig. 16 (a)[164], in 1 M H_2SO_4, MXene/PPy composite film provides a mass capacitance of 416 F g^{-1} at 0.5 A g^{-1}. Furthermore, SSC assembled with ITO-glasses electrodes covered with MXene/PPy films show high specific capacitance of 184 F g^{-1} at 10 mV s^{-1}, as well as good capacitance retention rate of about 86.4% after 5000 cycles at 5 A g^{-1} (Fig. 16 (b)[164]). Tong *et al.*[216] assembled the 400PPy175/$Ti_3C_2T_x$ composite electrode into an all-solid-state flexible SSC and provided a mass specific capacitance of 258.3 F g^{-1} in 1 M H_2SO_4 at 0.5 A g^{-1}. In 400PPy175, 400 and 175 denote 400 μL of pyrrole monomer and electrochemical polymerization time of 175 s. In addition, 400PPy175/$Ti_3C_2T_x$//400PPy175/$Ti_3C_2T_x$ devices exhibit energy densities of 10.82 μWh mg^{-1} and 3.99 μWh mg^{-1} at power densities of 0.11 mW mg^{-1} and 1.89 mW mg^{-1}, respectively.

Wu *et al.*[243] reported a method for preparing a composite film with high cycle stability, that is, a suspended PDT/$Ti_3C_2T_x$ composite film is formed by combining a dispersed conjugated

polymer (PDT) and layered $Ti_3C_2T_x$ MXene, as shown in Fig. 16 (c)[243]. There is a stable chemical bond between the PDT dispersed chain and the $Ti_3C_2T_x$ nanosheet (Fig. 16 (d)[243]), which effectively solves the performance problems caused by the volume expansion and contraction changes of the polymer chain.

In the meantime, the mechanical performances of the material are improved, and a high-speed path is provided for ion/charge transfer. In 0.5 M H_2SO_4, the PDT/$Ti_3C_2T_x$ composite electrode shows a surface capacitance of 284 mF cm^{-2} at 0.5 mA cm^{-2} (Fig. 16 (e)[243]), and nearly 100% capacitance retention after 10000 charge-discharge cycles (Fig. 16 (f)[243]). In addition, the all-solid SSC assembled based on PDT/$Ti_3C_2T_x$ film has excellent flexibility (0-90° static bending 10000 times, Fig. 16 (g)[243]) and a surface capacitance of up to 52.4 mF cm^{-2} at 0.1 mA cm^{-2}.

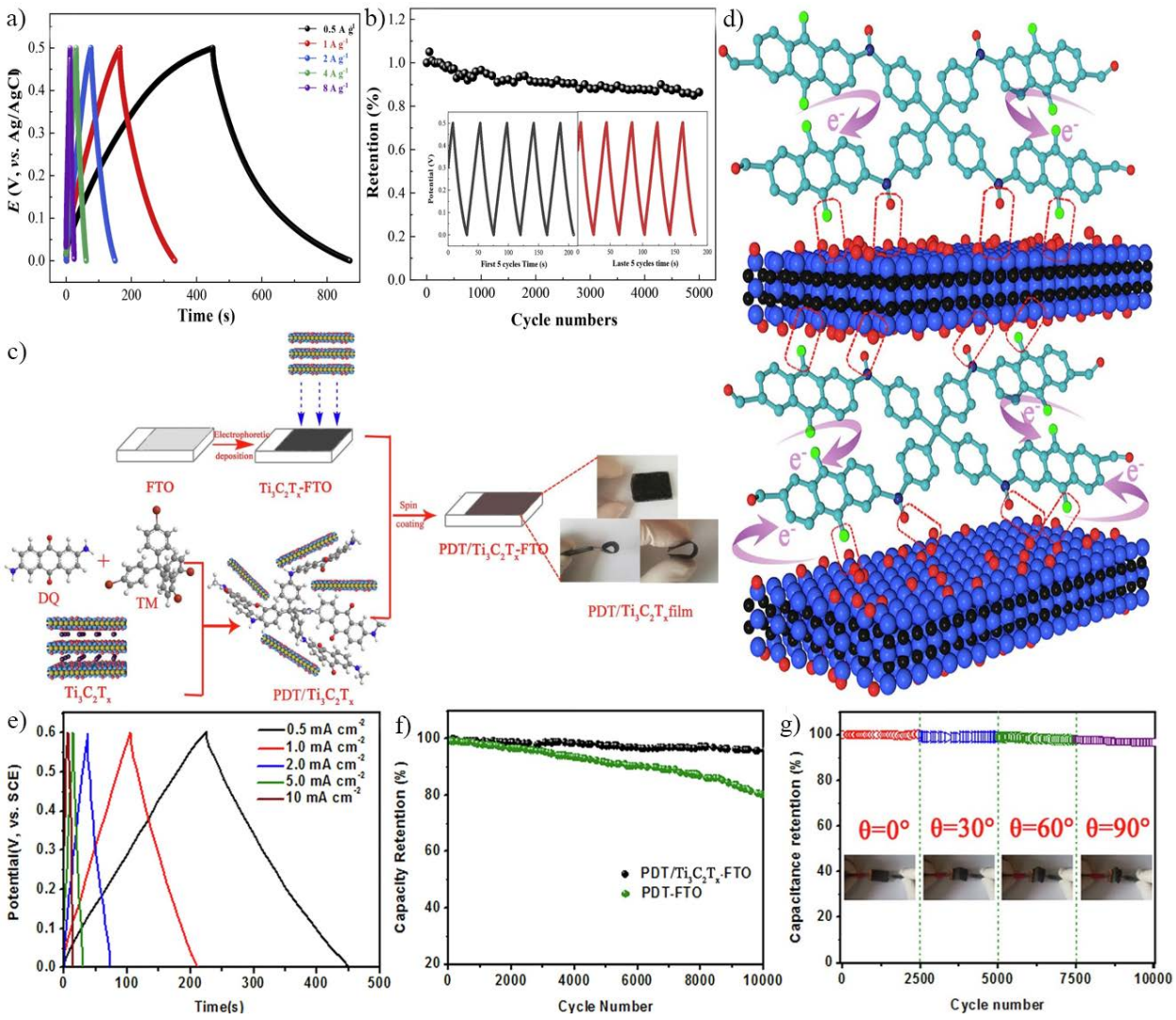

Fig. 16 (a) GCD curves of MXene/PPy electrodes at different current densities[164]. (b) The cycle stability curve of MXene/PPy//MXene/PPy SSC. (Inset is the GCD curves of the first five laps and the last five laps)[164]. Copyright 2019 Elsevier Ltd. (c) Schematic diagram for the fabrication of PDT/$Ti_3C_2T_x$ composite film[243]. (d) Atomic-scale schematic diagram of $Ti_3C_2T_x$ MXene and PDT chains binding[243]. (e) GCD curves of the PDT/$Ti_3C_2T_x$ electrodes at various current densities[243]. (f) Cyclic stability of PDT-FTO and PDT/$Ti_3C_2T_x$-FTO electrodes[243]. (g) Cycling performance of the all-solid SSC assembled based on PDT/$Ti_3C_2T_x$ film for 10000 cycles under different static bending angles[243]. Copyright 2019 Elsevier B.V.

Wu et al.[244] constructed Ti_3C_2/PANI nanotubes (Ti_3C_2/PANI-NTs) composites with a clear hierarchical structure (Fig. 17 (a)[244]) through one-pot in-situ polymerization, as shown in Fig. 17 (b)[244]. The Ti_3C_2 MXene nanosheets can ensure the mechanical stability and high conductivity of the composite material, and PANI-NTs serve as a one-dimensional high-speed transmission channel to further provide more active sites. The introduction of PANI-NTs effectively inhibited the self-stacking phenomenon of Ti_3C_2 nanosheets, and enlarged the spacing of MXene layers and the accessible surface area of ions. The electrochemical test of the three-electrode system indicates that under 1 M H_2SO_4 electrolyte, the Ti_3C_2/PANI-NTs composite electrode displays a specific capacitance of 596.6 F g^{-1} at 0.1 A g^{-1} (Fig. 17 (c)[244]), and the specific capacitance retention rate has 94.7% after 5000 cycles (Fig. 17 (d)[244]). More importantly, compared with the previously reported Ti_3C_2 MXene SSCs, the SSC assembled by Ti_3C_2/PANI-NTs exhibits an energy density of 25.6 Wh kg^{-1} at a power density of 153.2 W kg^{-1} in 1 M H_2SO_4. Even at 1610.8 W kg^{-1}, it still exhibits an energy density of 13.2 Wh kg^{-1}. In addition, as shown in Fig. 17 (e)[244], the Ti_3C_2/PANI-NTs//Ti_3C_2/PANI-NTs SSC device has a capacitance retention of 81.1% after 4000 cycles at 1 A g^{-1}.

Qin *et al*.[219] fabricated $Mo_{1.33}C$ MXene/PEDOT: PSS composites electrode by self-assembly method, which has super high conductivity because of the synergistic effect of acidified PEDOT: PSS and MXene. Under 1 M H_2SO_4 electrolyte, $Mo_{1.33}C$ MXene/PEDOT: PSS assembled flexible device provides a volume capacitance of 568 F cm^{-3} at 0.5 A g^{-1} (Fig. 17 (f)[219]), an energy density of 33.2 mWh cm^{-3} at an ultra-high-power density of 19470 mW cm^{-3}.

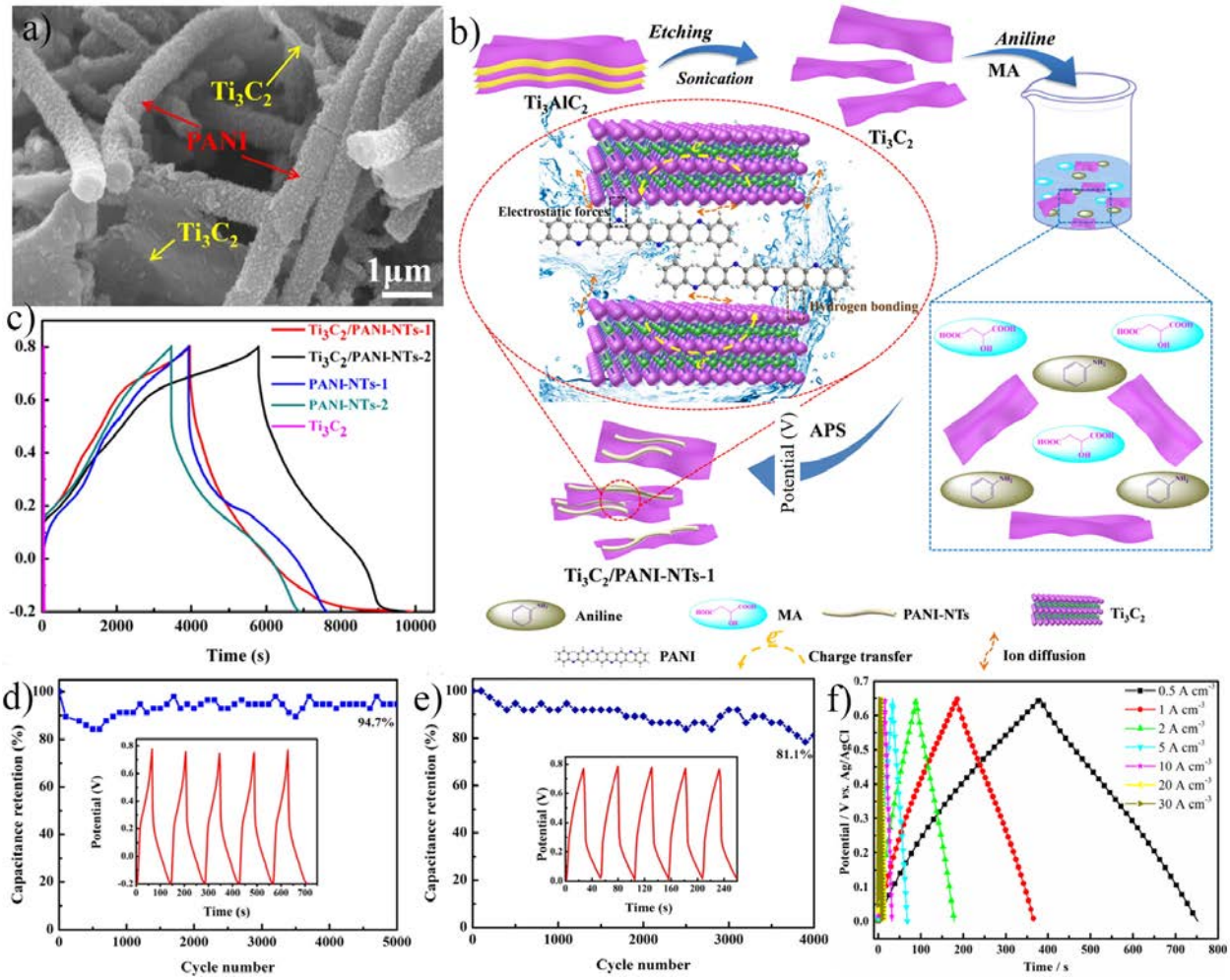

Fig. 17 (a) SEM image of Ti_3C_2/PANI-NTs[244]. (b) Schematic illustration for the preparation of Ti_3C_2/PANI-NTs composites[244]. (c) GCD curves of the electrodes at 0.1 A g^{-1}[244]. Cycle performance of the Ti_3C_2/PANI-NTs electrode (d) and the Ti_3C_2/PANI-NTs//Ti_3C_2/PANI-NTs SSC device (e)[244]. (Inset is GCD curves of the last five laps)[244]. Copyright 2020 Elsevier Inc. (f) GCD curves of the $Mo_{1.33}C$ MXene/PEDOT: PSS flexible device[219]. Copyright 2017 WILEY-VCH Verlag GmbH & Co. KGaA, Weinheim.

Zhou *et al.*[245] first prepared i-PANI@$Ti_3C_2T_x$ composites by in-situ non-oxidative polymerization, and then prepared Lig@$Ti_3C_2T_x$ and Lig@$Ti_3C_2T_x$/i-PANI@$Ti_3C_2T_x$ films through vacuum assisted filtration, as shown in Fig. 18 (a)[245]. SEM of Fig. 18 (b)[245] and

TEM of Fig. 18 (c)[245] manifest that the film presents a dense film with a regular hierarchical arrangement. The insertion of electroactive polymers (p-phenylenediamine as the initiator to prepare the PANI) i-PANI and (Lignosulfonate) Lig not only expands the spacing of $Ti_3C_2T_x$ layers to prevent self-stacking problems, but also provides considerable pseudo-capacitance, and at the same time promotes the rapid and effective transfer of ions/charges. Therefore, as shown in Fig. 18 (d)-(f)[245], in the PVA/H_2SO_4 electrolyte, the flexible SSCs assembled by i-PANI@$Ti_3C_2T_x$, Lig@$Ti_3C_2T_x$ and Lig@$Ti_3C_2T_x$/i-PANI@$Ti_3C_2T_x$ separately provides 310 F g^{-1} (~1001 F cm^{-3}), 271 F g^{-1} (~881 F cm^{-3}) and 295 F g^{-1} (~959 F cm^{-3}) at 1 A g^{-1}. Besides, i-PANI@$Ti_3C_2T_x$//i-PANI@$Ti_3C_2T_x$, Lig@$Ti_3C_2T_x$//Lig@$Ti_3C_2T_x$ and Lig@$Ti_3C_2T_x$/i-PANI@$Ti_3C_2T_x$//Lig@$Ti_3C_2T_x$/i-PANI@$Ti_3C_2T_x$ SSC devices separately show energy densities of 34.8 Wh L^{-1}, 30.6 Wh L^{-1} and 33.3 Wh L^{-1} at a power density of 1625 W L^{-1}. Interestingly, the SSC device assembled by Lig@$Ti_3C_2T_x$/i-PANI@$Ti_3C_2T_x$ displays superior mechanical durability, and after 2000 0-90° static bending experiments, it still exhibits a capacitance retention rate as high as 99.17%, as shown in Fig. 18 (g)[245]. This shows that the extremely flexible Lig@$Ti_3C_2T_x$/i-PANI@$Ti_3C_2T_x$ composite film is an electrode material that is practically used to flexible/wearable devices.

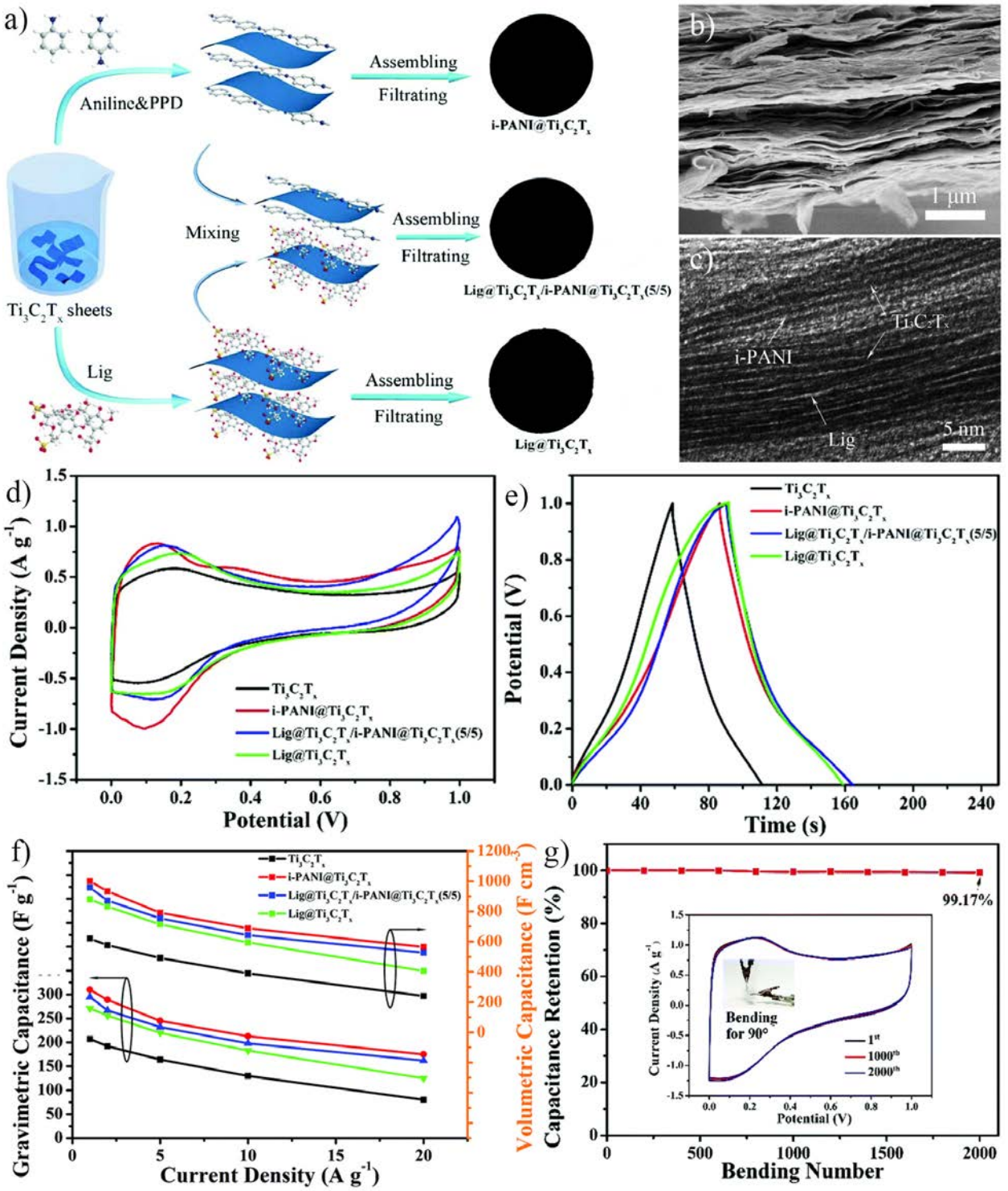

Fig. 18 (a) Schematic diagram for the preparation of i-PANI@$Ti_3C_2T_x$, Lig@$Ti_3C_2T_x$, and Lig@$Ti_3C_2T_x$/i-PANI@$Ti_3C_2T_x$ composite films[245]. SEM image (b) and TEM image (c) of Lig@$Ti_3C_2T_x$/i-PANI@$Ti_3C_2T_x$

film. (d) CV curves of different electrodes at 5 mV s^{-1} [245]. (e) GCD curves of different electrodes at 1 A g^{-1} [245]. (f) Specific gravimetric and volumetric capacitance at various current densities[245]. (g) Cycle performance after 2000 times of 90° bends measured at 10 mV s^{-1}. (Inset is CV curves at various 90° bending cycles.)[245] Copyright Royal Society of Chemistry.

4.2. Asymmetric supercapacitors

4.2.1. MXene for asymmetric supercapacitors

Compared with MXene-based SSCs, MXene is used as the negative electrode and combined with the positive electrode material to design ASCs device, which can broaden the voltage window of the device and further increase the energy density of the capacitor[246-249]. Nonetheless, ideal flexible cathodes that match the original MXene membrane electrodes are rare. Therefore, researchers have carried out a series of studies on the ideal flexible positive electrode that can be matched with it. Xia *et al*.[250] adopted a hydrothermal route to fabricate $Ti_3C_2T_x$ MXene nanocomposites decorated with NiO (Ni-dMXNC), as shown in Fig. 19 (a)[250]. In the Fig. 19 (b)[250], the NiO nanosheets are successfully attached to the surface of the MXene sheets. Compared to $Ti_3C_2T_x$ MXene prepared by traditional methods, TiO_2/C-$Ti_3C_2T_x$-MXene containing carbon-supported TiO_2 obtained by high temperature annealing has higher conductivity and higher specific surface area. The high specific surface area of the Ni-dMXNC special structure, the high surface activity of the NiO layer and the synergistic effect of the traditional $Ti_3C_2T_x$ MXene negative electrode enhance the capacitance performance of the device. Therefore, the ASC is assembled with Ni-dMXNC as the positive electrode and $Ti_3C_2T_x$ MXene as the negative electrode

(Fig. 19 (c)[250]). Compared with the previously reported pure $Ti_3C_2T_x$ MXene SSCs, the ASCs exhibit a high energy density of 1.04×10^{-2} Wh cm^{-3} at 0.22 W cm^{-3}. In addition, as shown in Fig. 19 (d&e)[250], the cycle performance of the device in the range of 0-1.8 V was observed at 1 A g^{-1}, and the capacitance retention rate was 72.1% after 5000 charge-discharge cycles.

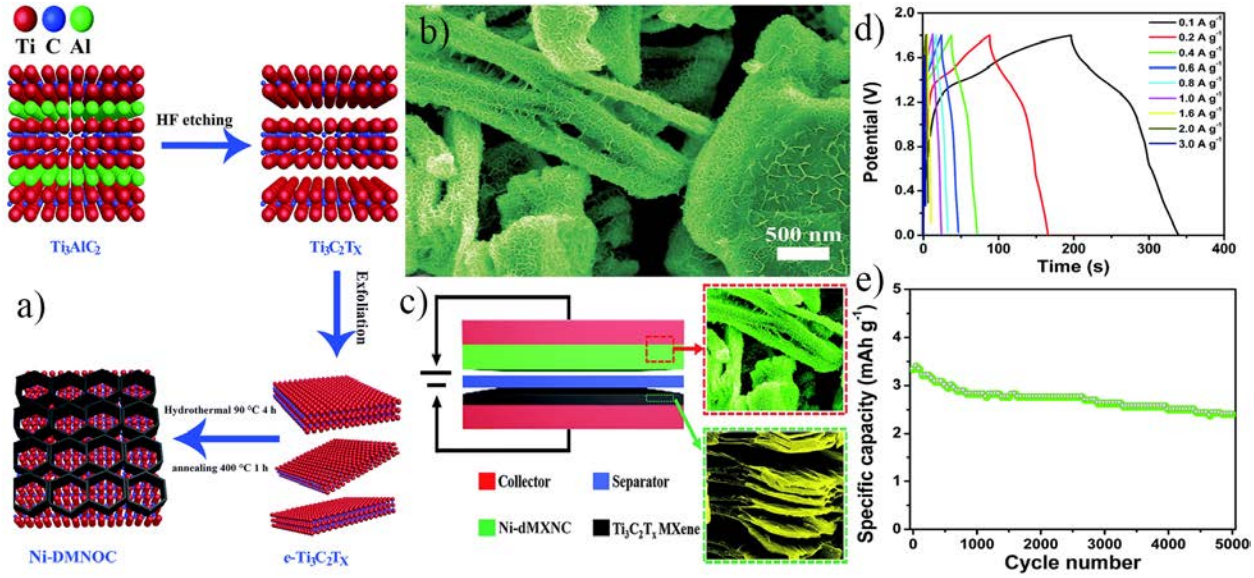

Fig. 19 (a) Illustration of the preparation of the Ni-dMXNC by hydrothermal method[250]. (b) SEM image of the Ni-dMXNC[250]. (c) Illustration of the Ni-dMXNC//$Ti_3C_2T_x$ ASC[250]. (d) GCD curves of the Ni-dMXNC//$Ti_3C_2T_x$ ASC at various densities[250]. (e) Cycle property of the Ni-dMXNC//$Ti_3C_2T_x$ ASC at 1 A g^{-1} [250]. Copyright Royal Society of Chemistry.

Zhao *et al*.[251] designed and prepared independent Ti_3C_2/FeOOH quantum dots (QDs) hybrid films through electrostatic self-assembly technology (Fig. 20 (a)[251]). Amorphous FeOOH QDs not only act as interlayer pillars to prevent self-stacking of Ti_3C_2 nanosheets, but also are active materials with high theoretical capacitance values[252]. In TEM of Fig. 20 (b)[251], FeOOH QDs are uniformly distributed on the periphery of the MXene nanosheets[253].

Combining Fig. 20 (c)[251] and Fig. 20 (d)[251], it is not difficult to see that the Ti_3C_2/Fe-15% hybrid film prepared when FeOOH QDs doping level is 15% has excellent electrochemical performance. It is worth noting that in 1 M Li_2SO_4, Ti_3C_2/Fe-15% electrode provides a surface capacitance of 485 mF cm^{-2} at 2 mV s^{-1}, 2.3 times than that of pure Ti_3C_2 thin film electrode (213 mF cm^{-2}), as displayed in Fig. 20 (d)[251]. Meanwhile, the capacitance of the Ti_3C_2/Fe-15% electrode remains 94.8% after 5000 cycles (Fig. 20 (e)[251]. In addition, a flexible Ti_3C_2/Fe-15%//MnO_2/CC ASC was assembled with Ti_3C_2/Fe-15% hybrid film as the negative electrode and MnO_2 grown on carbon cloth as the positive electrode. The ASC device has a wide voltage window of 1.6V (Fig. 20 (f)[251]), providing an energy density of 40 mWh cm^{-2} and a power density of 8.2 mW cm^{-2}, and keeps a capacitance value of 82% after 3000 cycles.

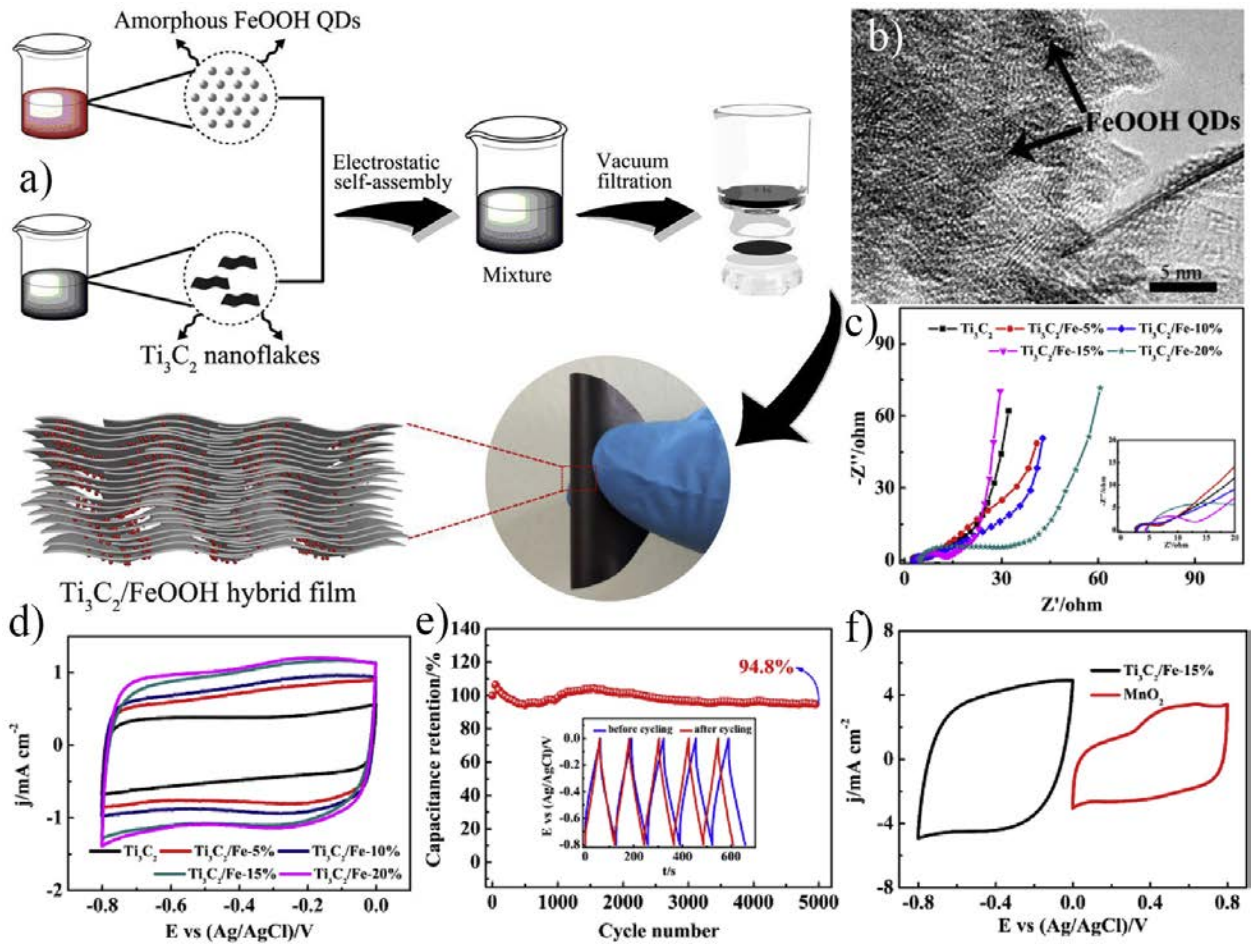

Fig. 20 (a) Schematic diagram for preparing Ti_3C_2/FeOOH hybrid films[251]. (b) TEM image of Ti_3C_2/FeOOH hybrid films[251]. (c) Nyquist plots of the different electrodes[251]. (d) CV curves of Ti_3C_2 and Ti_3C_2/FeOOH hybrid different electrodes at 2 mV s^{-1} in 1 M Li_2SO_4 electrolyte[251]. (e) Cycling performance of Ti_3C_2/Fe-15% electrode at 4 mA cm^{-2} (Inset is GCD curves before and after 5000 cycles)[251]. (f) CV curves of Ti_3C_2/Fe-15% and MnO_2/CC electrodes at 10 mV s^{-1} [251]. Copyright 2019 Elsevier Ltd.

4.2.2. MXene/conducting polymers for asymmetric supercapacitors

Researchers are not completely satisfied with the performance provided by MXene/conducting polymers SSCs, so they set their sights on MXene/conducting polymers ASCs with a higher operability[246, 254-256]. For example, Fu *et al*.[257] prepared a graphene

encapsulated Ti_2CT_x MXene@PANI (GMP) structure, as shown in Fig. 21 (a)[257]. From the SEM image of Fig. 21 (b)-(d)[257], it can be seen that the chemically inert graphene strengthens the MXene framework, and the embedding of conducting PANI provides more active sites. Affected by the hierarchical nanostructure and complementary synergistic effects, the GMP electrode shows excellent electrochemical property. In the presence of 1 M H_2SO_4, the GMP electrode provides a mass specific capacitance of 635 F g^{-1} (~1143 F cm^{-3}) at 1 A g^{-1}, and the capacitance remains 97.54% after 10000 cycles, as shown in Fig. 21 (e)-(g)[257]. In addition, an ASC is assembled with GMP and graphene serving as positive electrode and negative electrode, respectively. The ASC device provides an energy density of 42.3 Wh kg^{-1} at a power density of 950 W kg^{-1}, as well as still shows a cycle stability of 94.25% after 10000 cycles at 10 A g^{-1}.

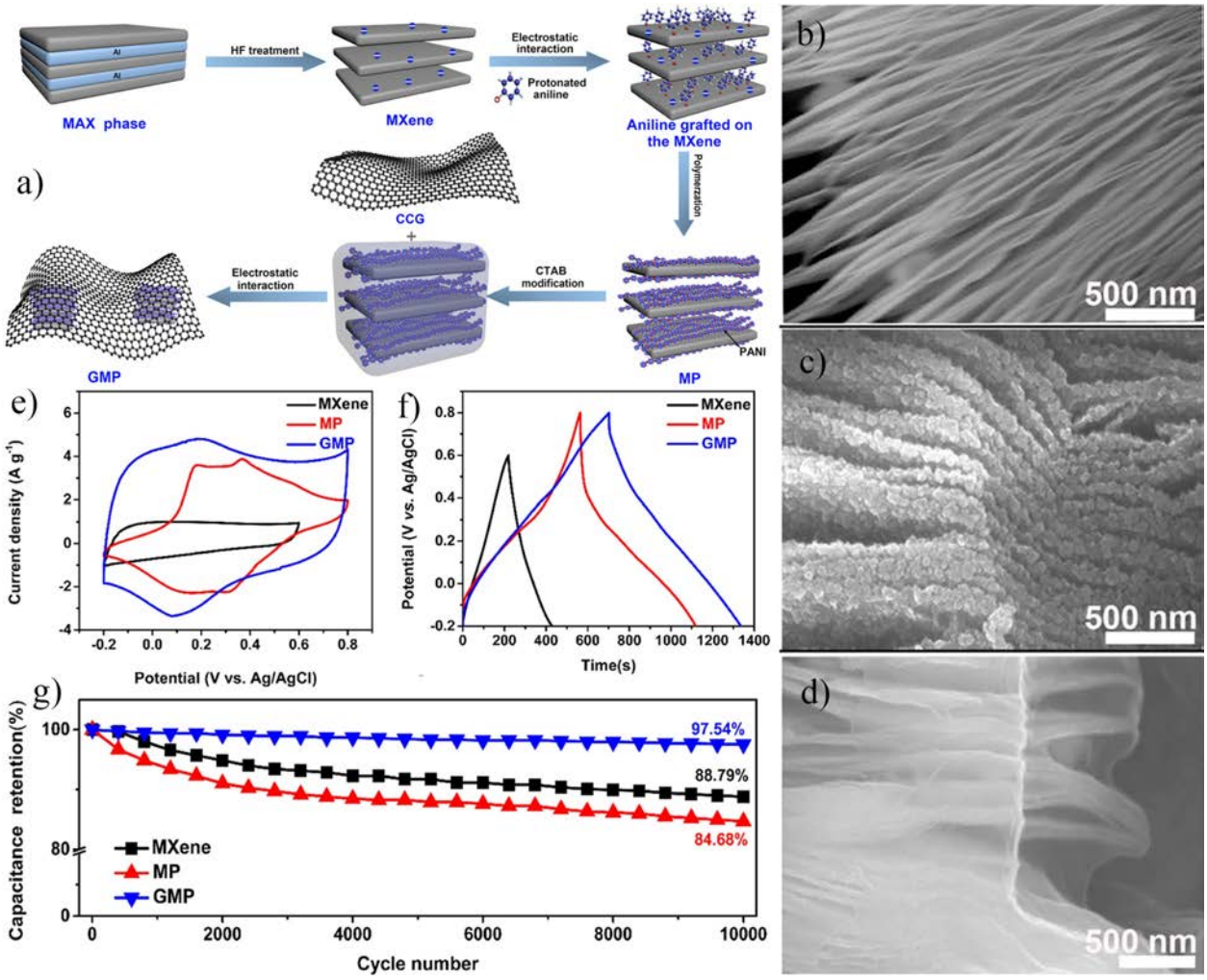

Fig. 21 (a) Schematic diagram for the preparation GMP composite electrode[257]. SEM images of MXene (b), MP (c), and GMP (d) [257]. (e) CV curves of GMP electrode at 5 mV s^{-1} in 1 M H_2SO_4[257]. (f) GCD curves of GMP electrode at 1 A g^{-1} in 1 M H_2SO_4[257]. (g) Cycle performance of the GMP electrode after 10000 charge-discharge at 10 A g^{-1} [257]. Copyright 2018 American Chemical Society.

Boota *et al*.[258] prepared CP@rGO composite electrodes by depositing PANI, PPy, and PEDOT on reduced graphene oxide (rGO). Using CP@rGO and $Ti_3C_2T_x$ MXene separately as the positive electrode and the negative electrode, a full pseudo-capacitance ASC was assembled (Fig. 22 (a)[258]). Among them, $Ti_3C_2T_x$//PANI@rGO has the most excellent performance. In 3 M

H_2SO_4, the voltage window of the $Ti_3C_2T_x$//PANI@rGO device reached 1.45 V, and the capacitance retention rate was 88.42% after 20000 charge-discharge cycles (Fig. 22 (b)[258]). Moreover, the voltage windows of $Ti_3C_2T_x$//PPy@rGO and $Ti_3C_2T_x$//PEDOT@rGO have also reached 1.4 V.

Li *et al*.[259] fabricated a PANI@ 3D macroporous $Ti_3C_2T_x$ (M-$Ti_3C_2T_x$) composites with ultra-high rate capability by depositing PANI on 3D $Ti_3C_2T_x$ MXene. Under 3 M H_2SO_4 electrolyte, the electrode provides a volume capacitance of 1632 F cm^{-3} at 10 mV s^{-1}, even at 5000 mV s^{-1}, it still provides up to 827 F cm^{-3}, as shown in Fig. 22 (c)[259]. According to energy matching, the MXene//PANI@M-$Ti_3C_2T_x$ ASC was prepared with PANI@M-$Ti_3C_2T_x$ and MXene as the positive electrode and the negative electrode. The device provides volumetric energy densities of 50.6 Wh L^{-1} and 24.4 Wh L^{-1} at energy densities of 1.7 kW L^{-1} and 127 kW L^{-1}.

Li *et al.*[208] used rGO/CNT/PANI and the wave-shaped $Ti_3C_2T_x$ MXene as the positive electrode and the negative electrode, respectively, and designed an all pseudo-capacitance $Ti_3C_2T_x$//rGO/CNT/PANI ASC, as shown in Fig. 22(d)[208]. From Fig. 22 (e)[208], one can observe that CNTs are uniformly dispersed between rGO/PANI layers as spacer materials. From the Fig. 22 (f)[208] that the wave $Ti_3C_2T_x$ film is densely packed with many folds, which provides many fast channels for ion transmission. Since the positive and negative electrodes are both highly dense structures and pseudo-capacitor energy storage mechanism, they can provide a sufficiently high-volume capacitance for asymmetric devices. In 3 M H_2SO_4, $Ti_3C_2T_x$//rGO/CNT/PANI ASC devices provide energy densities of 70 Wh L^{-1} and 34.8 Wh L^{-1} at power densities of 1.4 kW L^{-1}

and 111 kW L^{-1}, respectively. In addition, Li *et al.*[212] assembled ASC devices with MXene/PANI as the positive electrode and activated carbon (AC) as the negative electrode. This device provides an energy density of 22.67 Wh kg^{-1} at a power density of 217 W kg^{-1}.

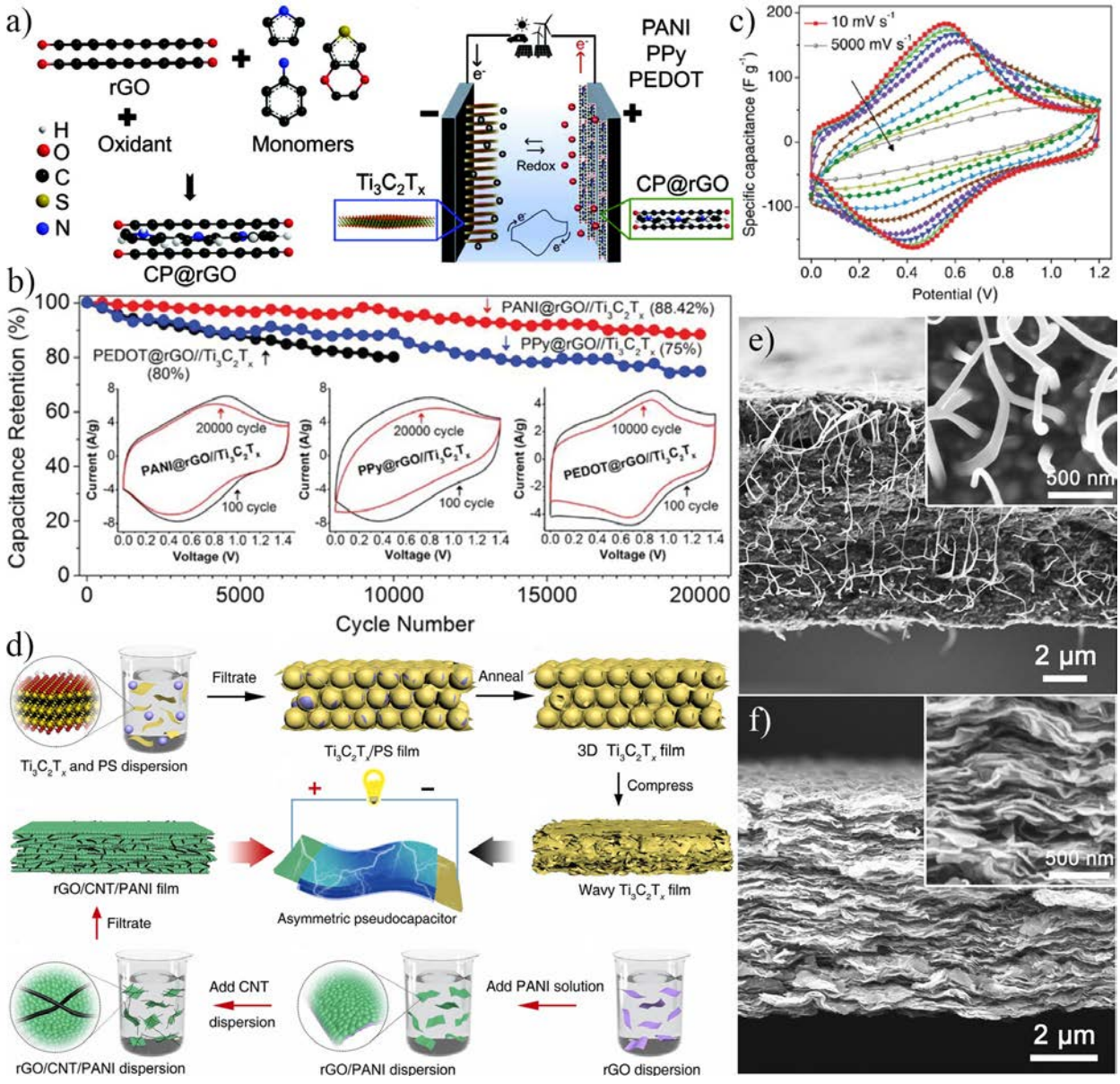

Fig. 22 (a) Illustration for electrodeposition preparation of CP@rGO composite electrodes and assembly of ASC[258]. (b) Cycle performance of $Ti_3C_2T_x$//CP@rGO ASC. (Inset is CV cuvres of different electrodes under different charge-discharge cycles.)[258] Copyright 2018 WILEY-VCH Verlag GmbH & Co. KGaA, Weinheim.

(c) CV curves of the $Ti_3C_2T_x$//CP@rGO ASC at different scan rates[259]. Copyright 2019 WILEY-VCH Verlag GmbH & Co. KGaA, Weinheim. (d) Illustration for preparation of all pseudo-capacitor $Ti_3C_2T_x$//rGO/CNT/PANI ASC[208]. SEM images of the wave $Ti_3C_2T_x$ film (e) and the rGO/CNT/PANI film (f)[208]. Copyright 2020 Elsevier Ltd.

Wang *et al*.[246] successfully prepared PANI/MXene inks into independent self-supporting PANI/MXene films by scraper coating technology, as shown in Fig. 23 (a). The insertion of nanoscale PANI particles facilitates a full contact with the MXene substrate, exposing more ion-accessible active sites to obtain an ideal pseudo-capacitance (Fig. 23 (b)[246]). From the Fig. 23 (c)[246] that the optimal performance of PANI/MXene composite film in 1 M H_2SO_4 was observed with a volume capacitance of 1167 F cm^{-3} at 5 mV s^{-1}. It is worth noting that the presence of a large number of PANI particles makes operating voltage window of the composite electrode extended to 0.8 V (Fig. 23 (d)[246]). In addition, a fully pseudocapacitive ASC device was prepared with MXene and PANI/MXene as the negative electrode and the positive electrode in Fig. 23 (e)[246]. This ASC device provides an energy density of 65.6 Wh L^{-1} at a power density of 1687.3 W L^{-1}.

Li *et al*.[72] prepared $Ti_3C_2T_x$/PEDOT: PSS ($Ti_3C_2T_x$/P-100-H) composite film with excellent performance through simple concentrated H_2SO_4 treatment. In Fig. 23 (f), the three-electrode test outcomes show that in 1 M H_2SO_4 electrolyte, the composite exhibits a volume capacitance of 1065 F cm^{-3} at 2 mV s^{-1}. Furthermore, an extremely tough $Ti_3C_2T_x$/P-100-H//rGO ASC was fabricated with rGO film (positive electrode) and the prepared composite film (negative

electrode). The ASC device provides an energy density of 23 mWh cm^{-3} at a high-power density of 7659 mW cm^{-3}. Since a single ASC can reach a voltage of 1.2V, several ASCs connected in series can be used to make simple light-emitting bracelets, etc., as shown in Fig. 23 (g)[72]. All the studies listed in this article show that MXene/conducting polymers composite films have a great potential as electrodes for SCs.

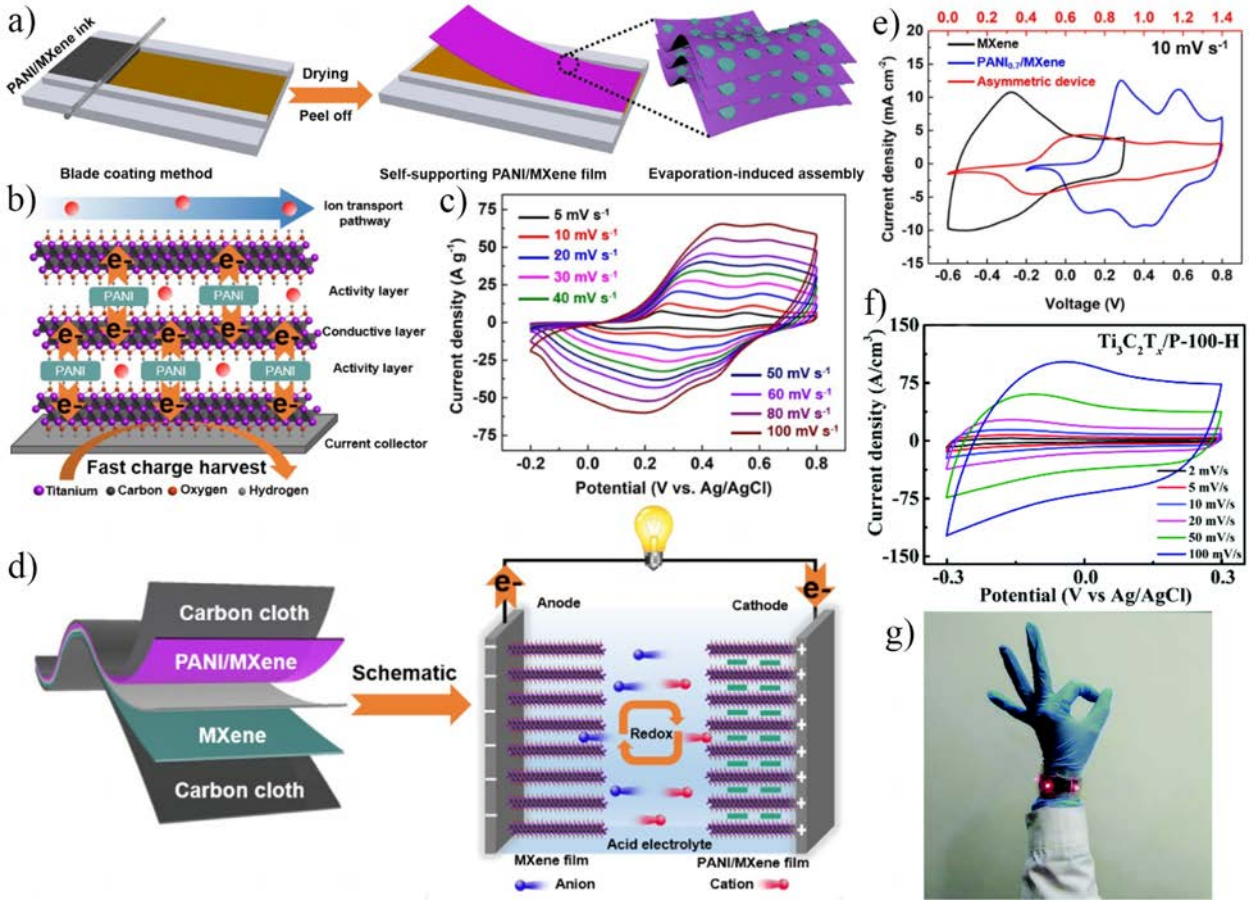

Fig. 23 (a) Schematic diagram of independent self-supporting PANI/MXene film prepared by scraper coating technology[246]. (b) Schematic diagram for the transmission path of ions and electrons in the PANI/MXene membrane electrode[246]. (c) CV curves of PANI/MXene at various scan rates[246]. (d) Schematic diagram of MXene//PANI/MXene ASC[246]. (e) CV curves of MXene electrode, PANI/MXene electrode, and

MXene//PANI/MXene ASC at 10 mV s^{-1} [246]. Copyright 2020 Elsevier B.V. (f) CV curves of $Ti_3C_2T_x$/P-100-H electrode at various scan rates[72]. (g) Optical image of a simple bracelet prepared by several $Ti_3C_2T_x$/P-100-H//rGO ASC in series[72]. Copyright Royal Society of Chemistry.

In general, the SCs assembled by MXene/conducting polymers composite electrodes show good electrochemical performance and stable cycling performance, and MXene/conducting polymers SCs have good application prospects. Table 3 summarizes the performance of MXene/conducting polymers in SCs devices.

Table 2. The applications of MXene/conducting polymers composite electrodes in SCs was mentioned in this review.

Method	Electrode	Electrolyte	Capacity
Ultrasonic stripping	Ti_3C_2 paper	1 M KOH	450 F cm^{-3} 280 F cm^{-3}
Mechanical rolling	Ti_3C_2	1 M H_2SO_4	900 F cm^{-3} 730 F cm^{-3}
Vacuum assisted filtration	$Ti_3C_2T_x$/P-100-H	1 M H_2SO_4	1065 F cm^{-3}
One-step co-electrodeposition	MXene/PPy	1 M H_2SO_4	416 F g^{-1}
Electrophoretic deposition, electrochemical polymerization	Ti_3C_2/PPy	2 M H_2SO_4 PVA/H_2SO_4	109 mF cm^{-2} 87 mF cm^{-2}
Electrochemical polymerization, co-doping	PEDOT: PSS: MXene	10 mM PBS	692 F cm^{-3}
Mechanical compression	Wavy Ti_3C_2	3 M H_2SO_4	1277 F cm^{-3} 790 F cm^{-3}
Two-step electrochemical polymerization	N-Ti_3C_2/PANI	0.5 M H_2SO_4	228 mF g^{-1}
Hydrothermal reaction	MXene/PANI	6 M KOH	563 F g^{-1} 477 F g^{-1}
Chemical oxidation polymerization	TDP	1 M H_2SO_4	452 F g^{-1}
Low-temperature chemical oxidation	$Ti_3C_2T_x$/PPy	1 M Na_2SO_4	184 F g^{-1}
Electrochemically depositing, vacuum assisted filtration	$Ti_3C_2T_x$/PPy	PVA/H_2SO_4	420 F g^{-1}
In-situ synthesis	3D $Ti_3C_2T_x$@PPy	3 M KOH	610 F g^{-1}
Hydrothermal reaction, vacuum assisted filtration	$Mo_{1.33}C$ MXene/PEDOT: PSS	1 M H_2SO_4	1310 F cm^{-3}
—	Ti_2CT_x	1 M KOH	517 F cm^{-3} 307 F cm^{-3}
—	$Ti_3C_2T_x$/PVA	1 M KOH	528 F cm^{-3} 306 F cm^{-3}
Vacuum assisted filtration	RAMX	3 M H_2SO_4	978 F cm^{-3} 736 F cm^{-3}
One-pot in-situ polymerization	$Ti_3C_2T_x$/PANI-NTs	1 M H_2SO_4	597 F g^{-1}
Doctor blade coating technology	PANI/MXene	1 M H_2SO_4	1167 F cm^{-3}
Electrostatic self-assembly	Ti_3C_2/Fe-15%	1 M Li_2SO_4	485 mF cm^{-2}
In-situ polymerization	GMP	1 M H_2SO_4	635 F g^{-1}
Chemical oxidation polymerization, vacuum assisted filtration	PANI@MXene	3 M H_2SO_4	1632 F cm^{-3} 827 F cm^{-3}

Table.3 The research of MXene/conducting polymers in SCs devices mentioned in this review.

Devices	Electrolyte	Capacitance	Energy density at po
$Ti_3C_2T_x$/P-100-H//rGO	1 M H_2SO_4	117 F cm^{-3}, 1.5 mA cm^{-2}	23 mWh cm^{-3} at 765
MXene/PPy//MXene/PPy	1 M H_2SO_4	184 F g^{-1}, 10 mV s^{-1}	—
$Ti_3C_2T_x$//rGO/CNT/PANI	3 M H_2SO_4	117 F g^{-1}, 10 mV s^{-1}	70 Wh L^{-1} at 1.4
		85 F g^{-1}, 1000 mV s^{-1}	34.8 Wh L^{-1} at 1.
AC//MXene/PANI	7 M KOH	262 F g^{-1}, 0.5 A g^{-1}	22.67 Wh kg^{-1} at 2
400PPy175/$Ti_3C_2T_x$//400PPy175/$Ti_3C_2T_x$	1 M H_2SO_4	258 F g^{-1}, 0.5 A g^{-1}	10.82 μWh mg^{-1} at 0.
			3.99 μWh mg^{-1} at 1.8
$Mo_{1.33}C$ MXene/PEDOT: PSS//$Mo_{1.33}C$ MXene/PEDOT: PSS	1 M H_2SO_4	568 F g^{-1}, 0.5 A g^{-1}	33.3 mWh cm^{-3} at 194
$Ti_3C_2T_x$//$Ti_3C_2T_x$	Sea water	27 F cm^{-3}, 0.25 A g^{-1}	1.74×10^{-3} Wh cm^{-3} at
		13 F cm^{-3}, 3 A g^{-1}	0.68×10^{-3} Wh cm^{-3} at
$Ti_3C_2T_x$//$Ti_3C_2T_x$	1 M Li_2SO_4	633 F cm^{-3}, 2 mV s^{-1}	22 Wh L
3D-PMCF//3D-PMCF	3 M H_2SO_4	375 F g^{-1}, 5 mV s^{-1}	9.2 Wh kg
		92 F g^{-1}, 10000 mV s^{-1}	
Ti_2CT_x//Ti_2CT_x	1 M KOH	452 F cm^{-3}, 2 mV s^{-1}	35 mWh cm^{-3} at 0.
		209 F cm^{-3}, 100 mV s^{-1}	17 mWh cm^{-3} at 1
RAMX//RAMX	3 M H_2SO_4	—	40 Wh L^{-1} at 0.8
			21 Wh L^{-1} at 41.
PDT/$Ti_3C_2T_x$//PDT/$Ti_3C_2T_x$	0.5 M H_2SO_4	284 mF cm^{-2}, 0.5mA cm^{-2}	24 mWh cm^{-3} at 5
Ti_3C_2/PANI-NTs//Ti_3C_2/PANI-NTs	1 M H_2SO_4	586 F g^{-1}, 0.1 A g^{-1}	25.6 Wh kg^{-1} at 15
			13.2 Wh kg^{-1} at 161
MXene//PANI/MXene	1 M H_2SO_4	231 F cm^{-3}, 10 mV s^{-1}	65.6 Wh L^{-1} at 168
			40.3 Wh L^{-1} at 10
Ni-dMXNC//$Ti_3C_3T_x$	1 M KOH	—	1.04×10^{-3} Wh cm^{-3} at
$Ti_3C_2T_x$/Fe-15%//MnO_2/CC	1 M Li_2SO_4	115 mF cm^{-2}, 2 mA cm^{-2}	40 mWh cm^{-2} at 8.2
GMP//graphene	1 M H_2SO_4	68 F g^{-1}, 10 A g^{-1}	42.3 Wh kg^{-1} at 9
			25 Wh kg^{-1} at 180
MXene//PANI@MXene	3 M H_2SO_4	87 F g^{-1}, 10 mV s^{-1}	50.6 Wh L^{-1} at 1.
			24.4 Wh L^{-1} at 12

5. Conclusion and outlook

Conducting polymers have been widely used in supercapacitors due to their high theoretical capacity, easy availability of raw materials, low preparation cost, and simple synthesis methods, etc. MXene, with its large graphene-like accessible ion surface area and excellent metal-like conductivity, has been rapidly gaining popularity among researchers in just a decade. This paper reviews the recent research progress of MXene/conducting polymer composites in the field of supercapacitors, including composite material preparation, electrode materials, SSCs and ASCs. Despite the extensive research on MXene and conducting polymers, there are still some challenges that hinder their practical applications.

From a material preparation perspective, conductive polymers have different morphologies and are prone to agglomeration, thus requiring rational design of preparation schemes and precise control of polymerization time. Etching of MXene materials involves corrosive and strong acids such as HF and concentrated HCl. From the reports mentioned previously in the paper, it is easy to see that the surface functional groups, size and morphology of MXene obtained by different etching methods are different. For the bulk preparation of MXene, it is necessary to explore gentler and more convenient etching methods. In addition, the utilization rate of the MAX phase of MXene precursor is relatively low, and it is also necessary to consider how to improve the utilization rate of the MAX phase when exploring a more gentle and convenient etching method.

From a material storage perspective, although low temperature can mitigate the oxidation of MXene, which does not prevent the oxidation of MXene to TiO_2 by oxygen and water molecules. To solve the problem of better utilization of MXene material, the researchers reduced the contact

of functional groups on the MXene surface with oxygen and water molecules by means of end-group protection. For example, Wu et al.[260] performed end-group protection of MXene using sodium citrate, and the results showed that the end-base protection had a significant improvement on the storage time of MXene. Nevertheless, the storage method of MXene is still a difficult problem that hinders its application.

From an electrode material application perspective, MXene is prone to self-stacking due to the lack of support material as the transition metal is etched away. Conducting polymers suffer from swelling during charging and discharging, which affects the electrochemical performance. The effective combination of MXene/conducting polymers not only solves the problem of self-accumulation of MXene and the expansion of the conducting polymers during charging and discharging, but also gives the electrode material practical characteristics such as higher stability and more relaxed use conditions (e.g. temperature, pH value).

Furthermore, since its introduction, MXene has been gradually applied in many fields such as SCs, batteries, sensors, electromagnetic shielding and adsorption. However, MXenes are diverse, with different constituent elements and surface functional groups. Conducting polymers also vary in structure, composition and morphology. The properties of MXene have not been fully exploited and many aspects remain unknown. In the future, it is possible to combine theoretical simulation calculations with experiments, in addition to the need to address the unresolved issues mentioned above. An effective computing system can not only improve research efficiency and reduce unnecessary exploration time, but also is expected to design composite materials with different structures according to different application scenarios. With the development of MXene research,

MXene is also expected to be applied in more different research fields due to its unique and excellent properties.

Acknowledgement

We gratefully appreciate the support of the Natural Science Foundation of Shandong (ZR2019BB063), the Fundamental Research Funds for the Central Universities, North Minzu University (2019KJ008) and the Natural Science Foundation of Ningxia Hui Autonomous Region (2020AAC03199). The author gratitude the environmental and function material team, supported by the Project of Shandong Province Higher Educational Young Innovative Talent Introduction and Cultivation.

Conflict of Interest

The authors declare that they have no conflict of interest.

Reference

[1] S. Bilgen, Structure and environmental impact of global energy consumption, Renewable & Sustainable Energy Reviews 38 (2014) 890-902.

[2] N. Kannan, D. Vakeesan, Solar energy for future world: - A review, Renewable and Sustainable Energy Reviews 62 (2016) 1092-1105.

[3] W.J. Liu, H. Jiang, H.Q. Yu, Emerging applications of biochar-based materials for energy storage and conversion, Energy Environ. Sci. 12 (2019) 1751-1779.

[4] C.C. Liu, K.H. Zheng, Y. Zhou, K. Zhu, Q. Huang, Experimental Thermal Hazard Investigation of Pressure and EC/PC/EMC Mass Ratio on Electrolyte, Energies 14 (2021) 2511.

[5] L. Tan, C. Wei, Y. Zhang, Y. An, S. Xiong, J. Feng, Long-life and dendrite-free zinc metal

anode enabled by a flexible, green and self-assembled zincophilic biomass engineered MXene based interface, Chem. Eng. J. 431 (2022) 134277.

[6] J. Sun, X. Zhang, Q. Du, V. Murugadoss, D. Wu, Z. Guo, The Contribution of Conductive Network Conversion in Thermal Conductivity Enhancement of Polymer Composite: A Theoretical and Experimental Study, ES Materials & Manufacturing 13 (2021) 53-65.

[7] Y. Ma, Z. Zhuang, M.L. Ma, Y.Y. Yang, W.T. Li, J. Lin, M.Y. Dong, S.D. Wu, T. Ding, Z.H. Guo, Solid polyaniline dendrites consisting of high aspect ratio branches self-assembled using sodium lauryl sulfonate as soft templates: Synthesis and electrochemical performance, Polymer 182 (2019) 121808.

[8] M. Zheng, Y. Wei, J. Ren, B. Dai, W. luo, M. Ma, T. Li, Y. Ma, 2-aminopyridine functionalized magnetic core–shell Fe_3O_4@polypyrrole composite for removal of Mn (VII) from aqueous solution by double-layer adsorption, Sep. Purif. Technol. 277 (2021) 119455.

[9] D.J. Xu, G. Huang, L. Guo, Y.J. Chen, C. Ding, C.C. Liu, Enhancement of catalytic combustion and thermolysis for treating polyethylene plastic waste, Adv. Compos. Hybrid Mater. (2021).

[10] X. Dong, X. Zhao, Y. Chen, C. Wang, Investigations about the influence of different carbon matrixes on the electrochemical performance of $Na_3V_2(PO_4)_3$ cathode material for sodium ion batteries, Adv. Compos. Hybrid Mater. 4 (2021) 1070-1081.

[11] C. Liu, D. Xu, J. Weng, S. Zhou, W. Li, Y. Wan, S. Jiang, D. Zhou, J. Wang, Q. Huang, Phase Change Materials Application in Battery Thermal Management System: A Review, Materials 13 (2020) 4622.

[12] J. Ruan, H. Sun, Y. Song, Y. Pang, J. Yang, D. Sun, S. Zheng, Constructing 1D/2D interwoven

carbonous matrix to enable high-efficiency sulfur immobilization in Li-S battery, Energy Mater. 1 (2021) 100018.

[13] H. Hu, F. Ding, H. Ding, J. Liu, M. Xiao, Y. Meng, L. Sun, Sulfonated poly(fluorenyl ether ketone)/Sulfonated α-zirconium phosphate Nanocomposite membranes for proton exchange membrane fuel cells, Adv. Compos. Hybrid Mater. 3 (2020) 498-507.

[14] S.A. Mahadik, A. Patil, H.M. Pathan, S. Salunke-Gawali, R.J. Butcher, Thionaphthoquinones as Photosensitizers for TiO_2 Nanorods and ZnO Nanograin Based Dye-sensitized Solar Cells: Effect of Nanostructures on Charge Transport and Photovoltaic Performance, Engineered Science 14 (2020) 46-58.

[15] J. Zhao, D. Wei, C. Zhang, Q. Shao, V. Murugadoss, Z. Guo, Q. Jiang, X. Yang, An Overview of Oxygen Reduction Electrocatalysts for Rechargeable Zinc-Air Batteries Enabled by Carbon and Carbon Composites, Engineered Science 15 (2021) 1-19.

[16] Y. Shi, J.Z. Wang, S.L. Chou, D. Wexler, H.J. Li, K. Ozawa, H.K. Liu, Y.P. Wu, Hollow structured Li_3VO_4 wrapped with graphene nanosheets in situ prepared by a one-pot template-free method as an anode for lithium-ion batteries, Nano Lett 13 (2013) 4715-4720.

[17] X. Peng, C. Wang, Y. Liu, W. Fang, Y. Zhu, L. Fu, J. Ye, L. Liu, Y. Wu, Critical advances in re-engineering the cathode-electrolyte interface in alkali metal-oxygen batteries, Energy Mater. 1 (2021) 100011.

[18] C. Zhan, X. Zeng, X. Ren, Y. Shen, R. Lv, F. Kang, Z.-H. Huang, Dual-ion hybrid supercapacitor: Integration of Li-ion hybrid supercapacitor and dual-ion battery realized by porous graphitic carbon, J. Energy Chem. 42 (2020) 180-184.

[19] L. Al-Ghussain, R. Samu, O. Taylan, M. Fahrioglu, Sizing renewable energy systems with energy storage systems in microgrids for maximum cost-efficient utilization of renewable energy resources, Sustainable Cities Soc. 55 (2020) 102059.

[20] Z. Dong, S.J. Kennedy, Y. Wu, Electrospinning materials for energy-related applications and devices, J. Power Sources 196 (2011) 4886-4904.

[21] Z. Sun, K. Qu, J. Li, S. Yang, B. Yuan, Z. Huang, Z. Guo, Self-template biomass-derived nitrogen and oxygen co-doped porous carbon for symmetrical supercapacitor and dye adsorption, Adv. Compos. Hybrid Mater. 4 (2021) 1413-1424.

[22] S.S. Patil, T.S. Bhat, A.M. Teli, S.A. Beknalkar, S.B. Dhavale, M.M. Faras, M.M. Karanjkar, P.S. Patil, Hybrid solid state supercapacitors (HSSC's) for high energy & power density: an overview, Engineered Science 12 (2020) 38-51.

[23] H. Dong, Y. Li, H. Chai, Y. Cao, X. Chen, Hydrothermal Synthesis of CuCo S Nano-structure and N-Doped Graphene for High- 2 4 Performance Aqueous Asymmetric Supercapacitors, ES Energy & Environment 4 (2019) 19-26.

[24] L.Y. Pu, J.X. Zhang, N.K.L. Jiresse, Y.F. Gao, H.J. Zhou, N. Naik, P. Gao, Z.H. Guo, N-doped MXene derived from chitosan for the highly effective electrochemical properties as supercapacitor, Adv. Compos. Hybrid Mater. (2021).

[25] K.Q. Qu, W.C. Wang, C. Shi, Z. Sun, H.J. Qi, J.M. Shi, S. Yang, Z.H. Huang, Z.H. Guo, Fungus bran-derived nanoporous carbon with layered structure and rime-like support for enhanced symmetric supercapacitors, J Nanostructure Chem 11 (2021) 769-784.

[26] M.S. Balogun, W. Qiu, W. Wang, P. Fa Ng, X. Lu, Y. Tong, Recent advances in metal nitrides

as high-performance electrode materials for energy storage devices, J. Mater. Chem. A 3 (2014) 1364-1387.

[27] Y. Lu, Q. Zhang, L. Li, Z.Q. Niu, J. Chen, Design Strategies toward Enhancing the Performance of Organic Electrode Materials in Metal-Ion Batteries, Chem 4 (2018) 2786-2813.

[28] Y. Wei, W. Luo, X. Li, Z. Lin, C. Hou, M. Ma, J. Ding, T. Li, Y. Ma, PANI-MnO_2 and $Ti_3C_2T_x$ (MXene) as electrodes for high-performance flexible asymmetric supercapacitors, Electrochim. Acta 406 (2022) 139874.

[29] J.S. Shayeh, M. Sadeghinia, S.O.R. Siadat, A. Ehsani, M. Rezaei, M. Omidi, A novel route for electrosynthesis of $CuCr_2O_4$ nanocomposite with p-type conductive polymer as a high performance material for electrochemical supercapacitors, J Colloid Interface Sci 496 (2017) 401-406.

[30] T. Wang, K. Li, Q. Le, S. Zhu, X. Guo, D. Jiang, Y. Zhang, Tuning parallel manganese dioxide to hollow parallel hydroxyl oxidize iron replicas for high-performance asymmetric supercapacitors, J Colloid Interface Sci 594 (2021) 812-823.

[31] L. Xiao, H. Qi, K. Qu, C. Shi, Y. Cheng, Z. Sun, B. Yuan, Z. Huang, D. Pan, Z. Guo, Layer-by-layer assembled free-standing and flexible nanocellulose/porous Co_3O_4 polyhedron hybrid film as supercapacitor electrodes, Adv. Compos. Hybrid Mater. 4 (2021) 306-316.

[32] K.L. Li, H. Teng, X.J. Dai, Y. Wang, D.S. Wang, X.F. Zhang, Y.J. Yao, X.Y. Liu, L. Feng, J.S. Rao, Y.X. Zhang, Atomic scale modulation strategies and crystal phase transition of flower-like CoAl layered double hydroxides for supercapacitors, CrystEngComm 24 (2022) 2081-2088.

[33] D. Wu, Z. Yao, X. Sun, X. Liu, L. Liu, R. Zhang, C. Wang, Mussel-tailored carbon

fiber/carbon nanotubes interface for elevated interfacial properties of carbon fiber/epoxy composites, Chem. Eng. J. 429 (2022) 132449.

[34] W. Gu, G. Yushin, Review of nanostructured carbon materials for electrochemical capacitor applications: advantages and limitations of activated carbon, carbide-derived carbon, zeolite-templated carbon, carbon aerogels, carbon nanotubes, onion-like carbon, and graphene, Wiley Interdisciplinary Reviews: Energy Environment 3 (2014) 424–473.

[35] J. Yan, Q. Wang, T. Wei, Z.J. Fan, Recent Advances in Design and Fabrication of Electrochemical Supercapacitors with High Energy Densities, Adv. Energy Mater. 4 (2014) 1300816.

[36] M. Zhi, C. Xiang, J. Li, M. Li, N. Wu, Nanostructured carbon-metal oxide composite electrodes for supercapacitors: a review, Nanoscale 5 (2013) 72-88.

[37] M. Ma, Y. Yang, W. Li, Y. Ma, Z. Tong, W. Huang, L. Chen, G. Wu, H. Wang, P. Lyu, Synthesis of yolk-shell structure Fe_3O_4/P(MAA-MBAA)-PPy/Au/ void/TiO_2 magnetic microspheres as visible light active photocatalyst for degradation of organic pollutants, J. Alloys Compd. 810 (2019) 151807.

[38] J. Yan, Z. Fan, W. Tong, W. Qian, M. Zhang, W. Fei, Fast and reversible surface redox reaction of graphene–MnO_2 composites as supercapacitor electrodes, Carbon 48 (2010) 3825-3833.

[39] T.P. Gujar, V.R. Shinde, C.D. Lokhande, W.Y. Kim, K.D. Jung, O.S. Joo, Spray deposited amorphous RuO_2 for an effective use in electrochemical supercapacitor, Electrochem. Commun. 9 (2007) 504-510.

[40] R.A. Fisher, M.R. Watt, W.J. Ready, Functionalized Carbon Nanotube Supercapacitor

Electrodes: A Review on Pseudocapacitive Materials, Ecs Journal of Solid State Science & Technology 2 (2013) M3170-M3177.

[41] L. Zhang, T. Song, L. Shi, N. Wen, Z. Wu, C. Sun, D. Jiang, Z. Guo, Recent progress for silver nanowires conducting film for flexible electronics, J Nanostructure Chem 11 (2021) 323-341.

[42] F. Wang, X. Wu, X. Yuan, Z. Liu, Y. Zhang, L. Fu, Y. Zhu, Q. Zhou, Y. Wu, W. Huang, Latest advances in supercapacitors: from new electrode materials to novel device designs, Chem Soc Rev 46 (2017) 6816-6854.

[43] K. Li, Z. Hu, R. Zhao, J. Zhou, C. Jing, Q. Sun, J. Rao, K. Yao, B. Dong, X. Liu, H. Li, Y. Zhang, J. Ji, A multidimensional rational design of nickel-iron sulfide and carbon nanotubes on diatomite via synergistic modulation strategy for supercapacitors, J Colloid Interface Sci 603 (2021) 799-809.

[44] J. Liang, X. Li, J. Zuo, J. Lin, Z. Liu, Hybrid 0D/2D heterostructures: in-situ growth of 0D g-C_3N_4 on 2D BiOI for efficient photocatalyst, Adv. Compos. Hybrid Mater. 4 (2021) 1122-1136.

[45] Q.-Y. Li, Q. Hao, T. Zhu, M. Zebarjadi, M. Zebarjadi, Nanostructured and Heterostructured 2D Materials for Thermoelectrics, Engineered Science 13 (2020) 24-50.

[46] Y.D. Wei, M.M. Zheng, W.L. Luo, B. Dai, J.J. Ren, M.L. Ma, T.X. Li, Y. Ma, All pseudocapacitive MXene-MnO_2 flexible asymmetric supercapacitor, J. Energy Storage 45 (2022).

[47] M. Xu, T. Liang, M. Shi, H.J.C.R. Chen, Graphene-like two-dimensional materials, Chem. Rev. 113 (2013) 3766-3798.

[48] A. Ehsani, A.A. Heidari, H.M. Shiri, Electrochemical Pseudocapacitors Based on Ternary

Nanocomposite of Conductive Polymer/Graphene/Metal Oxide: An Introduction and Review to it in Recent Studies, Chem Rec 19 (2019) 908-926.

[49] K. Li, S. Feng, C. Jing, Y. Chen, X. Liu, Y. Zhang, L. Zhou, Assembling a double shell on a diatomite skeleton ternary complex with conductive polypyrrole for the enhancement of supercapacitors, Chem Commun (Camb) 55 (2019) 13773-13776.

[50] Q. Gao, Y. Pan, G. Zheng, C. Liu, C. Shen, X. Liu, Flexible multilayered MXene/thermoplastic polyurethane films with excellent electromagnetic interference shielding, thermal conductivity, and management performances, Adv. Compos. Hybrid Mater. 4 (2021) 274-285.

[51] Y. Wang, Y. Liu, C. Wang, H. Liu, J. Zhang, J. Lin, J. Fan, T. Ding, J.E. Ryu, Z. Guo, Significantly Enhanced Ultrathin NiCo-based MOF Nanosheet Electrodes Hybrided with $Ti_3C_2T_x$ MXene for High Performance Asymmetric Supercapacitors, Engineered Science 9 (2020) 50-59.

[52] E. Kovalska, C. Kocabas, Organic electrolytes for graphene-based supercapacitor: Liquid, gel or solid, Materials Today Communications 7 (2016) 155-160.

[53] C. Young, J. Kim, Y.V. Kaneti, Y. Yamauchi, One-step Synthetic Strategy of Hybrid Materials from Bimetallic Metal-Organic Frameworks (MOFs) for Supercapacitor Applications, ACS Appl. Energy Mater. 1 (2018) 2007-2015.

[54] A. Ehsani, M. Bigdeloo, F. Assefi, M. Kiamehr, R. Alizadeh, Ternary nanocomposite of conductive polymer/chitosan biopolymer/metal organic framework: Synthesis, characterization and electrochemical performance as effective electrode materials in pseudocapacitors, Inorg. Chem. Commun. 115 (2020) 107885.

[55] D.F. Du, X.Z. Wu, S. Li, Y. Zhang, W. Xing, L. Li, Q.Z. Xue, P. Bai, Z.F. Yan, Remarkable supercapacitor performance of petal-like LDHs vertically grown on graphene/polypyrrole nanoflakes, J. Mater. Chem. A 5 (2017) 8964-8971.

[56] L. Pu, J. Zhang, N.K.L. Jiresse, Y. Gao, H. Zhou, N. Naik, P. Gao, Z. Guo, N-doped MXene derived from chitosan for the highly effective electrochemical properties as supercapacitor, Adv. Compos. Hybrid Mater. (2021).

[57] W. Luo, Y. Wei, Z. Zhuang, Z. Lin, X. Li, C. Hou, T. Li, Y. Ma, Fabrication of $Ti_3C_2T_x$ MXene/polyaniline composite films with adjustable thickness for high-performance flexible all-solid-state symmetric supercapacitors, Electrochim. Acta 406 (2022) 139871.

[58] A. Yz, D. Jie, B. Ch, C. Lxa, W.A. Qiang, Q.A. D, D. Wyac, Co-doped Mo-Mo_2C cocatalyst for enhanced g-C_3N_4 photocatalytic H_2 evolution, Appl. Catal., B 260 (2020) 118220-118220.

[59] S.J. Zhang, H. Zhuo, S.Q. Li, Z.K. Bao, S.W. Deng, G.L. Zhuang, X. Zhong, Z.Z. Wei, Z.H. Yao, J.G. Wang, Effects of surface functionalization of mxene-based nanocatalysts on hydrogen evolution reaction performance, Catal. Today 368 (2021) 187-195.

[60] B. Ahmed, D.H. Anjum, M.N. Hedhili, Y. Gogotsi, H.N. Alshareef, H2O2 assisted room temperature oxidation of Ti_2C MXene for Li-ion battery anodes, Nanoscale 8 (2016) 7580-7587.

[61] P. Urbankowski, B. Anasori, K. Hantanasirisakul, L. Yang, L. Zhang, B. Haines, S.J. May, S.J.L. Billinge, Y. Gogotsi, 2D molybdenum and vanadium nitrides synthesized by ammoniation of 2D transition metal carbides (MXenes), Nanoscale 9 (2017) 17722-17730.

[62] Z. Pan, F. Cao, X. Hu, X. Ji, A facile method for synthesizing CuS decorated Ti_3C_2 MXene with enhanced performance for asymmetric supercapacitors, J. Mater. Chem. A 7 (2019) 8984-

8992.

[63] A. VahidMohammadi, M. Mojtabavi, N.M. Caffrey, M. Wanunu, M. Beidaghi, Assembling 2D MXenes into Highly Stable Pseudocapacitive Electrodes with High Power and Energy Densities, Adv. Mater. 31 (2019) 1806931.

[64] J. Wang, H. Kang, H. Ma, Y. Liu, Z. Xie, Y. Wang, Z. Fan, Super-Fast Fabrication of MXene Film through a Combination of Ion Induced Gelation and Vacuum-Assisted Filtration, Engineered Science 15 (2021) 57-66.

[65] P.R.C.K. Y. Xie, Hybrid Density Functional Study of Structural and Electronic Properties of Functionalized $Ti_{n+1}X_n$ (X= C, N) monolayers, Physical Review B 87 (2013) 235441.

[66] X. Zang, J. Wang, Y. Qin, T. Wang, C. He, Q. Shao, H. Zhu, N. Cao, Enhancing Capacitance Performance of $Ti_3C_2T_x$ MXene as Electrode Materials of Supercapacitor: From Controlled Preparation to Composite Structure Construction, Nanomicro Lett 12 (2020) 77.

[67] J. Chen, Q. Huang, H. Huang, L. Mao, M. Liu, X. Zhang, Y. Wei, Recent progress and advances in the environmental applications of MXene related materials, Nanoscale 12 (2020) 3574-3592.

[68] M.A. Hope, A.C. Forse, K.J. Griffith, M.R. Lukatskaya, M. Ghidiu, Y. Gogotsi, C.P. Grey, NMR reveals the surface functionalisation of Ti_3C_2 MXene, Phys Chem Chem Phys 18 (2016) 5099-5102.

[69] M. Naguib, M. Kurtoglu, V. Presser, J. Lu, J. Niu, H. Min, L. Hultman, Y. Gogotsi, M.W.J.A.M. Barsoum, Two-Dimensional Nanocrystals: Two-Dimensional Nanocrystals Produced by Exfoliation of Ti3AlC2 (Adv. Mater. 37/2011), Advanced Materials 23 (2011) 4207-

4207.

[70] M.R. Lukatskaya, O. Mashtalir, C.E. Ren, Y. Dall'Agnese, P. Rozier, P.L. Taberna, M. Naguib, P. Simon, M.W. Barsoum, Y. Gogotsi, Cation Intercalation and High Volumetric Capacitance of Two-Dimensional Titanium Carbide, Science 341 (2013) 1502-1505.

[71] M. Ghidiu, M.R. Lukatskaya, M.Q. Zhao, Y. Gogotsi, M.W.J.N. Barsoum, Conductive two-dimensional titanium carbide 'clay' with high volumetric capacitance, Nature 516 (2014) 78-81.

[72] L. Li, N. Zhang, M. Zhang, X. Zhang, Z. Zhang, Flexible $Ti_3C_2T_x$/PEDOT:PSS films with outstanding volumetric capacitance for asymmetric supercapacitors, Dalton Trans 48 (2019) 1747-1756.

[73] C.C. Liu, Q. Huang, K.H. Zheng, J.W. Qin, D.C. Zhou, J. Wang, Impact of Lithium Salts on the Combustion Characteristics of Electrolyte under Diverse Pressures, Energies 13 (2020) 5373.

[74] I. Shown, A. Ganguly, L.C. Chen, K.H. Chen, Conducting polymer-based flexible supercapacitor, Energy Sci. Eng. 3 (2014) 2-26.

[75] Y.D. Wei, W.L. Luo, Z. Zhuang, B. Dai, J.X. Ding, T.X. Li, M.L. Ma, X.Q. Yin, Y. Ma, Fabrication of ternary MXene/MnO_2/polyaniline nanostructure with good electrochemical performances, Adv. Compos. Hybrid Mater. 4 (2021) 1082-1091.

[76] H. Cheng, Y. Pan, Q. Chen, R. Che, G. Zheng, C. Liu, C. Shen, X. Liu, Ultrathin flexible poly(vinylidene fluoride)/MXene/silver nanowire film with outstanding specific EMI shielding and high heat dissipation, Adv. Compos. Hybrid Mater. 4 (2021) 505-513.

[77] S.u. Rehman, R. Ahmed, K. Ma, S. Xu, T. Tao, M.A. Aslam, M. Amir, J. Wang, Composite of Strip-shaped ZIF-67 with Polypyrrole: A Conductive Polymer-MOF Electrode System for

Stable and High Specific Capacitance, Engineered Science 13 (2020) 71-78.

[78] M. Hassan, K.R. Reddy, E. Haque, S.N. Faisal, S. Ghasemi, A.I. Minett, V.G. Gomes, Hierarchical assembly of graphene/polyaniline nanostructures to synthesize free-standing supercapacitor electrode, Composites Science & Technology 98 (2014) 1-8.

[79] R. Ramya, R. Sivasubramanian, M.V. Sangaranarayanan, Conducting polymers-based electrochemical supercapacitors—Progress and prospects, Electrochim. Acta 101 (2013) 109-129.

[80] G.A. Snook, P. Kao, A.S. Best, Conducting-polymer-based supercapacitor devices and electrodes, J. Power Sources 196 (2011) 1-12.

[81] S.R. Sivakkumar, R. Saraswathi, Performance evaluation of poly(N-methylaniline) and polyisothianaphthene in charge-storage devices, J. Power Sources 137 (2004) 322-328.

[82] X. Luo, G. Yang, D.W. Schubert, Electrically conductive polymer composite containing hybrid graphene nanoplatelets and carbon nanotubes: synergistic effect and tunable conductivity anisotropy, Adv. Compos. Hybrid Mater. (2021).

[83] K. Lota, V. Khomenko, E. Frackowiak, Capacitance properties of poly(3,4-ethylenedioxythiophene)/carbon nanotubes composites, J. Phys. Chem. Solids 65 (2004) 295-301.

[84] X. Wang, X. Zeng, D. Cao, Biomass-derived nitrogen-doped porous carbons (NPC) and NPC/ polyaniline composites as high performance supercapacitor materials, Engineered Science 1 (2018) 55-63.

[85] S. Cao, W. Ge, Y. Yang, Q. Huang, X. Wang, High strength, flexible, and conductive graphene/polypropylene fiber paper fabricated via papermaking process, Adv. Compos. Hybrid Mater. (2021).

[86] J. Nan, X. Guo, J. Xiao, X. Li, W. Chen, W. Wu, H. Liu, Y. Wang, M. Wu, G. Wang, Nanoengineering of 2D MXene-Based Materials for Energy Storage Applications, Small 17 (2021) 1902085.

[87] Y.J. Wu, Y.J. Sun, J.F. Zheng, J.H. Rong, H.Y. Li, L. Niu, MXenes: Advanced materials in potassium ion batteries, Chem. Eng. J. 404 (2021) 126565.

[88] M.K. Aslam, T.S. AlGarni, M.S. Javed, S.S.A. Shah, S. Hussain, M.W. Xu, 2D MXene Materials for Sodium Ion Batteries: A review on Energy Storage, J. Energy Storage 37 (2021) 102478.

[89] T. Kshetri, D.T. Tran, H.T. Le, D.C. Nguyen, H.V. Hoa, N.H. Kim, J.H. Lee, Recent advances in MXene-based nanocomposites for electrochemical energy storage applications, Prog. Mater Sci. 117 (2021) 100733.

[90] Z. Chen, M. Asif, R. Wang, Y. Li, X. Zeng, W. Yao, Y. Sun, K. Liao, Recent Trends in Synthesis and Applications of Porous MXene Assemblies: A Topical Review, Chem Rec 22 (2022) e202100261.

[91] C.F. Zhang, V. Nicolosi, Graphene and MXene-based transparent conductive electrodes and supercapacitors, Energy Storage Mater. 16 (2019) 102-125.

[92] R. Ma, Z.T. Chen, D.N. Zhao, X.J. Zhang, J.T. Zhuo, Y.J. Yin, X.F. Wang, G.W. Yang, F. Yi, Ti3C2Tx MXene for electrode materials of supercapacitors, J. Mater. Chem. A 9 (2021) 11501-11529.

[93] K. Nasrin, V. Sudharshan, K. Subramani, M. Sathish, Insights into 2D/2D MXene Heterostructures for Improved Synergy in Structure toward Next-Generation Supercapacitors: A

Review, Adv. Funct. Mater. (2022) 2110267.

[94] Y. Guo, D. Wang, T. Bai, H. Liu, Y. Zheng, C. Liu, C. Shen, Electrostatic self-assembled $NiFe_2O_4/Ti_3C_2T_x$ MXene nanocomposites for efficient electromagnetic wave absorption at ultralow loading level, Adv. Compos. Hybrid Mater. 4 (2021) 602-613.

[95] P. Srivastava, A. Mishra, H. Mizuseki, K.R. Lee, A.K. Singh, Mechanistic Insight into the Chemical Exfoliation and Functionalization of Ti_3C_2 MXene, ACS Appl Mater Interfaces 8 (2016) 24256-24264.

[96] L.Y. Yu, L.F. Hu, B. Anasori, Y.T. Liu, Q.Z. Zhu, P. Zhang, Y. Gogotsi, B. Xu, MXene-Bonded Activated Carbon as a Flexible Electrode for High-Performance Supercapacitors, ACS Energy Lett. 3 (2018) 1597-1603.

[97] Michael Naguib, Olha Mashtalir, Joshua Carle, Volker Presser, Jun Lu, Lars Hultman, Yury Gogotsi, M.W. Barsoum, Two-Dimensional Transition Metal Carbides, ACS Nano 6 (2012) 1322–1331.

[98] M. Naguib, M. Kurtoglu, V. Presser, J. Lu, J. Niu, M. Heon, L. Hultman, Y. Gogotsi, M.W. Barsoum, Two-dimensional nanocrystals produced by exfoliation of Ti_3AlC_2, Adv Mater 23 (2011) 4248-4253.

[99] X. Sang, Y. Xie, M.W. Lin, M. Alhabeb, K.L. Van Aken, Y. Gogotsi, P.R.C. Kent, K. Xiao, R.R. Unocic, Atomic Defects in Monolayer Titanium Carbide ($Ti_3C_2T_x$) MXene, ACS Nano 10 (2016) 9193-9200.

[100] M.A. Hope, A.C. Forse, K.J. Griffith, M.R. Lukatskaya, C.P.J.P.C.C.P. Grey, NMR reveals the surface functionalisation of Ti 3 C 2 MXene, Physical Chemistry Chemical Physics 18 (2016).

[101] F. Wang, C. Yang, C. Duan, D. Xiao, Y. Tang, J. Zhu, An Organ-Like Titanium Carbide Material (MXene) with Multilayer Structure Encapsulating Hemoglobin for a Mediator-Free Biosensor, J. Electrochem. Soc. 162 (2015) B16-B21.

[102] M. Ghidiu, M.R. Lukatskaya, M.Q. Zhao, Y. Gogotsi, M.W. Barsoum, Conductive two-dimensional titanium carbide 'clay' with high volumetric capacitance, Nature 516 (2014) 78-81.

[103] T. Zhang, L.M. Pan, H. Tang, F. Du, Y.H. Guo, T. Qiu, J. Yang, Synthesis of two-dimensional $Ti_3C_2T_x$=MXene using HCl+LiF etchant: Enhanced exfoliation and delamination, J. Alloys Compd. 695 (2017) 818-826.

[104] C. Hou, J. Hou, H. Zhang, Y. Ma, X. He, W. Geng, Q. Zhang, Facile Synthesis of $LiMn_{0.75}Fe_{0.25}PO_4$/C Nanocomposite Cathode Materials of Lithium-Ion Batteries through Microwave Sintering, Engineered Science 11 (2020) 36-43.

[105] C. Hou, B. Wang, V. Murugadoss, S. Vupputuri, Y. Chao, Z. Guo, C. Wang, W. Du, Recent Advances in Co_3O_4 as Anode Materials for High-Performance Lithium-Ion Batteries, Engineered Science 11 (2020) 19-30.

[106] M.-S. Cao, Y.-Z. Cai, P. He, J.-C. Shu, W.-Q. Cao, J. Yuan, 2D MXenes: Electromagnetic property for microwave absorption and electromagnetic interference shielding, Chem. Eng. J. 359 (2019) 1265-1302.

[107] H. Li, Y. Hou, F. Wang, M.R. Lohe, X. Zhuang, L. Niu, X. Feng, Flexible All-Solid-State Supercapacitors with High Volumetric Capacitances Boosted by Solution Processable MXene and Electrochemically Exfoliated Graphene, Adv. Energy Mater. 7 (2017) 1601847.

[108] M.R. Lukatskaya, O. Mashtalir, C.E. Ren, Y. Dall'Agnese, P. Rozier, P.L. Taberna, M.

Naguib, P. Simon, M.W. Barsoum, Y.J.S. Gogotsi, Cation Intercalation and High Volumetric Capacitance of Two-Dimensional Titanium Carbide, Science 341 (2013) 1502-1505.

[109] O. Bubnova, Z.U. Khan, A. Malti, S. Braun, M. Fahlman, M. Berggren, X. Crispin, Optimization of the thermoelectric figure of merit in the conducting polymer poly(3,4-ethylenedioxythiophene), Nat. Mater. 10 (2011) 429.

[110] M. Wan, Conducting Polymers with Micro or Nanometer Structure, Conducting Polymers with Micro or Nanometer Structure2008.

[111] D. Wu, F. Xu, B. Sun, R. Fu, H. He, K. Matyjaszewski, Design and Preparation of Porous Polymers, Chem. Rev. 112 (2012) 3959.

[112] F. Xu, D. Bao, Y. Cui, Y. Gao, D. Lin, X. Wang, J. Peng, H. Geng, H. Wang, Copper nanoparticle-deposited graphite sheets for highly thermally conductive polymer composites with reduced interfacial thermal resistance, Adv. Compos. Hybrid Mater. (2021).

[113] D. Zhang, S. Hu, Y. Sun, X. Liu, H. Wang, H. Wang, Y. Chen, Y. Ni, XTe (X = Ge, Sn, Pb) Monolayers: Promising Thermoelectric Materials with Ultralow Lattice Thermal Conductivity and High-power Factor, ES Energy & Environment 10 (2020) 59-65.

[114] S.D. Li, J.C. Fan, S.Y. Li, Y. Ma, J.H. Wu, H.G. Jin, Z.S. Chao, D. Pan, Z.H. Guo, In situ-grown Co_3O_4 nanorods on carbon cloth for efficient electrocatalytic oxidation of urea, J Nanostructure Chem 11 (2021) 735-749.

[115] A. Ehsani, M.G. Mahjani, M. Bordbar, R. Moshrefi, Poly ortho aminophenol/TiO_2 nanocomposite: Electrosynthesis and characterization, Synth. Met. 165 (2013) 51-55.

[116] R.B. Ambade, S.B. Ambade, N.K. Shrestha, R.R. Salunkhe, W. Lee, S.S. Bagde, J.H. Kim,

F.J. Stadler, Y. Yamauchi, S.H. Lee, Controlled growth of polythiophene nanofibers in TiO_2 nanotube arrays for supercapacitor applications, J. Mater. Chem. A 5 (2017) 172-180.

[117] Y. Ma, M.L. Ma, X.Q. Yin, Q. Shao, N. Lu, Y.N. Feng, Y. Lu, E.K. Wujcik, X.M. Mai, C. Wang, Z.H. Guo, Tuning polyaniline nanostructures via end group substitutions and their morphology dependent electrochemical performances, Polymer 156 (2018) 128-135.

[118] K. Huang, J. Liu, S. Lin, Y. Wu, E. Chen, Z. He, M. Lei, Flexible silver nanowire dry electrodes for long-term electrocardiographic monitoring, Adv. Compos. Hybrid Mater. (2021).

[119] Y. Xue, S. Chen, J. Yu, B.R. Bunes, Z. Xue, J. Xu, B. Lu, L. Zang, Nanostructured conducting polymers and their composites: synthesis methodologies, morphologies and applications, J. Mater. Chem. C 8 (2020) 10136-10159.

[120] K. Qu, Z. Sun, C. Shi, W. Wang, L. Xiao, J. Tian, Z. Huang, Z. Guo, Dual-acting cellulose nanocomposites filled with carbon nanotubes and zeolitic imidazolate framework-67 (ZIF-67)–derived polyhedral porous Co_3O_4 for symmetric supercapacitors, Adv. Compos. Hybrid Mater. 4 (2021) 670-683.

[121] L. Pan, H. Qiu, C. Dou, Y. Li, L. Pu, J. Xu, Y. Shi, Conducting polymer nanostructures: template synthesis and applications in energy storage, Int J Mol Sci 11 (2010) 2636-2657.

[122] M. Xue, F. Li, C. Dong, Z. Yang, X. Wang, J. Ji, Gas Sensors: High-Oriented Polypyrrole Nanotubes for Next-Generation Gas Sensor Advanced Materials 28 (2016) 8067-8067.

[123] I.Y. Choi, J. Lee, H. Ahn, J. Lee, H.C. Choi, M.J. Park, High-Conductivity Two-Dimensional Polyaniline Nanosheets Developed on Ice Surfaces, Angew Chem Int Ed Engl 54 (2015) 10497-10501.

[124] D. Pan, J. Dong, G. Yang, F. Su, B. Chang, C. Liu, Y.-C. Zhu, Z. Guo, Ice template method assists in obtaining carbonized cellulose/boron nitride aerogel with 3D spatial network structure to enhance the thermal conductivity and flame retardancy of epoxy-based composites, Adv. Compos. Hybrid Mater. (2021).

[125] Y. Ma, C.Y. Zhang, C.P. Hou, H. Zhang, H.P. Zhang, Q.Y. Zhang, Z.H. Guo, Cetyl trimethyl ammonium bromide (CTAB) micellar templates directed synthesis of water-dispersible polyaniline rhombic plates with excellent processability and flow-induced color variation, Polymer 117 (2017) 30-36.

[126] W. Wang, Y. Ma, Z. Zhuang, S. Zhou, M. Ma, Q. Wu, R. Bai, T. Li, Synthesis of walnut-like polyaniline by using polyvinyl alcohol micellar template with excellent film transmission, J. Appl. Polym. Sci. 138 (2021).

[127] J. Zhuang, J. Sun, D. Wu, Y. Liu, R.R. Patil, D. Pan, Z. Guo, Multi-factor analysis on thermal conductive property of metal-polymer composite microstructure heat exchanger, Adv. Compos. Hybrid Mater. 4 (2021) 27-35.

[128] J. Chen, Y. Zhu, Z. Guo, A.G. Nasibulin, Recent Progress on Thermo-electrical Properties of Conductive Polymer Composites and Their Application in Temperature Sensors, Engineered Science 12 (2020) 13-22.

[129] C.Q. Zhao, T. Jing, J.Z. Tian, J. Guo, M. Wu, D.N. Shi, Z.Y. Zhao, Z.H. Guo, Visible light-driven photoelectrochemical enzyme biosensor based on reduced graphene oxide/titania for detection of glucose, J Nanostructure Chem (2021).

[130] M. Yong, C. Hou, Z. Hao, M. Qiao, Y. Chen, H. Zhang, Q. Zhang, Z.J.J.o.M.C.A. Guo,

Morphology-dependent electrochemical supercapacitors in multi-dimensional polyanilinenanostructures, Journal of Materials Chemistry A 5 (2017).

[131] A. Ehsani, H. Parsimehr, H. Nourmohammadi, R. Safari, S. Doostikhah, Environment-friendly electrodes using biopolymer chitosan/poly ortho aminophenol with enhanced electrochemical behavior for use in energy storage devices, Polym. Compos. 40 (2019) 4629-4637.

[132] K.L. Li, X.Y. Liu, T.X. Zheng, D.B. Jiang, Z. Zhou, C.Q. Liu, X.M. Zhang, Y.X. Zhang, D. Losic, Tuning MnO_2 to FeOOH replicas with bio-template 3D morphology as electrodes for high performance asymmetric supercapacitors, Chem. Eng. J. 370 (2019) 136-147.

[133] R.J. Deokate, Chemically Deposited $NiCo_2O_4$ Thin Films for Electrochemical Study, ES Materials & Manufacturing 11 (2020) 16-19.

[134] S.G. Sayyed, M.A. Mahadik, A.V. Shaikh, J.S. Jang, H.M. Pathan, Nano-Metal Oxide Based Supercapacitor Via Electrochemical Deposition, ES Energy & Environment 3 (2019) 25-44.

[135] A.B. Gite, B.M. Palve, V.B. Gaikwad, S.D. Shinde, G.H. Jain, H.M. Pathan, Physicochemical Properties and Thermoelectric Studies of Electrochemically Deposited Lead Telluride Films, ES Materials & Manufacturing 11 (2020) 40-49.

[136] H. Borate, A. Bhorde, A. Waghmare, S. Nair, S. Pandharkar, A. Punde, P. Shinde, P. Vairale, V. Jadkar, R. Waykar, S. Rondiya, Y. Hase, R. Aher, N. Patil, M. Prasad, S. Jadkar, Single-step Electrochemical Deposition of CZTS Thin Films with Enhanced Photoactivity, ES Materials & Manufacturing 11 (2020) 30-39.

[137] H.M. Shiri, A. Ehsani, R. Behjatmanesh-Ardakani, S. Hajghani, Electrosynthesis of Y_2O_3 nanoparticles and its nanocomposite with POAP as high efficient electrode materials in energy

storage device: Surface, density of state and electrochemical investigation, Solid State Ionics 338 (2019) 87-95.

[138] C. Debiemme-Chouvy, A. Fakhry, F. Pillier, Electrosynthesis of polypyrrole nano/micro structures using an electrogenerated oriented polypyrrole nanowire array as framework, Electrochim. Acta 268 (2018) 66-72.

[139] M. Berggren, X. Crispin, S. Fabiano, M.P. Jonsson, I. Zozoulenko, Organic Electrochemical Devices: Ion Electron–Coupled Functionality in Materials and Devices Based on Conjugated Polymers Adv. Mater. 31 (2019) 1970160.

[140] P.M. Mana, P.K. Bhujbal, H.M. Pathan, Fabrication and Characterization of ZnS based Photoelectrochemical Solar Cell, ES Energy & Environment 12 (2020) 77-85.

[141] A. Hajian, A.A. Rafati, A. Af Raz, M. Najafi, Electrosynthesis of high-density polythiophene nanotube arrays and their application for sensing of riboflavin, J. Mol. Liq. 199 (2014) 150-155.

[142] M. Raaijmakers, N.E. Benes, Current trends in interfacial polymerization chemistry, Prog. Polym. Sci. 63 (2016) 86-142.

[143] L. Zhang, W. Du, A. Nautiyal, Z. Liu, X. Zhang, Recent progress on nanostructured conducting polymers and composites: synthesis, application and future aspects, Sci. China Mater. 61 (2018) 303–352.

[144] R.V. Ingle, S.F. Shaikh, P.K. Bhujbal, H.M. Pathan, V.A. Tabhane, Polyaniline Doped with Protonic Acids: Optical and Morphological Studies, ES Materials & Manufacturing 8 (2020) 54-59.

[145] L. Chen, C. Lan, B. Xu, K. Bi, Progress on material characterization methods under big data

environment, Adv. Compos. Hybrid Mater. 4 (2021) 235-247.

[146] X. Tang, X. Guo, W. Wu, G. Wang, 2D Metal Carbides and Nitrides (MXenes) as High-Performance Electrode Materials for Lithium-Based Batteries, Adv. Energy Mater. 8 (2018) 1801897.

[147] L. Yu, Z. Fan, Y. Shao, Z. Tian, Z. Liu, Versatile N-Doped MXene Ink for Printed Electrochemical Energy Storage Application, Adv. Energy Mater. 9 (2019) 1901839.

[148] J.H. Huang, X.Q. Cheng, Y.D. Wu, Y.Q. Zhang, S.W. Li, C.H. Lau, L. Shao, Critical operation factors and proposed testing protocol of nanofiltration membranes for developing advanced membrane materials, Adv. Compos. Hybrid Mater. 4 (2021) 1092-1101.

[149] S. Buczek, M.L. Barsoum, S. Uzun, N. Kurra, R. Andris, E. Pomerantseva, K.A. Mahmoud, Y. Gogotsi, Rational Design of Titanium Carbide MXene Electrode Architectures for Hybrid Capacitive Deionization, Energy Environ. Mater. 3 (2020) 398-404.

[150] Y.Z. Zhang, J.K. El-Demellawi, Q. Jiang, G. Ge, H. Liang, K. Lee, X. Dong, H.N. Alshareef, MXene hydrogels: fundamentals and applications, Chem Soc Rev 49 (2020) 7229-7251.

[151] M.Q. Zhao, C.E. Ren, Z. Ling, M.R. Lukatskaya, C. Zhang, K.L. Van Aken, M.W. Barsoum, Y. Gogotsi, Flexible MXene/carbon nanotube composite paper with high volumetric capacitance, Adv Mater 27 (2015) 339-345.

[152] J. Yan, C.E. Ren, K. Maleski, C.B. Hatter, B. Anasori, P. Urbankowski, A. Sarycheva, Y. Gogotsi, Flexible MXene/Graphene Films for Ultrafast Supercapacitors with Outstanding Volumetric Capacitance, Adv. Funct. Mater. 27 (2017) 1701264.

[153] M.R. Lukatskaya, S. Kota, Z. Lin, M.Q. Zhao, N. Shpigel, M. Levi, J. Halim, P.L. Taberna,

M.W. Barsoum, P. Simon, Ultra-high-rate pseudocapacitive energy storage in two-dimensional transition metal carbides, Nat. Energy 2 (2017) 17105.

[154] A. Ehsani, Influence of counter ions in electrochemical properties and kinetic parameters of poly tyramine electroactive film, Prog. Org. Coat. 78 (2015) 133-139.

[155] A. VahidMohammadi, J. Moncada, H. Chen, E. Kayali, J. Orangi, C.A. Carrero, M. Beidaghi, Thick and freestanding MXene/PANI pseudocapacitive electrodes with ultrahigh specific capacitance, J. Mater. Chem. A 6 (2018) 22123-22133.

[156] Q. Zhu, Y. Huang, Y. Li, M. Zhou, S. Xu, X. Liu, C. Liu, B. Yuan, Z. Guo, Aluminum dihydric tripolyphosphate/polypyrrole-functionalized graphene oxide waterborne epoxy composite coatings for impermeability and corrosion protection performance of metals, Adv. Compos. Hybrid Mater. 4 (2021) 780-792.

[157] X. Li, W. Zhao, R. Yin, X. Huang, L. Qian, A Highly Porous Polyaniline-Graphene Composite Used for Electrochemical Supercapacitors, Engineered Science 3 (2018) 89-95.

[158] Y. Ma, C.P. Hou, H.P. Zhang, Q.Y. Zhang, H. Liu, S.D. Wu, Z.H. Guo, Three-dimensional core-shell Fe_3O_4/Polyaniline coaxial heterogeneous nanonets: Preparation and high performance supercapacitor electrodes, Electrochim. Acta 315 (2019) 114-123.

[159] H. Xu, D. Zheng, F. Liu, W. Li, J. Lin, Synthesis of an MXene/polyaniline composite with excellent electrochemical properties, J. Mater. Chem. A 8 (2020) 5853-5858.

[160] M. Boota, B. Anasori, C. Voigt, M.Q. Zhao, M.W. Barsoum, Y. Gogotsi, Pseudocapacitive Electrodes Produced by Oxidant-Free Polymerization of Pyrrole between the Layers of 2D Titanium Carbide (MXene), Adv Mater 28 (2016) 1517-1522.

[161] L. Zhao, K. Wang, W. Wei, L. Wang, W. Han, High-performance flexible sensing devices based on polyaniline/MXene nanocomposites, InfoMat 1 (2019) 407-416.

[162] H. Gu, H. Zhang, C. Gao, C. Lian, J. Gu, Z. Guo, New Functions of Polyaniline, ES Materials & Manufacturing 1 (2018) 3-12.

[163] J. Guo, Z. Chen, W. Abdul, J. Kong, M.A. Khan, D.P. Young, J. Zhu, Z. Guo, Tunable positive magnetoresistance of magnetic polyaniline nanocomposites, Adv. Compos. Hybrid Mater. 4 (2021) 534-542.

[164] X. Jian, M. He, L. Chen, M.-m. Zhang, R. Li, L.-j. Gao, F. Fu, Z.-h. Liang, Three-dimensional carambola-like MXene/polypyrrole composite produced by one-step co-electrodeposition method for electrochemical energy storage, Electrochim. Acta 318 (2019) 820-827.

[165] Y. Huang, H.F. Li, Z.F. Wang, M.S. Zhu, Z.X. Pei, Q. Xue, Y. Huang, C.Y. Zhi, Nanostructured Polypyrrole as a flexible electrode material of supercapacitor, Nano Energy 22 (2016) 422-438.

[166] V. Elayappan, V. Murugadoss, Z. Fei, P.J. Dyson, S. Angaiah, Influence of Polypyrrole Incorporated Electrospun Poly(vinylidene fluoride-co-hexafluoropropylene) Nanofibrous Composite Membrane Electrolyte on the Photovoltaic Performance of Dye Sensitized Solar Cell, Engineered Science 10 (2020) 78-84.

[167] C. Zhang, S.K. Xu, D. Cai, J.M. Cao, L.L. Wang, W. Han, Planar supercapacitor with high areal capacitance based on Ti_3C_2/Polypyrrole composite film, Electrochim. Acta 330 (2020) 135277.

[168] D. Wei, W. Wu, J. Zhu, C. Wang, C. Zhao, L. Wang, A facile strategy of polypyrrole nanospheres grown on Ti_3C_2-MXene nanosheets as advanced supercapacitor electrodes, J. Electroanal. Chem. 877 (2020) 114538.

[169] H. Wei, A. Li, D. Kong, Z. Li, D. Cui, T. Li, B. Dong, Z. Guo, Polypyrrole/reduced graphene aerogel film for wearable piezoresisitic sensors with high sensing performances, Adv. Compos. Hybrid Mater. 4 (2021) 86-95.

[170] J. Guo, X. Li, H. Liu, D.P. Young, G. Song, K. Song, J. Zhu, J. Kong, Z. Guo, Tunable magnetoresistance of core-shell structured polyaniline nanocomposites with 0-, 1-, and 2-dimensional nanocarbons, Adv. Compos. Hybrid Mater. 4 (2021) 51-64.

[171] L.F. Gao, C. Li, W.C. Huang, S. Mei, H. Lin, Q. Ou, Y. Zhang, J. Guo, F. Zhang, S.X. Xu, H. Zhang, MXene/Polymer Membranes: Synthesis, Properties, and Emerging Applications, Chem. Mater. 32 (2020) 1703-1747.

[172] Y.J. Wan, X.M. Li, P.L. Zhu, R. Sun, C.P. Wong, W.H. Liao, Lightweight, flexible MXene/polymer film with simultaneously excellent mechanical property and high-performance electromagnetic interference shielding, Composites Part a-Applied Science and Manufacturing 130 (2020) 105764.

[173] S. Wustoni, A. Saleh, J.K. El-Demellawi, A. Koklu, A. Hama, V. Druet, N. Wehbe, Y.Z. Zhang, S. Inal, MXene improves the stability and electrochemical performance of electropolymerized PEDOT films, APL Mater. 8 (2020) 121105.

[174] C.L. Hou, H.Z. Yu, Modifying the nanostructures of PEDOT:PSS/$Ti_3C_2T_X$ composite hole transport layers for highly efficient polymer solar cells, J. Mater. Chem. C 8 (2020) 4169-4180.

[175] X. Guan, W. Feng, X. Wang, R. Venkatesh, J. Ouyang, Significant Enhancement in the Seebeck Coefficient and Power Factor of p-Type Poly(3,4-ethylenedioxythiophene):Poly(styrenesulfonate) through the Incorporation of n-Type MXene, ACS Appl Mater Interfaces 12 (2020) 13013-13020.

[176] Z. Chen, Y. Han, T. Li, X. Zhang, T. Wang, Z. Zhang, Preparation and electrochemical performances of doped MXene/poly(3,4-ethylenedioxythiophene) composites, Mater. Lett. 220 (2018) 305-308.

[177] X. Li, J. Yan, K. Zhu, Fabrication and Characterization of Pt doped Ti/Sb-SnO_2 Electrode and its Efficient Electro-Catalytic Activity toward Phenol, Engineered Science 15 (2021) 38-46.

[178] C. Chen, M. Boota, X. Xie, M. Zhao, B. Anasori, C.E. Ren, L. Miao, J. Jiang, Y. Gogotsi, Charge transfer induced polymerization of EDOT confined between 2D titanium carbide layers, J. Mater. Chem. A 5 (2017) 5260-5265.

[179] W.W. Chiu, J. Travas-Sejdic, R.P. Cooney, G.A. Bowmaker, Studies of dopant effects in poly(3,4-ethylenedi-oxythiophene) using Raman spectroscopy, J. Raman Spectrosc. 37 (2010) 1354-1361.

[180] A. Umar, R. Kumar, H. Algadi, J. Ahmed, M. Jalalah, A.A. Ibrahim, F.A. Harraz, M.A. Alsaiari, H. Albargi, Highly sensitive and selective 2-nitroaniline chemical sensor based on Ce-doped SnO_2 nanosheets/Nafion-modified glassy carbon electrode, Adv. Compos. Hybrid Mater. 4 (2021) 1015-1026.

[181] X. Zheng, J. Shen, Q. Hu, W. Nie, Z. Wang, L. Zou, C. Li, Vapor phase polymerized conducting polymer/MXene textiles for wearable electronics, Nanoscale 13 (2021) 1832-1841.

[182] S. Hwang, N.I. Park, Y.J. Choi, S.M. Lee, S.Y. Han, D.W. Chung, S. Lee, PEDOT:PSS nanocomposite via partial intercalation of monomer into colloidal graphite prepared by in-situ polymerization, J. Ind. Eng. Chem. 76 (2019) 116-121.

[183] J. Zhang, S. Seyedin, Z. Gu, W. Yang, X. Wang, J.M. Razal, MXene: a potential candidate for yarn supercapacitors, Nanoscale 9 (2017) 18604-18608.

[184] S. Hussain, H.L. Liu, D. Vikraman, M. Hussain, S.H.A. Jaffery, A. Ali, H.S. Kim, J.W. Kang, J.W. Jung, Characteristics of Mo_2C-CNTs hybrid blended hole transport layer in the perovskite solar cells and X-ray detectors, J. Alloys Compd. 885 (2021) 161039.

[185] H.G. Liu, Z. Hu, Q.L. Liu, P. Sun, Y.F. Wang, S.L. Chou, Z.Z. Hu, Z.Q. Zhang, Single-atom Ru anchored in nitrogen-doped MXene ($Ti_3C_2T_x$) as an efficient catalyst for the hydrogen evolution reaction at all pH values, J. Mater. Chem. A 8 (2020) 24710-24717.

[186] K. Zhang, Z. Ma, H. Deng, Q. Fu, Improving high-temperature energy storage performance of PI dielectric capacitor films through boron nitride interlayer, Adv. Compos. Hybrid Mater. (2021).

[187] S. Najib, E. Erdem, Current progress achieved in novel materials for supercapacitor electrodes: mini review, Nanoscale Adv. 1 (2019) 2817-2827.

[188] M. Xu, Y. Huang, R. Chen, Q. Huang, Y. Yang, L. Zhong, J. Ren, X. Wang, Green conversion of Ganoderma lucidum residues to electrode materials for supercapacitors, Adv. Compos. Hybrid Mater. 4 (2021) 1270-1280.

[189] S. Kasap, I.I. Kaya, S. Repp, E. Erdem, Superbat: battery-like supercapacitor utilized by graphene foam and zinc oxide (ZnO) electrodes induced by structural defects, Nanoscale Adv. 1

(2019) 2586-2597.

[190] S. Liu, H. Du, K. Liu, M.-G. Ma, Y.-E. Kwon, C. Si, X.-X. Ji, S.-E. Choi, X. Zhang, Flexible and porous Co_3O_4-carbon nanofibers as binder-free electrodes for supercapacitors, Adv. Compos. Hybrid Mater. 4 (2021) 1367-1383.

[191] R. Sahoo, D.T. Pham, T.H. Lee, T.H.T. Luu, J. Seok, Y.H. Lee, Redox-Driven Route for Widening Voltage Window in Asymmetric Supercapacitor, ACS Nano 12 (2018) 8494-8505.

[192] L.L. Tu, C.Y. Jia, Conducting Polymers as Electrode Materials for Supercapacitors, Progress in Chemistry 22 (2010) 1610-1618.

[193] C. Xia, Y.B. Xie, H.X. Du, W. Wang, Ternary nanocomposite of polyaniline/manganese dioxide/titanium nitride nanowire array for supercapacitor electrode, J. Nanopart. Res. 17 (2015) 1-12.

[194] P. Wang, L. Yang, S. Gao, X. Chen, T. Cao, C. Wang, H. Liu, X. Hu, X. Wu, S. Feng, Enhanced dielectric properties of high glass transition temperature PDCPD/CNT composites by frontal ring-opening metathesis polymerization, Adv. Compos. Hybrid Mater. 4 (2021) 639-646.

[195] S.H. Kazemi, B. Hosseinzadeh, H. Kazemi, M.A. Kiani, S. Hajati, Facile Synthesis of Mixed Metal-Organic Frameworks: Electrode Materials for Supercapacitors with Excellent Areal Capacitance and Operational Stability, ACS Appl Mater Interfaces 10 (2018) 23063-23073.

[196] S.Y. Sun, M.J. Huang, P.C. Wang, M. Lu, Controllable Hydrothermal Synthesis of Ni/Co MOF as Hybrid Advanced Electrode Materials for Supercapacitor, J. Electrochem. Soc. 166 (2019) A1799-A1805.

[197] Y. Wang, Y.-J. Hu, X. Hao, P. Peng, J.-Y. Shi, F. Peng, R.-C. Sun, Hydrothermal synthesis

and applications of advanced carbonaceous materials from biomass: a review, Adv. Compos. Hybrid Mater. 3 (2020) 267-284.

[198] P. Saxena, P. Shukla, A comprehensive review on fundamental properties and applications of poly(vinylidene fluoride) (PVDF), Adv. Compos. Hybrid Mater. 4 (2021) 8-26.

[199] X. He, D. Ou, S. Wu, Y. Luo, Y. Ma, J. Sun, A mini review on factors affecting network in thermally enhanced polymer composites: filler content, shape, size, and tailoring methods, Adv. Compos. Hybrid Mater. 5 (2021) 21-38.

[200] J. Yang, Y. Liu, S.L. Liu, L. Li, C. Zhang, T.X. Liu, Conducting polymer composites: material synthesis and applications in electrochemical capacitive energy storage, Mater. Chem. Front. 1 (2017) 251-268.

[201] P.P. Bag, G.P. Singh, S. Singha, G. Roymahapatra, Synthesis of Metal-Organic Frameworks (MOFs) and Their Applications to Biology, Catalysis and Electrochemical Charge Storage: A Mini Review, Engineered Science 13 (2020) 1-10.

[202] Y. Ma, X. Xie, W. Yang, Z. Yu, X. Sun, Y. Zhang, X. Yang, H. Kimura, C. Hou, Z. Guo, W. Du, Recent advances in transition metal oxides with different dimensions as electrodes for high-performance supercapacitors, Adv. Compos. Hybrid Mater. 4 (2021) 906-924.

[203] C.J. Zhang, B. Anasori, A. Seral-Ascaso, S.H. Park, N. Mcevoy, A. Shmeliov, G.S. Duesberg, J.N. Coleman, Y. Gogotsi, V. Nicolosi, Transparent, Flexible, and Conductive 2D Titanium Carbide (MXene) Films with High Volumetric Capacitance, Adv. Mater. 29 (2017) 1702678.

[204] X. Sang, Y. Xie, M.W. Lin, M. Alhabeb, R.R.J.A.N. Unocic, Atomic Defects in Monolayer

Titanium Carbide (Ti3C2Tx) MXene, Acs Nano 10 (2016) 9193-9200.

[205] Fafarman, T. Aaron, Ghidiu, J. Michael, Gogotsi, Yury, Barsoum, W. Michel, Krick, L. Alex, Highly Conductive Optical Quality Solution-Processed Films of 2D Titanium Carbide, Adv. Funct. Mater. 26 (2016) 4162-4168.

[206] H.M. Jiang, Z.G. Wang, Q. Yang, M. Hanif, Z.M. Wang, L.C. Dong, M.D. Dong, A novel $MnO_2/Ti_3C_2T_x$ MXene nanocomposite as high performance electrode materials for flexible supercapacitors, Electrochim. Acta 290 (2018) 695-703.

[207] C.X. Lu, A.R. Li, T.F. Zhai, C.R. Niu, H.P. Duan, L. Guo, W. Zhou, Interface design based on Ti_3C_2 MXene atomic layers of advanced battery-type material for supercapacitors, Energy Storage Mater. 26 (2020) 472-482.

[208] K. Li, X.H. Wang, X.F. Wang, M.Y. Liang, V. Nicolosi, Y.X. Xu, Y. Gogotsi, All-pseudocapacitive asymmetric MXene-carbon-conducting polymer supercapacitors, Nano Energy 75 (2020) 104971.

[209] Z. Fan, J. Wang, H. Kang, Y. Wang, Z. Xie, Z. Cheng, Y. Liu, A Compact MXene Film with Folded Structure for Advanced Supercapacitor Electrode Material, ACS Appl. Energy Mater. 3 (2020) 1811-1820.

[210] R. Nie, Q. Wang, P. Sun, R. Wang, Q. Yuan, X. Wang, Pulsed Laser Deposition of $NiSe_2$ Film on Carbon Nanotubes for High-Performance Supercapacitor, Engineered Science 6 (2018) 22-29.

[211] W.L. Wu, D.J. Niu, J.F. Zhu, Y. Gao, D. Wei, X.H. Liu, F. Wang, L. Wang, L.Q. Yang, Organ-like Ti_3C_2 Mxenes/polyaniline composites by chemical grafting as high-performance

supercapacitors, J. Electroanal. Chem. 847 (2019) 113203.

[212] Y. Li, P. Kamdem, X.J. Jin, Hierarchical architecture of MXene/PANI hybrid electrode for advanced asymmetric supercapacitors, J. Alloys Compd. 850 (2021) 156608.

[213] Y. Ma, C. Hou, H. Zhang, M. Qiao, Y. Chen, H. Zhang, Q. Zhang, Z. Guo, Morphology-dependent electrochemical supercapacitors in multi-dimensional polyaniline nanostructures, J. Mater. Chem. A 5 (2017) 14041-14052.

[214] Z. Chen, Y. Wang, J. Han, T. Wang, Y. Leng, Y. Wang, T. Li, Y. Han, Preparation of Polyaniline onto dl-Tartaric Acid Assembled MXene Surface as an Electrode Material for Supercapacitors, ACS Appl. Energy Mater. 3 (2020) 9326-9336.

[215] W.L. Wu, D. Wei, J.F. Zhu, D.J. Niu, F. Wang, L. Wang, L.Q. Yang, P.P. Yang, C.W. Wang, Enhanced electrochemical performances of organ-like Ti_3C_2 MXenes/polypyrrole composites as supercapacitors electrode materials, Ceram. Int. 45 (2019) 7328-7337.

[216] L. Tong, C. Jiang, K.F. Cai, P. Wei, High-performance and freestanding PPy/Ti3C2Tx composite film for flexible all-solid-state supercapacitors, Journal of Power Sources 465 (2020).

[217] T.A. Le, N.Q. Tran, Y. Hong, H. Lee, Intertwined Titanium Carbide MXene within a 3 D Tangled Polypyrrole Nanowires Matrix for Enhanced Supercapacitor Performances, Chemistry 25 (2019) 1037-1043.

[218] Q. Tao, M. Dahlqvist, J. Lu, S. Kota, R. Meshkian, J. Halim, J. Palisaitis, L. Hultman, M.W. Barsoum, P.O.A. Persson, J. Rosen, Two-dimensional $Mo_{1.33}C$ MXene with divacancy ordering prepared from parent 3D laminate with in-plane chemical ordering, Nat Commun 8 (2017) 14949.

[219] L. Qin, Q. Tao, A. El Ghazaly, J. Fernandez-Rodriguez, P.O.Å. Persson, J. Rosen, F. Zhang,

High-Performance Ultrathin Flexible Solid-State Supercapacitors Based on Solution Processable $Mo_{1.33}C$ MXene and PEDOT:PSS, Adv. Funct. Mater. 28 (2018) 1703808.

[220] X. Wang, S. Kajiyama, H. Iinuma, E. Hosono, S. Oro, I. Moriguchi, M. Okubo, A. Yamada, Pseudocapacitance of MXene nanosheets for high-power sodium-ion hybrid capacitors, Nat Commun 6 (2015) 6544.

[221] J. Cai, W. Xu, Y. Liu, Z. Zhu, G. Liu, W. Ding, G. Wang, H. Wang, Y. Luo, Robust Construction of Flexible Bacterial Cellulose@Ni(OH) Paper: Toward High 2 Capacitance and Sensitive H_2O_2 Detection, Engineered Science 5 (2018) 21-29.

[222] J. Huang, Q. Chen, S. Chen, L. Luo, J. Li, C. Lin, Y. Chen, Al^{3+}-doped $FeNb_{11}O_{29}$ anode materials with enhanced lithium-storage performance, Adv. Compos. Hybrid Mater. 4 (2021) 733-742.

[223] H. Yan, X. Dai, K. Ruan, S. Zhang, X. Shi, Y. Guo, H. Cai, J. Gu, Flexible thermally conductive and electrically insulating silicone rubber composite films with BNNS@Al_2O_3 fillers, Adv. Compos. Hybrid Mater. 4 (2021) 36-50.

[224] (!!! INVALID CITATION !!! [145]).

[225] Q. Jiang, N. Kurra, M. Alhabeb, Y. Gogotsi, H.N. Alshareef, All Pseudocapacitive MXene-RuO_2 Asymmetric Supercapacitors, Adv. Energy Mater. 8 (2018) 1703043.

[226] S. De, C.K. Maity, S. Sahoo, G.C. Nayak, Polyindole Booster for $Ti_3C_2T_x$ MXene Based Symmetric and Asymmetric Supercapacitor Devices, ACS Appl. Energy Mater. 4 (2021) 3712-3723.

[227] F. Ding, H. Hu, H. Ding, J. Liu, Y. Chen, M. Xiao, Y. Meng, L. Sun, Sulfonated

poly(fluorene ether ketone) (SPFEK)/α-zirconium phosphate (ZrP) nanocomposite membranes for fuel cell applications, Adv. Compos. Hybrid Mater. 3 (2020) 546-550.

[228] C. Chen, J. Hu, Z. Xu, Z. Wang, Y. Wang, L. Zeng, X. Liu, Y. Li, Y. Mai, F. Guo, Natural methionine-passivated $MAPbI_3$ perovskite films for efficient and stable solar devices, Adv. Compos. Hybrid Mater. 4 (2021) 1261-1269.

[229] Q.X. Xia, N.M. Shinde, T. Zhang, J.M. Yun, A. Zhou, R.S. Mane, S. Mathur, K.H. Kim, Seawater electrolyte-mediated high volumetric MXene-based electrochemical symmetric supercapacitors, Dalton Trans 47 (2018) 8676-8682.

[230] C.H. Yang, Y. Tang, Y.P. Tian, Y.Y. Luo, Y.C. He, X.T. Yin, W.X. Que, Achieving of Flexible, Free-Standing, Ultracompact Delaminated Titanium Carbide Films for High Volumetric Performance and Heat-Resistant Symmetric Supercapacitors, Adv. Funct. Mater. 28 (2018) 1705487.

[231] P. Zhang, Q. Zhu, R.A. Soomro, S. He, N. Sun, N. Qiao, B. Xu, In Situ Ice Template Approach to Fabricate 3D Flexible MXene Film-Based Electrode for High Performance Supercapacitors, Adv. Funct. Mater. 30 (2020) 2000922.

[232] K. Zhu, Y. Jin, F. Du, S. Gao, Z. Gao, X. Meng, G. Chen, Y. Wei, Y. Gao, Synthesis of Ti_2CT_x MXene as electrode materials for symmetric supercapacitor with capable volumetric capacitance, J. Energy Chem. 31 (2019) 11-18.

[233] Z. Ling, C.E. Ren, M.Q. Zhao, J. Yang, J.M. Giammarco, J. Qiu, M.W. Barsoum, Y. Gogotsi, Flexible and conductive MXene films and nanocomposites with high capacitance, Proc Natl Acad Sci U S A 111 (2014) 16676-16681.

[234] Z.T. Wu, X.C. Liu, T.X. Shang, Y.Q. Deng, N. Wang, X.M. Dong, J. Zhao, D.R. Chen, Y. Tao, Q.H. Yang, Reassembly of MXene Hydrogels into Flexible Films towards Compact and Ultrafast Supercapacitors, Adv. Funct. Mater. 31 (2021) 2102874.

[235] M.Q. Zhao, X. Xie, C.E. Ren, T. Makaryan, B. Anasori, G. Wang, Y. Gogotsi, Hollow MXene Spheres and 3D Macroporous MXene Frameworks for Na-Ion Storage, Adv Mater 29 (2017) 1702410.

[236] P. Das, Z.S. Wu, MXene for energy storage: present status and future perspectives, Journal of Physics-Energy 2 (2020) 032004.

[237] G.K. Rahane, S.B. Jathar, S.R. Rondiya, Y.A. Jadhav, S.V. Barma, A. Rokade, R.W. Cross, M.P. Nasane, V. Jadkar, N.Y. Dzade, S.R. Jadkar, Photoelectrochemical Investigation on the Cadmium Sulfide (CdS) Thin Films Prepared using Spin Coating Technique, ES Materials & Manufacturing 11 (2020) 57-64.

[238] J. Wang, J. Wang, Z. Kong, K. Lv, C. Teng, Y. Zhu, Conducting-Polymer-Based Materials for Electrochemical Energy Conversion and Storage, Adv Mater 29 (2017) 1703044.

[239] G.S. Gund, J.H. Park, R. Harpalsinh, M. Kota, J.H. Shin, T.-i. Kim, Y. Gogotsi, H.S. Park, MXene/Polymer Hybrid Materials for Flexible AC-Filtering Electrochemical Capacitors, Joule 3 (2019) 164-176.

[240] J.M. Li, A. Levitt, N. Kurra, K. Juan, N. Noriega, X. Xiao, X.H. Wang, H.Z. Wang, H.N. Alshareef, Y. Gogotsi, MXene-conducting polymer electrochromic microsupercapacitors, Energy Storage Mater. 20 (2019) 455-461.

[241] M.O. Faruk, A. Ahmed, B. Adak, M. Marzana, M.M. Hossain, S. Mukhopadhyay, High

performance 2D MXene based conducting polymer hybrids: synthesis to emerging applications, J. Mater. Chem. C 9 (2021) 10193-10215.

[242] B. Wang, X. Sun, X. Xie, J. Wang, L. Li, K. Jiao, Experimental Investigation of a Novel Cathode Matrix Flow Field in Proton Exchange Membrane Fuel Cell, ES Energy & Environment 12 (2021) 95-107.

[243] X.M. Wu, B. Huang, R.Y. Lv, Q.G. Wang, Y. Wang, Highly flexible and low capacitance loss supercapacitor electrode based on hybridizing decentralized conjugated polymer chains with MXene, Chem. Eng. J. 378 (2019) 122246.

[244] W. Wu, C. Wang, C. Zhao, D. Wei, J. Zhu, Y. Xu, Facile strategy of hollow polyaniline nanotubes supported on Ti_3C_2-MXene nanosheets for High-performance symmetric supercapacitors, J Colloid Interface Sci 580 (2020) 601-613.

[245] Y. Zhou, Y. Zou, Z. Peng, C. Yu, W. Zhong, Arbitrary deformable and high-strength electroactive polymer/MXene anti-exfoliative composite films assembled into high performance, flexible all-solid-state supercapacitors, Nanoscale 12 (2020) 20797-20810.

[246] Y. Wang, X. Wang, X. Li, Y. Bai, H. Xiao, Y. Liu, G. Yuan, Scalable fabrication of polyaniline nanodots decorated MXene film electrodes enabled by viscous functional inks for high-energy-density asymmetric supercapacitors, Chem. Eng. J. 405 (2021) 126664.

[247] C. Couly, M. Alhabeb, K.L. Van Aken, N. Kurra, L. Gomes, A.M. Navarro-Suárez, B. Anasori, H.N. Alshareef, Y. Gogotsi, Asymmetric Flexible MXene-Reduced Graphene Oxide Micro-Supercapacitor, Adv. Electron. Mater. 4 (2017) 1700339.

[248] M. Boota, M. Bécuwe, Y. Gogotsi, Phenothiazine–MXene Aqueous Asymmetric

Pseudocapacitors, ACS Appl. Energy Mater. 3 (2020) 3144-3149.

[249] Y. Su, H. Yin, X. Wang, Y. Ma, S. Vupputuri, Z. Guo, G. Song, Preparation and properties of ethylene-acrylate salt ionomer/polypropylene antistatic alloy, Adv. Compos. Hybrid Mater. 4 (2021) 104-113.

[250] Q.X. Xia, J. Fu, J.M. Yun, R.S. Mane, K.H. Kim, High volumetric energy density annealed-MXene-nickel oxide/MXene asymmetric supercapacitor, RSC Adv. 7 (2017) 11000-11011.

[251] K. Zhao, H. Wang, C. Zhu, S. Lin, Z. Xu, X. Zhang, Free-standing MXene film modified by amorphous FeOOH quantum dots for high-performance asymmetric supercapacitor, Electrochim. Acta 308 (2019) 1-8.

[252] J. Liu, M. Zheng, X. Shi, H. Zeng, H. Xia, Amorphous FeOOH Quantum Dots Assembled Mesoporous Film Anchored on Graphene Nanosheets with Superior Electrochemical Performance for Supercapacitors, Adv. Funct. Mater. 26 (2016) 919-930.

[253] Y. Guo, Q. Jiang, B. Peng, X. Zan, Investigating Dynamic Processes of Nanomaterials Using in Situ Liquid Phase TEM Technologies: 2014-2019, Engineered Science 9 (2020) 17-24.

[254] L. Qin, Q. Tao, X. Liu, M. Fahlman, J. Halim, P.O.Å. Persson, J. Rosen, F. Zhang, Polymer-MXene composite films formed by MXene-facilitated electrochemical polymerization for flexible solid-state microsupercapacitors, Nano Energy 60 (2019) 734-742.

[255] M. Boota, M. Rajesh, M. Becuwe, Multi-electron redox asymmetric supercapacitors based on quinone-coupled viologen derivatives and $Ti_3C_2T_x$ MXene, Mater. Today Energy 18 (2020) 100532.

[256] W. Liang, I. Zhitomirsky, MXene–carbon nanotube composite electrodes for high active

mass asymmetric supercapacitors, J. Mater. Chem. A 9 (2021) 10335-10344.

[257] J. Fu, J. Yun, S. Wu, L. Li, L. Yu, K.H. Kim, Architecturally Robust Graphene-Encapsulated MXene Ti_2CT_x@Polyaniline Composite for High-Performance Pouch-Type Asymmetric Supercapacitor, ACS Appl Mater Interfaces 10 (2018) 34212-34221.

[258] M. Boota, Y. Gogotsi, MXene-Conducting Polymer Asymmetric Pseudocapacitors, Adv. Energy Mater. 9 (2019) 1802917.

[259] K. Li, X. Wang, S. Li, P. Urbankowski, J. Li, Y. Xu, Y. Gogotsi, An Ultrafast Conducting Polymer@MXene Positive Electrode with High Volumetric Capacitance for Advanced Asymmetric Supercapacitors, Small 16 (2020) 1906851.

[260] C.-W. Wu, B. Unnikrishnan, I.W.P. Chen, S.G. Harroun, H.-T. Chang, C.-C. Huang, Oxidation resistive MXene aqueous ink for micro-supercapacitor application, Energy Storage Mater. 25 (2020) 563-571.